Title: Neutrophils restrain allergic airway inflammation by limiting ILC2 function and monocyte-dendritic cell antigen presentation.

One sentence summary: G-CSF augments T_H2 responses in allergen sensitized mice and is negatively regulated by transmigrated lung neutrophils.

Authors:

Dhiren F. Patel[1], Teresa Peiró[1,2], Nicoletta Bruno[1], Juho Vuononvirta[1], Samia Akthar[1], Franz Puttur[1], Chloe J. Pyle[1], Kornelija Suveizdytė[1], Simone A. Walker[1], Aran Singanayagam[1], Leo M. Carlin[3,4], Lisa G. Gregory[1], Clare M. Lloyd[1], Robert J. Snelgrove[1*].

Affiliations:

[1]Inflammation Repair and Development, National Heart and Lung Institute, Imperial College London, London SW7 2AZ, United Kingdom.

[2]Departamento de Enfermería, Universidad de Valencia, Valencia 46010, Spain.

[3]Cancer Research UK Beatson Institute, Garscube Estate, Glasgow, G61 1BD, UK.

[4]Institute of Cancer Sciences, University of Glasgow, Garscube Estate, Glasgow, G61 1QH, UK.

[*]**Corresponding author:**

Robert J. Snelgrove

National Heart and Lung Institute, Imperial College London, London SW7 2AZ, United Kingdom

Tel: +44 (0)207 594 8192

robert.snelgrove@imperial.ac.uk

Abstract:

Neutrophil mobilization, recruitment and clearance must be tightly regulated as over-exuberant neutrophilic inflammation is implicated in the pathology of chronic diseases, including asthma. Efforts to target neutrophils therapeutically have failed to consider their pleiotropic functions and the implications of disrupting fundamental regulatory pathways that govern their turnover during homeostasis and inflammation. Using the house dust mite (HDM) model of allergic airways disease, we demonstrate that neutrophil depletion unexpectedly resulted in exacerbated T_H2 inflammation, epithelial remodelling and airway resistance. Mechanistically, this was attributable to a striking increase in systemic G-CSF concentrations, which are ordinarily negatively regulated in the periphery by transmigrated lung neutrophils. Intriguingly, we found that increased G-CSF augmented allergic sensitization in HDM exposed animals by directly acting on airway ILC2s to elicit cytokine production. Moreover, increased systemic G-CSF promoted expansion of bone marrow monocyte progenitor populations, which resulted in enhanced antigen presentation by an augmented peripheral monocyte-derived dendritic cell pool. By modelling the effects of neutrophil depletion, our studies have therefore uncovered previously unappreciated roles for G-CSF in modulating ILC2 function and antigen presentation. More broadly, they highlight an unexpected regulatory role for neutrophils in limiting T_H2 allergic airway inflammation.

Introduction:

Neutrophils are essential components of the body's immune surveillance and host defence owing to their capacity to readily eliminate invading pathogens. However, due to their considerable destructive capacity and potential to cause damage to healthy tissue, it is critical that neutrophil homeostasis is tightly regulated. Neutrophil homeostasis is maintained by a fine balance between granulopoiesis, bone marrow storage and release, intravascular margination, and ensuing clearance and destruction. The principle regulator of granulopoiesis at steady-state is granulocyte colony stimulating factor (G-CSF) / CSF3, with mice lacking the G-CSF receptor shown to be severely neutropenic *(1–4)*. Following stress or an inflammatory insult, G-CSF and an array of other mediators, such as ELR^+ CXC chemokines, are increased and function to further promote granulopoiesis and neutrophil recruitment to a tissue *(5, 6)*. However, it is critical that this neutrophilic inflammation is tightly regulated and efficiently resolved and a homeostatic state restored. Increasingly, there is a growing comprehension for the prominent role neutrophils play in regulating their own turnover both during homeostasis and inflammation *(7, 8)*.

Over-exuberant and persistent neutrophilic responses have been implicated in the pathology of an array of chronic diseases including chronic obstructive pulmonary disease, cystic fibrosis and asthma. In the context of asthma, elevated neutrophil numbers are associated with enhanced severity of disease, impaired lung function, diminished responsiveness to corticosteroids, exacerbations and fatality *(8–14)*. However, manipulation of neutrophilic inflammation in a clinical setting has been disappointing and failed to ameliorate disease pathology *(15–21)*. One potential explanation for this is that strategies seeking to reduce neutrophilic inflammation may inadvertently disrupt regulatory functions performed by neutrophils.

In this study, we demonstrate that chronic, systemic depletion of neutrophils in a house dust mite (HDM) murine model of allergic airways disease unexpectedly resulted in exacerbated T_H2 inflammation, augmented mucus production and increased airway resistance. Central to this augmented inflammation in neutrophil-depleted animals was a striking increase in G-CSF concentrations, which arose due to a failure of apoptotic neutrophils to trigger a negative feedback IL-23 – IL-17 – G-CSF regulatory axis in the periphery, classically designed to limit neutrophil production and mobilization from the bone marrow. In the context of our allergic airways disease model, the accumulated G-CSF directly potentiated allergen sensitization at early time points by promoting T_H2 cytokine production by type 2 innate lymphoid cells (ILC2s) and acting on bone marrow progenitors to drive monocytosis. This monocytosis consequently resulted in augmented antigen presentation by monocyte-derived dendritic cells. Thus, we highlight unappreciated roles for G-CSF in promoting ILC2 function and antigen presentation, and more broadly for neutrophils in negatively regulating type 2 allergic airway inflammation.

Results:

HDM administration elicits a neutrophilic inflammation in the lung and airways of mice.

Our well-established HDM model of allergic airways disease (Supplementary Fig. 1A) *(22)* provokes a mixed granulocytic inflammation with prominent neutrophilia. In this model, a robust increase in neutrophil numbers and percentages in the lung (Supplementary Fig. 1B and C, respectively) and airways (Supplementary Fig. 1D and E, respectively) were observed from 1 week of HDM exposure and persisted until 3 weeks – by which time eosinophils were the prominent granulocyte (Supplementary Fig. 1B-E). The elevated neutrophilic inflammation observed in HDM treated animals coincided with increased expression levels and protein concentrations of classical ELR^+ CXC chemokine CXCL1/KC (Supplementary Fig. 1F-H) and neutrophil granulopoiesis regulator G-CSF (Supplementary Fig. 1I-K). Neutrophil-derived proteases myeloperoxidase (MPO; Supplementary Fig. 2A and B) and metalloproteinase-9 (MMP-9; Supplementary Fig. 2C and D) are often used as a clinical surrogate for neutrophilic inflammation, and levels were indeed found to be elevated in the lung and airways of HDM exposed mice. Whilst MPO levels temporally correlated with neutrophilic infiltrate, MMP-9 levels in the airways continued to increase when neutrophilia had stabilized, likely reflective of the multitude of cellular sources of this protease.

Neutrophil depletion exacerbates T_H2 inflammation and airway remodelling in HDM exposed mice.

To interrogate the role of neutrophils in our model of allergic airways disease, mice were administered an anti-Ly6G (1A8) neutrophil-depleting antibody *(23)*. Differential 1A8 dosing regimens were utilized to assess the optimal strategy to deplete neutrophils in mice exposed to HDM (Supplementary Fig. 3A), and a previously reported *(24)* flow cytometry gating protocol was employed and modified to identify neutrophils independently of their Ly6G expression (Supplementary Fig. 3B) – with neutrophils defined as $CD11b^+$ $CD11c^{lo}$, $F480^-$ and

Ly6C^{intermediate}. A single intraperitoneal administration of 100 µg 1A8 was sufficient to completely ablate neutrophil numbers in the lung (Supplementary Fig. 3C and E), airways (Supplementary Fig. 3D and E), blood (Supplementary Fig. 3F) and spleen (Supplementary Fig. 3G) 24 hrs after a single HDM exposure, with neutrophil numbers in the bone marrow (Supplementary Fig. 3H) also partially reduced. When this dosing regimen was employed throughout the 3 week duration of the HDM allergic airways disease model (Fig. 1A; Supplementary Fig. 3I), a consistent reduction in neutrophil numbers was observed at all time points in the lung (Fig. 1B), airways (Fig. 1C) and blood (Supplementary Fig. 3J) relative to mice treated with an IgG2a isotype control antibody (2A3). However, depletion of bone marrow neutrophils was not apparent at later time points (Supplementary Fig. 3K). The anti-Ly6G 1A8 antibody has become the preferential strategy to deplete neutrophils *(23)*, owing to its purported selective expression by these cells *(25, 26)*. The neutrophil specificity of Ly6G expression is further supported by the Catchup Ly6G reporter mice, though low transgene activity was reported in a small number of eosinophils within this study *(27)*. In our hands, Ly6G expression was largely absent on lymphocytes and monocytes, but low levels were detectable on a subset of eosinophils in the bone marrow, blood and lungs of PBS and HDM treated mice (Supplementary Fig. 4A-C). However, 1A8 administration selectively depleted neutrophils in HDM treated mice, with no effect on numbers of eosinophils and lymphocyte numbers, whilst monocytes were surprisingly increased in HDM/1A8 treated animals (Supplementary Fig. 4D-F). A marginal reduction in lung eosinophil numbers was, however, observed in PBS mice administered 1A8 (Supplementary Fig. 4F).

The hallmark clinical features of allergic airways disease are established within our model by 3 weeks of HDM exposure *(22)*. At this time point, despite the substantial reduction in neutrophil numbers in 1A8 treated HDM-exposed mice, these animals actually exhibited an increase in total cell numbers in their lungs (Fig. 1D), whereas total numbers in the airways

were modestly elevated, albeit not significantly relative to control animals (Supplementary Fig. 5A). The increase in pulmonary inflammation in HDM exposed neutrophil-depleted mice was clearly visible by observation of haematoxylin and eosin stained lung sections (Fig. 1E). We next sought to determine the nature of the populations that must be elevated in HDM treated neutrophil-depleted mice to account for the increase in total inflammation despite the loss of neutrophils. HDM-exposed neutrophil-depleted mice displayed increased eosinophils in their lungs (Fig. 1F) and airways (Supplementary Fig. 5B) relative to control treated mice administered HDM, although this again failed to reach significance in the airways. Furthermore, the number of $CD4^+$ T_H2 cells in both the lungs (Fig. 1G and H) and airways (Supplementary Fig. 5C) were significantly elevated in neutrophil-depleted mice relative to control animals after 3 weeks of HDM administration. In keeping with greater T_H2 inflammation in neutrophil depleted animals after 3 weeks of HDM exposure, was a significant increase in classical type 2 antibodies, with serum levels of both total (Supplementary Fig. 5D) and HDM-specific (Fig. 1I) IgE and IgG1 being elevated compared to 2A3 control animals. Observation of haematoxylin and eosin stained lung sections (Fig. 1E) revealed that many of the airways of HDM-exposed neutrophil depleted mice were plugged with mucus. Accordingly, 1A8-treated HDM exposed mice exhibited increased lung tissue expression of the major airway mucin *Muc5ac* (Supplementary Fig. 5E) with an associated increase in airway MUC5AC protein (Supplementary Fig. 5F) relative to 2A3/HDM animals. IL-13 is a major instigator of epithelial MUC5AC production within our model of allergic airways disease, and accordingly IL-13 concentrations were elevated in the BALF of neutrophil depleted mice exposed to HDM (Supplementary Fig. 5G), in keeping with the augmented T_H2 response within this group. Furthermore, BALF IL-13 concentrations showed a significant correlation with MUC5AC protein levels across HDM groups (Supplementary Fig. 5H). In keeping with airway obstruction and plugging by mucus, the neutrophil-depleted HDM treated animals exhibited an

increase in baseline airway resistance relative to 2A3/HDM controls (Supplementary Fig. 5I), with airway resistance correlating with BALF MUC5AC concentrations (Supplementary Fig. 5J). Changes in lung function of HDM exposed mice following neutrophil depletion were, however, restricted to baseline airway resistance, with no differences detectable in airway hyperresponsiveness to increasing doses of methacholine relative to 2A3/HDM mice (Supplementary Fig. 6).

An early increase in ILC2-derived T_H2 cytokines supports the augmented type 2 inflammation observed in neutrophil-depleted mice administered HDM.

Given the prominent effect of neutrophil depletion on antigen-specific T cell responses and type 2 antibody generation, we questioned the potential role of neutrophils in regulating allergen sensitization at early time points after HDM exposure when neutrophil numbers were at their peak (Fig. 2A). T_H2 cytokines are of fundamental importance in driving the type 2 inflammation and associated antibody responses in allergen models of allergic airways disease *(28)*. Accordingly, levels of prototypic T_H2 cytokines IL-4, IL-5 and IL-13 were significantly increased in the airways of neutrophil-depleted mice relative to controls after 1 week of HDM exposure, both in terms of protein levels in BAL fluid (Fig. 2B) and *Il4*, *Il5* and *Il13* message in cells derived from the airways (Supplementary Fig. 7A). This phenotype was conserved in lung tissue, albeit less pronounced, at the level of protein (Supplementary Fig. 7B) and transcript (Supplementary Fig. 7C). We next sought to ascertain the cellular source of the elevated T_H2 cytokines in neutrophil depleted animals at 1 week of HDM exposure. Lung epithelial ($CD45^-$ $EpCAM^+$), endothelial ($CD45^-$ $EpCAM^-$ $CD31^+$) and leukocytes ($CD45^+$) were isolated via fluorescence-activated cell sorting (FACS) from mice administered PBS or HDM for 1 week (Supplementary Fig. 8A) to assess the gene expression of T_H2 cytokines. *Il4*, *Il5* and *Il13* message were only detected in the leukocyte population and were increased upon HDM challenge (Supplementary Fig. 8B). ILC2s and $CD4^+$ T_H2 cells are classically

acknowledged as primary sources of T_H2 cytokines in allergen models of allergic airways disease *(28)*, and assessment of IL-13 gfp-reporter mice *(29)* administered HDM for 1 week demonstrated that ILC2s were the prominent source of this cytokine at this early time point (Supplementary Fig. 8C).

Subsequently, ILC2s and $CD4^+$ T cells were isolated by FACS (Supplementary Fig. 9) from the airways (Fig. 2C) and lungs (Supplementary Fig. 10) of control and neutrophil-depleted mice challenged with HDM for 1 week and assessed for expression of genes encoding T_H2 cytokines. At this early time point, $CD4^+$ T cells were the prominent source of IL-4 and expression was significantly elevated in cells derived from the lungs of neutrophil-depleted animals (Supplementary Fig. 10). Conversely, ILC2s were clearly the primary source of IL-5 and IL-13 (Fig. 2C and Supplementary Fig. 10) and their levels were strikingly elevated in airway ILC2s derived from neutrophil-depleted animals (Fig. 2C), in keeping with the prominent increase in levels of these cytokines in BAL fluid of these mice. Supportive of these findings, the master transcriptional regulator of T_H2 cytokine production, GATA-3, showed elevated mRNA expression in lung $CD4^+$ T cells (Supplementary Fig. 10) and airway ILC2s (Fig. 2C) derived from neutrophil-depleted mice. Intracellular cytokine staining and flow cytometry analysis supported these assertions, since whilst the total number of lung and airway ILC2s (Supplementary Fig. 11A) and the proportion (Supplementary Fig. 11B and C) and number (Fig. 2D and Supplementary Fig. 11D-F) of ILC2s producing IL-13 or IL-5 were not consistently elevated in neutrophil-depleted animals administered HDM, the amount of cytokines the ILC2s produced on a per cell basis (as adjudged by assessment of geometric mean) were significantly elevated (Fig. 2E and Supplementary Fig. 11D-F).

Elevated monocyte-derived dendritic cells and ensuing antigen presentation in HDM exposed neutrophil-depleted mice as a consequence of perturbations in bone marrow progenitor pools.

In addition to a T_H2 milieu, antigen sampling and presentation by dendritic cells is central to allergen sensitization and establishment of a type 2 adaptive response in models of allergic airways disease. Concomitant with an increase in ILC2-derived T_H2 cytokines in neutrophil depleted mice administered HDM for 1 week was a significant increase in lung $Ly6C^{low}$ and $Ly6C^{high}$ monocytes (Fig. 3A). Whilst this increase was most pronounced in neutrophil-depleted mice given HDM, it was also apparent in neutrophil-depleted PBS treated animals. This increase in monocyte populations in the lungs of HDM administered neutrophil-depleted animals was clearly apparent in precision cut lung slices (PCLS) stained for monocyte marker CD115 (Supplementary Fig. 12A). Subsequently, neutrophil-depleted animals also presented with an increase in lung monocyte-derived dendritic cells (moDCs) that was again most pronounced in those animals administered HDM for 1 week (Fig. 3B). Surprisingly, this phenotype was not restricted to moDCs, with a significant increase in lung $CD11b^+$ conventional dendritic cells (cDCs) and $CD103^+$ cDCs (Supplementary Fig. 12B) also observed in neutrophil-depleted mice.

Activation and migration of DCs to draining lymph nodes and ensuing priming of allergen-specific T cell responses is integral to allergen sensitization. In the HDM model, moDCs and $CD11b^+$ cDCs are integral to transporting antigen to draining mediastinal lymph nodes (MLNs) *(28, 30)*. Numbers of total and activated moDCs (Fig. 3C and D) and $CD11b^+$ cDCs (Supplementary Fig. 12C and D) were increased in the MLNs of neutrophil-depleted animals administered HDM. To ascertain whether antigen presentation was augmented in neutrophil-depleted animals exposed to HDM, 2A3 and 1A8 treated mice were administered HDM for 1 week, with Alexa Fluor-488 tagged ovalbumin (OVA) administered concomitantly with the final dose of allergen (Fig. 3E). Importantly, numbers of OVA^+ moDCs in neutrophil-depleted mice were also significantly elevated in MLNs (Fig. 3F), demonstrating that they were effectively transporting antigen to localized lymph nodes. Whilst the same trend was observed

with OVA^+ $CD11b^+$ cDCs (Supplementary Fig. 12E), the increase in neutrophil-depleted animals did not reach statistical significance. Supportive of the assertion of increased antigen presentation in HDM treated neutrophil depleted mice, MLN T cells from these animals expressed higher levels of activation markers ICOS (Supplementary Fig. 12F) and PD1 (Supplementary Fig. 12G) and showed greater proliferation (Supplementary Fig. 12H). Thus, enhanced antigen presentation in the context of an augmented T_H2 cytokine environment observed in neutrophil depleted animals during allergen sensitization at 1 week of HDM exposure is conducive to the elevated T_H2 inflammation seen at later time points.

To rationalize the accumulation of monocyte populations and ensuing moDCs in the lungs of neutrophil depleted mice, we assessed lung concentrations of classical monocyte chemokines CCL2 and CX_3CL1 after 1 week of HDM exposure. Whilst HDM administration resulted in an increase in concentrations of CCL2 and CX_3CL1, these chemokines were not further elevated in mice depleted of neutrophils and could not therefore account for the tissue monocytosis observed in these animals (Supplementary Fig. 13A). Analysis of PCLS revealed increased intra-vascular pools of monocytes in neutrophil depleted HDM exposed animals (Supplementary Fig. 12A). Accordingly, flow cytometry analysis demonstrated that neutrophil depletion resulted in increased numbers of blood $Ly6C^{low}$ and $Ly6C^{high}$ monocytes – in both PBS and HDM treated animals (Fig. 4A) – thus providing a greater circulating pool of monocytes to extravasate into the lung in response to localized chemokine gradients. Subsequently, we questioned whether alteration in bone marrow progenitor pools could account for systemic changes in monocyte numbers following neutrophil depletion. Accordingly, the percentage of monocyte dendritic cell progenitors (MDPs) *(31, 32)*, defined as $CD115^+$, $Lineage^-$, $c\text{-}Kit^+$ and $FLT\text{-}3^+$ (Supplementary Fig. 13B), were shown to be elevated in the bone marrow of neutrophil depleted mice after 1 week of HDM exposure (Fig. 4B). Recently, it has been suggested that MDPs differentiate into common dendritic cell progenitor

cells (CDPs) *(32)*, which are the first committed dendritic cell progenitor to give rise to the cDC subsets that were also shown to be universally elevated in neutrophil depleted mice. Consequently, the percentage of CDPs, defined as $CD115^+$, $Lineage^-$, $c\text{-}Kit^-$, $FLT\text{-}3^+$, $CD11b^-$ and $CD11c^-$ (Supplementary Fig. 13B), were also shown to be elevated in neutrophil depleted animals (Fig. 4B). Thus neutrophil depletion gives rise to increased MDPs and CDPs in the bone marrow, which ultimately drives elevated monocyte and DC populations in the lung.

A dysregulated IL-23 – IL-17 – G-CSF axis in neutrophil depleted mice.

We next sought to ascertain what mediator/s was driving the augmented progenitor pools in the bone marrow of neutrophil depleted animals and the ensuing increase in lung monocytes and DCs. A proteome profiler array was used to semi-quantitatively assess broad changes in cytokines, chemokines and proteases in serum of control and neutrophil depleted mice after 1 week of HDM administration. Whilst differential levels of various mediators were observed via proteome profiler analysis, a striking increase in G-CSF in neutrophil depleted animals was particularly noteworthy (Supplementary Fig. 14). This was deemed to be especially pertinent given that CSF3R, the G-CSF receptor, is expressed on MDPs and CDPs *(33)*, and that an increase in monocytes has been reported in neutropenic patients administered G-CSF to promote granulopoiesis *(34)*. Subsequently, serum, lung homogenate and BALF G-CSF levels were assessed by ELISA and demonstrated to be strikingly elevated in both PBS and HDM treated mice depleted of neutrophils (Fig. 4C). The increase in G-CSF concentration did not simply reflect a reduced internalization of the G-CSF following ablation of neutrophils, since lung *Csf3* gene expression was elevated in neutrophil depleted mice (Fig. 4D).

Previous studies have demonstrated that G-CSF expression is prominently controlled by IL-17 *(35–37)*, with IL-17 derived from tissue resident T cell populations central to G-CSF regulation during homeostasis *(38, 39)*. It was noteworthy therefore that the proteome profiler revealed

an increase in IL-17 levels in HDM-exposed neutrophil depleted animals (Supplementary Fig. 14). Accordingly, it was demonstrated that *Il17a* expression was significantly elevated in the lungs of neutrophil depleted mice, with the increase potentiated by HDM exposure (Fig. 4E). Expression analysis in T cells and ILC2s isolated from the lungs of HDM treated animals at this time point demonstrated that T cells were the primary source of IL-17 and that those derived from neutrophil depleted mice produced more of this cytokine (Supplementary 15A). This was supported by flow cytometry, with both $CD4^+$ αβ T cells and γδ T cells derived from neutrophil depleted mice producing more IL-17 following 1 week of HDM administration (Supplementary 15B and C). IL-23 is a potent regulator of IL-17 expression and it has previously been demonstrated during homeostasis, that phagocytosis of transmigrated, apoptotic neutrophils by resident macrophages and dendritic cells suppresses their intrinsic IL-23 production *(38, 39)*. We thus questioned whether the failure of neutrophils to reach the lung in HDM challenged neutrophil-depleted mice would lead to an increase in IL-23 concentrations which would rationalize an ensuing increase in IL-17 and ultimately G-CSF. Consequently, *Il23* expression was shown to be elevated in the lungs of neutrophil depleted animals administered HDM for 1 week (Fig. 4F). Flow cytometry analysis demonstrated that resident $CD11c^+$ macrophages and moDCs were the primary sources of IL-23 in HDM treated mice, with increased numbers of IL-23^+ moDCs present in neutrophil depleted animals (Supplementary 15D). Furthermore, both the $CD11c^+$ macrophages and moDCs derived from neutrophil depleted HDM exposed mice produced more IL-23 on a per cell basis than those from HDM/control antibody treated animals (Supplementary 15E and F). Thus disruption of a peripheral feedback system, normally regulated by lung infiltrating, apoptotic neutrophils, resulted in the increased G-CSF levels observed in our 1A8 treated mice (Fig. 4G).

Neutralization of G-CSF reduces the monocytosis and elevated T_H2 cytokine levels observed in neutrophil depleted HDM exposed mice.

We next sought to determine whether neutralization of G-CSF in our HDM model would abrogate the augmentation of bone marrow progenitors and tissue monocytes seen in neutrophil depleted animals. Mice exposed to HDM for 1 week were concomitantly treated with 2A3/1A8 and anti-G-CSF neutralising antibody/control (Fig. 5A). Neutralization of G-CSF resulted in a significant reduction in neutrophils in HDM exposed animals (Fig. 5B), highlighting a prominent role for this mediator in defining neutrophilia in this model. Importantly, the increase in lung $Ly6C^{low}$ and $Ly6C^{high}$ (Fig. 5C) monocytes observed in HDM treated mice depleted of neutrophils was completely negated following anti-G-CSF treatment. Furthermore, anti-G-CSF administration also reduced the percentage of bone marrow MDPs and CDPs (Fig. 5D) in neutrophil depleted mice exposed to HDM for 1 week to a level observed in 2A3 treated animals. Thus, G-CSF, elevated as a consequence of neutrophil depletion, is driving the augmentation in bone marrow progenitors and ensuing increase in circulating and tissue monocytes. Reassuringly, the phenotype was largely recapitulated when IL-17 was neutralized in HDM exposed neutrophil-depleted mice, validating the importance of this cytokine in defining G-CSF levels (Supplementary Fig. 16A), and consequential changes in tissue neutrophils (Supplementary Fig. 16B) and monocytes (Supplementary Fig. 16C) and bone marrow progenitors (Supplementary Fig. 16D).

Previously, we demonstrated that HDM-exposed neutrophil depleted mice exhibited a prominent increase in T_H2 cytokine levels at 1 week of HDM exposure, which was attributable to augmented production on a per cell basis by ILC2s. Remarkably, the increase in BAL fluid concentrations of IL-4, IL-5 and IL-13 observed in neutrophil depleted mice after 1 week of HDM administration were significantly reduced upon anti-G-CSF administration (Fig. 5E).

Similarly, the amount of T_H2 cytokines produced by ILC2s on a per cell basis, as exemplified by IL-13 and assessed by flow cytometry, were significantly reduced following anti-G-CSF administration to neutrophil depleted animals exposed to HDM (Fig. 5F) – a phenotype that was again conserved with anti-IL-17 treatment (Supplementary Fig. 16E).

Recombinant G-CSF can augment ILC2 T_H2 cytokine production.

We next questioned whether the profound capacity of G-CSF to modulate ILC2 T_H2 cytokine production and the expansion of bone marrow progenitor populations in HDM exposed animals was unique to mice depleted of neutrophils, or whether it could also operate comparably in fully immunocompetent animals. HDM exposed mice were therefore administered recombinant G-CSF for 1 week (Fig. 6A). Administration of recombinant G-CSF to HDM exposed mice further increased tissue neutrophils (Fig. 6B), but also augmented tissue monocytes (Fig. 6C) and bone marrow progenitors (Fig. 6D) – as seen following neutrophil depletion. Furthermore, HDM-driven increases in BALF IL-4, IL-5 and IL-13 (Fig. 6E) and ILC2 T_H2 cytokine production (Fig. 6F) were also further accentuated by recombinant G-CSF administration. Thus G-CSF is a physiologically relevant regulator of ILC2 function and monocyte numbers.

We next questioned whether G-CSF could directly act on ILC2s to potentiate cytokine production. Data mining of previous RNAseq data sets indicated that ILC2s express the G-CSF receptor, csf3r *(40, 41)*, and this was confirmed in our HDM model with ILC2s isolated from the airways by FACS expressing *Csf3r* (Fig. 7A). *Csf3r* expression was completely absent in T cells isolated from airways (Fig. 7A), rationalizing earlier observations that the primary source of IL-5 and IL-13 in neutrophil depleted animals was ILC2s and not $CD4^+$ T cells. IL-33 is a potent regulator of ILC2s, and a week-long model of intranasal recombinant IL-33

administration (Fig. 7B) induces substantial ILC2 numbers in the absence of an antigen-specific T_H2 cell response. Once again, ILC2s isolated from the airways of recombinant IL-33 treated mice expressed *Csf3r* – which was again absent from T cells derived from these animals (Fig. 7C). When recombinant G-CSF was co-administered with recombinant IL-33 into the airways of mice (Fig. 7B) it augmented *Il5* and *Il13* expression within isolated airway ILC2s but not T cells, as adjudged by qPCR (Fig. 7D). Furthermore, co-administration of recombinant G-CSF with IL-33 increased BALF concentrations of IL5 and IL-13 (Fig. 7E).

To validate that G-CSF was able to directly augment T_H2 cytokine production from ILC2s, ILC2s were isolated from the airways of recombinant IL-33 treated mice (Supplementary Fig. 17A) or from peripheral blood of healthy donors (Fig. 8A) and then stimulated with or without G-CSF. As observed with mouse ILC2s, human ILC2s exhibited robust expression of G-CSF receptor, *CSF3R* (Fig. 8B). Mouse and human ILC2s stimulated with G-CSF released significantly more IL-5 and IL-13 than medium treated control cells (Supplementary Fig. 17B and Fig. 8C, respectively), whereas levels IL-4, IL-17, IFN-γ and IL-12 were undetectable and levels of IL-6 and TNF-α were extremely low and comparable. Accordingly, *IL5* and *IL13* message was significantly elevated in human ILC2s stimulated with G-CSF, as were levels of T_H2 master transcriptional regulator *GATA3* (Fig. 8D). Expression of *IL4* and *IL17* message was undetectable. Similarly, *Il4*, *Il5* and *Gata3* transcripts were dose-dependently augmented in mouse ILC2s stimulated with G-CSF (Supplementary Fig. 17C). Thus G-CSF is a previously unrecognised potentiator of T_H2 cytokine production by ILC2s which, together with the augmented G-CSF-driven moDC antigen presentation, facilitates the greater type 2 inflammation observed in HDM exposed neutrophil depleted mice at 3 weeks.

Discussion:

An over-exuberant or persistent neutrophilic response is implicated in the pathology of an array of inflammatory diseases, and neutrophils have consequently represented an attractive therapeutic target. However, therapeutic strategies that seek to ameliorate neutrophilic inflammation have failed to fully consider the potential regulatory roles fulfilled by these cells. In this study, we demonstrate that depletion of neutrophils in a HDM model of allergic airways disease led to perturbations of an IL-23 – IL-17 – G-CSF regulatory feedback pathway. The accumulated G-CSF subsequently promoted allergen sensitization and exacerbated type 2 inflammation, epithelial remodelling and lung function. This was mediated by the capacity of G-CSF to promote T_H2 cytokine production by airway ILC2s and to drive monocytosis and ensuing moDC-mediated antigen presentation (Supplementary Fig. 18).

We demonstrate that G-CSF acts on $Csf3r^+$ ILC2s to potentiate their production of IL-5 and IL-13 on a per cell basis. IL-4 levels were also elevated *in vivo* in a G-CSF-dependent manner, but was derived from $Csf3r^-$ $CD4^+$ T cells - potentially attributable to the reported capacity of ILC2s to promote IL-4 production by $CD4^+$ T cells *(42–44)*. ILC2s are early effectors in type 2 inflammation that sense and respond to cytokines and stress signals evoked from the proximal environment upon disruption of tissue homeostasis *(45)*. It is, thus, rational that an innate mediator such as G-CSF can function to potentiate ILC2 function. We also reveal the capacity to G-CSF to drive the expansion of bone marrow MDPs and CDPs and an ensuing monocytosis. Rationalizing this effect, G-CSF has previously been demonstrated to drive the expansion of granulocyte macrophage progenitor compartments (GMPs) within the bone marrow *(46)*. GMPs lie developmentally upstream of MDPs and CDPs and may thus account for the accumulation of the latter in neutrophil depleted animals. Data mining of historic RNA-seq data sets *(47)* revealed that GMPs, MDPs and CDPs all express csf3r, supportive of the notion

that G-CSF is able to drive the proliferation of one or more of these progenitors. Whilst G-CSF is classically recognized as a potent regulator of granulopoiesis, G-CSF administration has been reported to stimulate monocyte production and release in neutropenic patients *(48–50)*. In our allergen sensitized mice these expanded monocyte populations gave rise to augmented moDC numbers, which in keeping with previous literature *(28, 30)*, transported antigen to draining MLNs and activated T cells - potentially further licensed by the elevated ILC2-derived IL-13 *(42)*. Thus, enhanced antigen presentation, in the context of elevated ILC2-derived type 2 cytokines, in neutrophil depleted mice facilitated the increase in $CD4^+$ T_H2 cells after 3 weeks of allergen exposure. Similarly, the elevated levels of IL-4 would function to promote B cell responses and class switching that underlie the augmented levels of HDM-specific IgE and IgG1.

Given the novel roles ascribed to G-CSF in this study, it is worth re-evaluating the broader implications of G-CSF in the context of asthma. Increased levels of G-CSF have been reported in the BALF of asthmatic patients relative to healthy controls *(51)*, and in serum of patients with unstable asthma *(52)*. Pertinent to our current findings, G-CSF has been shown to increase concomitantly with IL-5 in unstable asthma *(52)*, whilst treatment of people with G-CSF augmented the number of circulating dendritic cells with the capacity to prime T cells to produce T_H2 cytokines *(53)*. Consequently, it is also appropriate to contextualize our findings with regards to the perceived role of neutrophils in asthma. The general consensus, based primarily on circumstantial clinical data, is that neutrophils are detrimental in the context of asthma and indicate a worse prognosis *(8, 10–14)*. Based upon our current findings, it could be argued that neutrophils also represent a compensatory mechanism to indirectly restrain T_H2 inflammation in the context of allergic disease by negatively regulating the bioavailability of G-CSF. In keeping with this hypothesis, adoptive transfer of neutrophils has recently been

shown to attenuate T_H2 responses in a mouse model of allergic airways disease *(54)*. Our data in mice that neutrophils negatively regulate type 2 inflammation is supported by a previously reported case of a patient with cyclic neutropenia that suffered episodic acute asthma, whereby the cyclical depreciation in neutrophils concomitantly correlated with a substantial increase in eosinophils, serum IgE levels and asthma exacerbation *(55)*. Additionally, eosinophilia is a well-recognised feature of a number of primary immunodeficiency disorders associated with neutropenia *(56)*.

Our study demonstrates the complex regulatory feedback pathways that define neutrophil turnover, and the intrinsic challenges of targeting neutrophils as a therapeutic modality in the context of asthma. Any intervention that impacts on the ability of neutrophils to transmigrate into tissues at steady-state will likely modify G-CSF levels. Thus, mice deficient in CXCR2 *(39)* or specific adhesion molecules *(38)* display increased baseline levels of G-CSF. Accordingly, therapeutic strategies employed to ameliorate neutrophilic inflammation in asthma may inadvertently augment G-CSF levels and potentiate T_H2 inflammation. It is noteworthy, therefore, that CXCR2 antagonist AZD5069 reduced peripheral blood neutrophils in healthy volunteers but also caused a significant increase in serum G-CSF concentrations *(57)*. Similarly, AZD5069 reduced lung, sputum and blood neutrophil numbers in patients with persistent asthma but again significantly increased G-CSF expression *(57, 58)*. Furthermore, CXCR2 antagonist SCH526123 reduced sputum neutrophils in patients with severe asthma, but concomitantly increased the percentage sputum eosinophils *(15)*. It is feasible, therefore, that augmented G-CSF levels leading to increased T_H2 inflammation could be a confounding factor that has contributed to the disappointing results of clinical trials with CXCR2 antagonists. Alternative approaches which target neutrophilic inflammation in combination with reducing the compensatory increase in G-CSF could potentially be more clinically

beneficial. Alternatively, would we be better equipped with strategies that seek to promote neutrophil apoptosis in tissues *(59–62)*, so as to reduce neutrophil numbers but simultaneously suppress the IL-23 – IL-17 – G-CSF axis? More broadly, our study highlights the complexities of targeting neutrophils within the clinic and implies that broad-sword approaches to block neutrophils may be sub-optimal given neutrophils' heterogeneity, pleiotropic functionality and regulatory capacity. It would be prudent to gain a fuller understanding of pathways by which neutrophils instigate pathology in asthma so that these facets of their biology may be targeted more specifically. Our findings may also, of course, have implications outside the remit of asthma, whereby a multitude of animal studies have studied depletion or manipulation of neutrophil numbers in diverse inflammatory models, and numerous clinical trials have assessed therapies aimed at attenuating neutrophilic inflammation. Whilst we have demonstrated the consequence of G-CSF accumulation in the context of antigen sensitization and type 2 inflammation of the airways, it will be intriguing to ascertain the implications in other experimental systems.

In conclusion, we demonstrate that depletion of neutrophils in the context of a murine model of allergic airways disease, results in a dysregulated IL-23 – IL-17 – G-CSF feedback loop. Ensuing accumulation of G-CSF functioned to augment allergen sensitization by directly potentiating ILC2 T_H2 cytokine production and acting on bone marrow progenitors to drive a monocytosis, which in turn resulted in augmented antigen presentation by moDCs. These studies are of basic biological significance in that they demonstrate previously unrecognized roles for G-CSF, and of translational significance in that they highlight the capacity of neutrophils to indirectly restrain allergic airway inflammation, potentially rationalizing the failure of previous neutrophil-targeting therapeutic strategies.

Materials and Methods:

Study Design.

The primary objective of this study was to define the importance of neutrophils in governing inflammation and pathology in allergic airway disease. In all experiments, appropriate control groups were utilised, and mice were housed under the same environmental conditions and were age-matched. Adult female mice were randomly placed in distinct experimental groups. Authors were blinded for cell counts and histology analysis. The number of mice in each group was determined by power calculations based on extensive previous experience with the model system and is defined in the respective figure legends. The number of independent replicates for each experiment is defined within the respective figure legends. No samples or animals were excluded from data analyses.

Human isolated ILC2s were utilised to determine the direct effects of G-CSF on ILC2 functionality. Blood was obtained from 3 male and 2 female donors. The number of donors was determined by previous experience with blood-derived ILC2 culturing methods. Authors were blinded from analysis of supernatant cytokine and mRNA expression analysis. All research ethics and patient consent were in place and further detailed below in "Human ILC2 culture".

Experimental Animals.

Eight to twelve-week-old female Balb/c mice were purchased from Envigo (Huntingdon, UK). All mice were randomly assigned to experimental groups. IL13-eGFP mice were kindly provided by A.N. McKenzie (MRC Laboratory of Molecular Biology, Cambridge) and subsequently bred in house *(29)*. Mice were kept in specified pathogen-free conditions and provided autoclaved food, water and bedding. All mouse experiments were performed in accordance with the recommendations in the Guide for the Use of Laboratory Animals of

Imperial College London, with the ARRIVE (Animal Research: Reporting of In Vivo Experiments) guidelines. All animal procedures and care conformed strictly to the UK Home Office Guidelines under the Animals (Scientific Procedures) Act 1986, and the protocols were approved by the Home Office of Great Britain.

Allergic airway disease murine model.

Balb/c mice were administered 25 μg House Dust Mite (HDM) extract (10.17 μg/l DerP1, 9 EU/ endotoxin content; Greer Laboratories) in 50 μl sterile PBS intranasally (i.n.) three times per week for up to 3 weeks. Control mice were administered 50 μl sterile PBS i.n. at analogous time points. All mice were culled 24 hours post the final dose of HDM or PBS.

Recombinant IL-33 and G-CSF administration.

Mice were intranasally administered 1 μg recombinant IL-33 protein (ThermoFisher Scientific) in 50μl PBS three times over a period of 1 week. In some experiments, mice were concomitantly intranasally administered 100 ng recombinant G-CSF (Peprotech, New Jersey, USA) in 50μl PBS (or PBS vehicle control) on a daily basis. When necessary, IL-33 was admixed with G-CSF for treatment of mice. Harvests were performed 24 hours post the final dose of IL-33.

In other experiments, mice administered HDM (i.n.) for 1 week (as detailed above) were also treated daily with 2.5 μg of recombinant G-CSF i.p. in 200μl PBS (or PBS vehicle control) and 100 ng G-CSF i.n. in 50μl PBS (or PBS vehicle control). Harvests were performed 24 hours post the final dose of G-CSF/HDM.

In vivo neutrophil depletion.

In order to deplete neutrophils, Balb/c mice received intraperitoneal (i.p.) administration of 100 μg anti-Ly6G (clone 1A8, BioXCell) in 200 μl PBS. Control mice received 100 μg isotype control antibody (clone 2A3, BioXCell) in 200 μl PBS. During the allergic airways disease model, mice were administered the respective antibodies 24 hours prior to each HDM or PBS treatment.

In vivo G-CSF neutralisation.

Neutralisation of G-CSF was achieved by i.p. administration of 100 μg anti-mouse G-CSF antibody (R&D Systems). Respective control mice for G-CSF neutralisation received i.p. administration of 100 μg isotype control antibody (clone 2A3, R&D Systems). Where appropriate, the respective antibodies were admixed with anti-Ly6G antibody (clone 1A8, BioXCell) for neutrophil depleted mice or isotype control antibody (clone 2A3, BioXCell) for control mice. Antibodies were administered 24 hours prior to each HDM or PBS i.n. exposure.

In-vivo IL-17 neutralisation.

Neutralisation of IL-17 was achieved by i.p. administration of 20 μg anti-mouse IL-17A antibody (R&D Systems). Respective control mice for IL-17 neutralisation received i.p. administration of 20 μg isotype control antibody (clone 2A3, R&D Systems). Where appropriate, the respective antibodies were admixed with anti-Ly6G antibody (clone 1A8, BioXCell) for neutrophil depleted mice or isotype control antibody (clone 2A3, BioXCell) for control mice. Antibodies were administered 24 hours prior to each HDM or PBS i.n. exposure.

Administration of fluorescently-tagged ovalbumin.

Ovalbumin (Invivogen) was tagged with Alexa Fluor 488 fluorophore utilising an Alexa Fluor 488 Protein Labelling kit as per the manufacturer's guidelines (ThermoFisher Scientific). Mice

were administered HDM i.n. for 1 week and upon the last HDM dose, mice received HDM mixed with 100 μg of Alexa Fluor-488 tagged Ovalbumin i.n.

Lung function measurements.

For studies where mice were administered HDM for 3 weeks, measurements of dynamic resistance, elastance and compliance were performed in anaesthetized and tracheotomized mice using a Flexi-vent system (SCIREQ) in response to increasing concentrations (0, 3, 10, 30, and 100 mg/mL) of methacholine (Sigma-Aldrich), as described previously *(63)*.

Cell recovery and isolation.

Mice were exsanguinated via cardiac puncture and 200 μl of blood was immediately lysed in ACK buffer (0.15 M ammonium chloride, 1 M potassium hydrogen carbonate and 0.01 mM EDTA, pH 7.2) for 5 minutes and subsequently centrifuged at 800 x g for 5 minutes before the cells were resuspended in 0.5 ml complete media (R10F; RPMI supplemented with 10% heat inactivated fetal bovine serum). Serum was isolated from excess clotted blood by centrifugation (8 min at 5,000 x g). Broncho-alveolar lavage (BAL) was performed by inflating the lungs 3 times each with 0.4 ml of PBS via a tracheal cannula. The BAL fluid was then pooled and centrifuged at 800 x g for 5 minutes, and the BAL supernatant was collected and frozen at -80 °C until required. The remaining cell pellet was re-suspended in 0.5 ml R10F.

The accessory, middle and superior lobes of the right lung were snap frozen in liquid nitrogen and subsequently stored at -80 ºC until required. The left lobe was chopped finely and incubated at 37 ºC for 30 minutes in complete media containing 0.15 mg/mL Liberase (Sigma-Aldrich) and 25 μg/mL DNAse (Type 1, Sigma-Aldrich). The cells were recovered by disruption through a 70 μm sieve before being centrifuged at 800 x g for 5 minutes. Lysis of red blood cells in ACK buffer was performed for 3 minutes at room temperature before a final

centrifugation at 800 x g for 5 minutes and re-suspension of the remaining cell pellet in 2 ml R10F.

Both femurs from each mouse were removed and freed of soft tissue attachments, and the extreme distal tip of each femur cut off. Both ends of the femurs were flushed with 1 ml of PBS containing 0.1% (wt/vol) sodium azide and 1% (wt/vol) BSA. The cells were carefully dispersed by filtration through a 70 μm sieve before being centrifuged at 800 x g for 5 minutes. Lysis of red blood cells in ACK buffer was performed for 3 minutes at room temperature before a final centrifugation at 800 x g for 5 minutes and re-suspension of the remaining cell pellet in 2 ml R10F.

The spleens of respective mice were disrupted through a 70 μm sieve and the suspension was centrifuged at 800 xg for 5 minutes. Red blood cell lysis was performed for 3 minutes utilising ACK buffer and the cells were centrifuged at 800 x g for 5 minutes before the final re-suspension of the cell pellet in 2 ml R10F.

Mediastinal lymph nodes were digested in 0.15 mg/mL Liberase (Sigma-Aldrich) for 30 minutes. The cells were recovered by disruption through a 70 μm sieve before being centrifuged at 800 x g for 5 minutes. The cell pellet was subsequently resuspended in 2 ml R10F.

FACS of leukocytes and stromal cells.

Lungs of mice were inflated with 1.5 ml of 5 mg/ml Dispase II (Sigma-Aldrich) and then allowed to collapse naturally. Low-melting-point agarose (0.5 ml of 1% (wt/vol)) was then slowly injected into the lungs and was immediately solidified by packing of the lungs in ice. Lungs were then removed and incubated for 40 min in dispase solution. Lung tissue was subsequently transferred to DMEM containing Hepes (25 mM; ThermoFisher) and DNAse I (50 μg/ml; Sigma-Aldrich), and the digested tissue was 'teased away' from the upper airways

and incubated with gentle agitation for a further 30 minutes. Digested lung tissue was disrupted into single-cell suspensions by passage through a 70 μm sieve (BD Labware) before being centrifuged at 800 x g for 5 minutes. Lysis of red blood cells in ACK buffer was performed for 3 minutes before a final centrifugation at 800 x g for 5 minutes and re-suspension of the remaining cell pellet in 2 ml R10F. Cell suspensions were stained with anti–mouse CD45-PerCP, anti-mouse EpCAM-PE and anti–mouse CD31-APC as detailed below, and populations (endothelial cells: $CD45^-$ $CD31^+$ $EpCAM^-$; epithelial cells: $CD45^-$ $CD31^-$ $EpCAM^+$; hematopoietic cells $CD45^+$ $CD31^-$ $EpCAM^-$) isolated by fluorescent-activated cell sorting (FACS) on a BD FACS LSR Aria III sorter. Isolated cells were centrifuged 800 x g for 5 minutes and re-suspended in 350 μl RLT buffer (Qiagen) and stored at -80 ºC for real time PCR (see below).

FACS of T cells and ILC2s.

Single cell suspensions were obtained from lung tissue and BAL as described above in "Cell recovery and isolation". For interrogation of airway T cells and ILC2s it was necessary to pool the BAL from 3 mice for each data point. Cell suspensions were stained with anti–mouse CD4-FITC, anti-mouse CD45-PerCP, anti–mouse ICOS-PE-Cy7 and an internally made lineage (Lin) cocktail (consisting of TCRβ-APC, CD5-APC, CD19-APC, TCRγδ-APC, CD11b-APC, CD11c-APC, NKp46-APC, FCεR1-APC, GR-1-APC, F4/80-APC, TER-119-APC) as detailed in Supplementary Table 2, and populations (T cells: Lin^+ $CD45^+$ $CD4^+$; ILC2s: Lin^- $CD45^+$ $CD4^-$ $ICOS^+KLRG1^+$) were isolated by FACS on a BD FACS LSR Aria III sorter. Isolated cells were centrifuged 800 x g for 5 minutes and re-suspended in 350 μl RLT buffer (Qiagen) and stored at -80 ºC for real time PCR (see below).

Human ILC2 cultures.

Blood from healthy, non-allergic male (n = 3) and female (n=2) volunteers, with an age range of 24 - 40 years, was collected with written informed consent approved by the Brompton, Harefield and NHLI ethics committee. All experiments were carried out in accordance with the approved guidelines. Blood (50 ml) was collected from each donor via venepuncture and placed in 1 ml EDTA (0.5M, ThermoFisher Scientific). Whole blood ILC2s were enriched utilising the RosetteSep^{TM} Human ILC2 Enrichment Kit (Stemcell Technologies, UK) as per manufacturer's instructions. The enriched ILCs were then stained with anti-human lineage cocktail-FITC (ThermoFisher Scientific), anti-human CD45-PERCP (ThermoFisher Scientific) and anti-human CRTH2-BV421 (Biolegend) antibodies for 30 minutes before being sorted utilising a BD LSR Aria III cell sorter (BD Biosystems). The ILCs were identified as Lin^{-} $CD45^{+}$ $CRTH2^{+}$. The isolated ILC2s were cultured in medium containing DMEM + 10 % FCS, IL-7 (5 ng/ml; PeproTech) and IL-33 (10 ng/ml; PeproTech) for 2 weeks. The cells were subsequently split and cultured in control medium or media supplemented with G-CSF (100 ng/ml; PeproTech) for 72 hours. After stimulation, the cell supernatant was collected for protein analysis and the cells were lysed with 350 µl RLT buffer (Qiagen).

Mouse ILC2 culture.

Mice were administered 1 µg recombinant IL-33 (ThermoFisher Scientific) for 1 week as detailed above in "Recombinant IL-33 and G-CSF administration". At 24 hours after the final IL-33 dose, lung tissue was extracted and single cell suspensions were obtained as described above in "Cell recovery and isolation". ILC2s were sorted as described in "FACS of T cells and ILC2s". Post sort, the isolated ILC2s were immediately plated in medium containing DMEM + 10% FCS, IL-7 (5 ng/ml; PeproTech) containing IL-33 (10 ng/ml; PeproTech) or lacking IL-33. Respective wells were subsequently supplemented with either media, 10 ng/ml G-CSF or 100 ng/ml G-CSF for 72 hours. After 72 hours, the supernatant was collected for the

measurement of IL-5 and IL-13 by ELISA and the cells were lysed in 350 µl RLT buffer (Qiagen) for RNA analysis. The lysed cells were assessed for mRNA expression of *Il5*, *Il13* and *Gata3*.

Flow cytometry.

Cells were stained with the LIVE/DEAD Fixable Near-IR-Dead Cell staining kit (Molecular Probes, Invitrogen) for 10 minutes in PBS before being blocked with anti-CD16/CD32 Fc receptor block (BD Pharmingen) for 20 minutes. Cells were then washed in PBS and stained for surface markers for 30 minutes at 4 ºC in PBS that contained 0.1% (wt/vol) sodium azide and 1% (wt/vol) BSA and were fixed with 2% (vol/vol) paraformaldehyde. All samples were acquired immediately on a BD LSR Fortessa cell analyser (BD Biosystems) and analysed using BD FACS DIVA (BD Biosystems). Cells were defined by markers, as described in Supplementary Table 2.

For intracellular cytokine staining, single cell suspensions from lung tissue and BAL were stimulated with 40 ng/ml PMA (Sigma Aldrich) and 3 µg/ml ionomycin (MERCK Millipore) in complete medium supplemented with 10 µg/ml Brefeldin A (Sigma Aldrich) at 37 ºC, 0.5% CO_2 for 3 hours. The cells were then stained for extracellular markers and fixed as stated above. Cells were subsequently permeabilized with saponin buffer (PBS with 0.05% (wt/vol) sodium azide, 1% (wt/vol) BSA and 1% (wt/vol) saponin (Sigma Aldrich)) containing anti-mouse IL-13-PE, anti-mouse IL-5-BV421, anti-mouse IL-4-FITC, anti-mouse IL-17A-AlexaFluor 700 and / or anti-mouse IL-23-PE-CY7. For Ki-67 staining, the cells were incubated with anti-mouse Ki67-Alexa Fluor 488 antibodies. Then, 30 minutes later, cells were washed once in saponin buffer and once in PBS containing 0.1% (wt/vol) sodium azide and 1% (wt/vol) BSA and data were acquired immediately on a BD LSR Fortessa cell analyser.

Cytokine Analysis.

Murine superior and middle lung lobes were homogenized at a concentration of 50 mg/ml in PBS. Lung homogenates were centrifuged for 10 minutes (800 x g) and supernatant harvested for cytokine analysis. Lung homogenates, BAL fluid, serum and mouse ILC2 supernatants were assessed for concentrations of MMP-9, MPO, CCL2, CX_3CL1, G-CSF (DuoSet; R&D Systems), IL-13 (ThermoFisher Scientific), IL-4 and IL-5 (BD Pharmingen), where relevant, by ELISA.

Human ILC2 cell supernatants were assessed for cytokines using the LegendPlex Human Th helper cytokine kit. The preparation of samples was performed as per manufacturer's instructions and recorded on a BD LSR FORTESSA flow cytometer (BD Biosystems).

Measurement of Immunoglobulin concentrations.

Total IgG1 and IgE (BD Biosciences, UK) were measured in diluted serum using standardized sandwich ELISAs according to the manufacturer's protocol. Allergen specific IgE and IgG1 were measured in diluted serum as previously described *(64)*.

Measurement of airway mucin concentrations.

BALF MUC5AC protein was determined using a previously described protocol *(65)*. In brief, BAL fluid was placed on a 96 well plate (Corning, U.K.) and allowed to evaporate overnight at 37 ºC. The plate was subsequently washed and blocked with 2% BSA for 2 hours. Protein Muc5ac was measured using a biotinylated anti-Muc5ac detection antibody (400 ng/ml; ThermoFisher Scientific).

Quantitative RT-PCR.

For whole lung, tissue was homogenised in RLT buffer (Qiagen) and total RNA was extracted using RNeasy Plus Mini Kit (Qiagen). Reverse transcription was subsequently performed

using the High-Capacity cDNA Reverse Transcription Kit (ThermoFisher). For suspensions of isolated cell populations (in RLT buffer (Qiagen)), total RNA was extracted using RNeasy Plus Micro Kit (Qiagen) and reverse transcription was performed using GoScript™ Reverse Transcriptase kit (Promega). Taqman gene expression assays (ThermoFisher Scientific) were used to assess relative expression of murine *Csf3*, *Csf3r*, *Cxcl1*, *Il4*, *Il5*, *Il13*, *Il17*, *Il23*, *Gata3* and *Muc5ac* mRNA expression and normalised to *Gapdh*. Similarly, relative expression of human *IL5*, *IL13* and *GATA3* expression was normalised to *GAPDH*. Quantitative RT-PCR was performed on a Viaa7 Real-Time PCR System (ThermoFisher Scientific). Data were obtained from two technical replicates and expressed as fold change in ΔΔCT from respective control groups or relative expression of gene (calculated as $1000*\Delta CT^2$).

Precision cut lung slicing.

Control and neutrophil depleted mice were administered HDM i.n. for 1 week. 24 hours post the final HDM dose, anti-mouse CD31-Alexa Fluor 647 (ThermoFisher Scientific), anti-mouse CD115-PE (Biolegend) and anti-mouse Ly6G-Alexa Fluor-488 (Biolegend) antibodies (at a concentration of 50 µg/ml) were injected i.v. to stain blood cells approximately 5 minutes before harvesting. Anti-mouse CD115-PE (Biolegend), anti-mouse Ly6G- Alexa Fluor 488 (Biolegend) and anti-mouse CD11c-BV421 (Biolegend) antibodies (at a concentration of 50 µg/ml) was also administered i.n. to stain cells within the airways. Mice were harvested and the tracheas were exposed, and the lungs were inflated with 1 ml of 2 % low melting point agarose (ThermoFisher Scientific). Once the agarose was solidified, the right lung lobe was isolated and sliced to 300 µl thickness using a BIO-RAD H1200 vibratome (BIO-RAD, France). The lung slices were immediately washed twice in R10F. To ensure staining of tissue resident cells, the lung slices were incubated with anti-mouse CD115-PE (Biolegend), anti-mouse Ly6G-Alexa Fluor-488 (Biolegend), anti-mouse CD115-PE (Biolegend), anti-mouse

Ly6G- Alexa Fluor 488 (Biolegend) and anti-mouse CD11c-BV421 (Biolegend) antibodies (at a concentration of 50 µg/ml) for 30 minutes at room temperature. The fully stained lung slices were washed three times with R10F before being mounted onto an imaging µ-plate (IBIDI). Images were obtained with an inverted SP5 confocal microscope using a 20x objective (Leica, UK). The images were subsequently analysed and prepared using Imaris software version 8.1 (Bitplane, Oxford Instruments, UK).

Lung sectioning for H&E staining.

Following 3 weeks of HDM / PBS exposure, histology assessment was performed as previously described *(63)*. In brief, the inferior lobe of the right lung was fixed with 10% neutral buffered formalin for 24 hours. The lungs were then paraffin wax embedded and cut to 4 µm thickness. The sections were subsequently stained with H&E to assess general inflammation and airway morphology.

Statistical Analysis.

Statistical significance was calculated with a nonparametric Mann-Whitney test (two-sided) and Prism software (GraphPad Software, Inc.). Statistical significance for Human ILC2 experiments was calculated using a paired t-test. Statistical significance for Mouse ILC2 experiments was calculated using an ANOVA test with Bonferroni correction. Results are depicted as mean ± SEM unless stated otherwise. Statistical significance for correlations was calculated using a Spearman Rank test with p-values and r-values noted on the respective graphs. All P values of <0.05 (*), <0.01 (**), <0.001 (***) and <0.0001 (****) were considered significant and are referred to as such in the text.

Supplementary Materials:

Supplementary Fig. 1: Intranasal administration of HDM induces neutrophilic inflammation in the lungs and airways of mice.

Supplementary Fig. 2: Intranasal administration of HDM induces an increase in neutrophil proteases in the lungs and airways of mice.

Supplementary Fig. 3: Intraperitoneal administration of anti-Ly6G antibody, 1A8, systemically depletes neutrophils in HDM treated mice.

Supplementary Fig. 4: Intraperitoneal administration of anti-Ly6G antibody, 1A8, specifically depletes neutrophils.

Supplementary Fig. 5: Neutrophil depleted mice display augmented type 2 inflammation, epithelial remodelling and airway resistance after 3 weeks of HDM exposure.

Supplementary Fig. 6: Neutrophil depleted mice display comparable airway hyperresponsiveness after 3 weeks of HDM exposure.

Supplementary Fig. 7: Augmented T_H2 cytokine levels in neutrophil depleted mice administered HDM for 1 week.

Supplementary Fig. 8: ILC2s are the predominant source of IL-13 after 1 week of HDM administration.

Supplementary Fig. 9: Gating strategy for isolation of ILC2s and $CD4^+$ T cells by fluorescence activated cell sorting.

Supplementary Fig. 10: Augmented IL-5 and IL-13 levels in lungs of neutrophil depleted mice administered HDM for 1 week are primarily derived from ILC2s.

Supplementary Fig. 11: ILC2s from neutrophil depleted mice administered HDM for 1 week produce more IL-5 and IL-13 on a per cell basis.

Supplementary Fig. 12: HDM exposed, neutrophil depleted mice exhibit augmented dendritic cell numbers and antigen presentation.

Supplementary Fig. 13: Lung concentrations of classical monocyte chemokines and flow cytometry gating strategy to identify monocyte dendritic cell progenitors (MDPs) and common dendritic cell progenitors (CDPs).

Supplementary Fig. 14: G-CSF is elevated in the serum of neutrophil depleted mice administered HDM.

Supplementary Fig. 15: Neutrophil depleted mice administered HDM produce elevated levels of IL-17 and IL-23.

Supplementary Fig. 16: Neutralization of IL-17 reverts the effects of neutrophil depletion in HDM administered mice.

Supplementary Fig. 17: G-CSF directly augments T_H2 cytokine production from mouse ILC2s.

Supplementary Fig. 18: Neutrophil depletion alters the IL-23 – IL-17 – G-CSF regulatory feedback pathway to exacerbate T_H2 cytokine production and allergen sensitisation.

Supplementary Table 1: Raw data file.

Supplementary Table 2: List of antibodies utilised for flow cytometry staining.

References:

1. M. K. Richards, F. Liu, H. Iwasaki, K. Akashi, D. C. Link, Pivotal role of granulocyte colony-stimulating factor in the development of progenitors in the common myeloid pathway., *Blood* **102**, 3562–8 (2003).

2. B. I. Lord, M. H. Bronchud, S. Owens, J. Chang, A. Howell, L. Souza, T. M. Dexter, The kinetics of human granulopoiesis following treatment with granulocyte colony-stimulating factor in vivo., *Proc. Natl. Acad. Sci. U. S. A.* **86**, 9499–503 (1989).

3. G. J. Lieschke, D. Grail, G. Hodgson, D. Metcalf, E. Stanley, C. Cheers, K. J. Fowler, S. Basu, Y. F. Zhan, A. R. Dunn, Mice lacking granulocyte colony-stimulating factor have chronic neutropenia, granulocyte and macrophage progenitor cell deficiency, and impaired neutrophil mobilization., *Blood* **84**, 1737–46 (1994).

4. F. Liu, H. Y. Wu, R. Wesselschmidt, T. Kornaga, D. C. Link, Impaired production and increased apoptosis of neutrophils in granulocyte colony-stimulating factor receptor-deficient mice., *Immunity* **5**, 491–501 (1996).

5. C. Summers, S. M. Rankin, A. M. Condliffe, N. Singh, A. M. Peters, E. R. Chilvers, Neutrophil kinetics in health and disease., *Trends Immunol.* **31**, 318–24 (2010).

6. A. M. Wengner, S. C. Pitchford, R. C. Furze, S. M. Rankin, The coordinated action of G-CSF and ELR + CXC chemokines in neutrophil mobilization during acute inflammation., *Blood* **111**, 42–9 (2008).

7. A. Mantovani, M. a Cassatella, C. Costantini, S. Jaillon, Neutrophils in the activation and regulation of innate and adaptive immunity., *Nat. Rev. Immunol.* **11**, 519–31 (2011).

8. R. J. Snelgrove, D. F. Patel, T. Patel, C. M. Lloyd, The enigmatic role of the neutrophil in

asthma: Friend, foe or indifferent?, *Clin. Exp. Allergy* **48**, 1275–1285 (2018).

9. J. V Fahy, K. W. Kim, J. Liu, H. A. Boushey, Prominent neutrophilic inflammation in sputum from subjects with asthma exacerbation, *J Allergy Clin Immunol* **95**, 843–852 (1995).

10. M. Gauthier, A. Ray, S. E. Wenzel, Evolving concepts of asthma, *Am. J. Respir. Crit. Care Med.* **192**, 660–668 (2015).

11. R. Louis, L. C. Lau, A. O. Bron, A. C. Roldaan, M. Radermecker, R. Djukanović, The relationship between airways inflammation and asthma severity., *Am. J. Respir. Crit. Care Med.* **161**, 9–16 (2000).

12. W. C. Moore, A. T. Hastie, X. Li, H. Li, W. W. Busse, N. N. Jarjour, S. E. Wenzel, S. P. Peters, D. A. Meyers, E. R. Bleecker, and B. I. S. A. R. P. National Heart, Lung, Sputum neutrophil counts are associated with more severe asthma phenotypes using cluster analysis., *J. Allergy Clin. Immunol.* **133**, 1557–63.e5 (2014).

13. S. E. Wenzel, S. J. Szefler, D. Y. Leung, S. I. Sloan, M. D. Rex, R. J. Martin, Bronchoscopic evaluation of severe asthma. Persistent inflammation associated with high dose glucocorticoids, *Am J Respir Crit Care Med* **156**, 737–743 (1997).

14. S. E. Wenzel, Asthma phenotypes: the evolution from clinical to molecular approaches, *Nat Med* **18**, 716–725 (2012).

15. P. Nair, M. Gaga, E. Zervas, K. Alagha, F. E. Hargreave, P. M. O'Byrne, P. Stryszak, L. Gann, J. Sadeh, P. Chanez, Study Investigators, Safety and efficacy of a CXCR2 antagonist in patients with severe asthma and sputum neutrophils: a randomized, placebo-controlled clinical trial., *Clin. Exp. Allergy* **42**, 1097–103 (2012).

16. P. M. O'Byrne, H. Metev, M. Puu, K. Richter, C. Keen, M. Uddin, B. Larsson, M. Cullberg,

P. Nair, Efficacy and safety of a CXCR2 antagonist, AZD5069, in patients with uncontrolled persistent asthma: a randomised, double-blind, placebo-controlled trial., *Lancet. Respir. Med.* **4**, 797–806 (2016).

17. D. J. Evans, P. J. Barnes, S. M. Spaethe, E. L. van Alstyne, M. I. Mitchell, B. J. O'Connor, Effect of a leukotriene B4 receptor antagonist, LY293111, on allergen induced responses in asthma., *Thorax* **51**, 1178–84 (1996).

18. Y. S. Wasfi, C. Villarán, C. L. B. de Tilleghem, S. S. Smugar, W. D. Hanley, T. F. Reiss, B. A. Knorr, The efficacy and tolerability of MK-0633, a 5-lipoxygenase inhibitor, in chronic asthma., *Respir. Med.* **106**, 34–46 (2012).

19. R. Chaudhuri, V. Norris, K. Kelly, C.-Q. Zhu, C. Ambery, J. Lafferty, E. Cameron, N. C. Thomson, Effects of a FLAP inhibitor, GSK2190915, in asthmatics with high sputum neutrophils., *Pulm. Pharmacol. Ther.* **27**, 62–9 (2014).

20. W. Barchuk, J. Lambert, R. Fuhr, J. Z. Jiang, K. Bertelsen, A. Fourie, X. Liu, P. E. Silkoff, E. S. Barnathan, R. Thurmond, Effects of JNJ-40929837, a leukotriene A4 hydrolase inhibitor, in a bronchial allergen challenge model of asthma., *Pulm. Pharmacol. Ther.* **29**, 15–23 (2014).

21. W. W. Busse, S. Holgate, E. Kerwin, Y. Chon, J. Feng, J. Lin, S.-L. Lin, Randomized, double-blind, placebo-controlled study of brodalumab, a human anti-IL-17 receptor monoclonal antibody, in moderate to severe asthma., *Am. J. Respir. Crit. Care Med.* **188**, 1294–302 (2013).

22. L. G. Gregory, B. Causton, J. R. Murdoch, S. A. Mathie, V. O'Donnell, C. P. Thomas, F. M. Priest, D. J. Quint, C. M. Lloyd, Inhaled house dust mite induces pulmonary T helper 2 cytokine production, *Clin Exp Allergy* **39**, 1597–1610 (2009).

23. J. M. Daley, A. a Thomay, M. D. Connolly, J. S. Reichner, J. E. Albina, Use of Ly6G-specific monoclonal antibody to deplete neutrophils in mice., *J. Leukoc. Biol.* **83**, 64–70 (2008).

24. I. R. Dunay, A. Fuchs, L. D. Sibley, Inflammatory monocytes but not neutrophils are necessary to control infection with Toxoplasma gondii in mice., *Infect. Immun.* **78**, 1564–70 (2010).

25. J.-X. Wang, A. M. Bair, S. L. King, R. Shnayder, Y.-F. Huang, C.-C. Shieh, R. J. Soberman, R. C. Fuhlbrigge, P. A. Nigrovic, Ly6G ligation blocks recruitment of neutrophils via a β2-integrin-dependent mechanism., *Blood* **120**, 1489–98 (2012).

26. B. Becher, A. Schlitzer, J. Chen, F. Mair, H. R. Sumatoh, K. W. W. Teng, D. Low, C. Ruedl, P. Riccardi-Castagnoli, M. Poidinger, M. Greter, F. Ginhoux, E. W. Newell, High-dimensional analysis of the murine myeloid cell system., *Nat. Immunol.* **15**, 1181–9 (2014).

27. A. Hasenberg, M. Hasenberg, L. Männ, F. Neumann, L. Borkenstein, M. Stecher, A. Kraus, D. R. Engel, A. Klingberg, P. Seddigh, Z. Abdullah, S. Klebow, S. Engelmann, A. Reinhold, S. Brandau, M. Seeling, A. Waisman, B. Schraven, J. R. Göthert, F. Nimmerjahn, M. Gunzer, Catchup: a mouse model for imaging-based tracking and modulation of neutrophil granulocytes., *Nat. Methods* **12**, 445–52 (2015).

28. B. N. Lambrecht, H. Hammad, The immunology of asthma., *Nat. Immunol.* **16**, 45–56 (2015).

29. D. R. Neill, S. H. Wong, A. Bellosi, R. J. Flynn, M. Daly, T. K. A. Langford, C. Bucks, C. M. Kane, P. G. Fallon, R. Pannell, H. E. Jolin, A. N. J. McKenzie, Nuocytes represent a new innate effector leukocyte that mediates type-2 immunity, *Nature* **464**, 1367–1370 (2010).

30. M. Plantinga, M. Guilliams, M. Vanheerswynghels, K. Deswarte, F. Branco-Madeira, W.

Toussaint, L. Vanhoutte, K. Neyt, N. Killeen, B. Malissen, H. Hammad, B. N. Lambrecht, Conventional and Monocyte-Derived CD11b+ Dendritic Cells Initiate and Maintain T Helper 2 Cell-Mediated Immunity to House Dust Mite Allergen, *Immunity* **38**, 322–335 (2013).

31. D. K. Fogg, C. Sibon, C. Miled, S. Jung, P. Aucouturier, D. R. Littman, A. Cumano, F. Geissmann, A Clonogenic Bone Marrow Progenitor Specific for Macrophages and Dendritic Cells, *Science (80-.).* **311**, 83–87 (2006).

32. A. Schlitzer, V. Sivakamasundari, J. Chen, H. R. Bin Sumatoh, J. Schreuder, J. Lum, B. Malleret, S. Zhang, A. Larbi, F. Zolezzi, L. Renia, M. Poidinger, S. Naik, E. W. Newell, P. Robson, F. Ginhoux, Identification of cDC1- and cDC2-committed DC progenitors reveals early lineage priming at the common DC progenitor stage in the bone marrow, *Nat. Immunol.* **16**, 718–728 (2015).

33. M. A. Meyer, J. M. Baer, B. L. Knolhoff, T. M. Nywening, R. Z. Panni, X. Su, K. N. Weilbaecher, W. G. Hawkins, C. Ma, R. C. Fields, D. C. Linehan, G. A. Challen, R. Faccio, R. L. Aft, D. G. DeNardo, Breast and pancreatic cancer interrupt IRF8-dependent dendritic cell development to overcome immune surveillance., *Nat. Commun.* **9**, 1250 (2018).

34. S. Sivakumaran, S. Henderson, S. Ward, P. S. E. Sousa, T. Manzo, L. Zhang, T. Conlan, T. K. Means, M. D'Aveni, O. Hermine, M.-T. Rubio, R. Chakraverty, C. L. Bennett, Depletion of $CD11c^+$ cells in the CD11c.DTR model drives expansion of unique $CD64^+$ $Ly6C^+$ monocytes that are poised to release TNF-α., *Eur. J. Immunol.* **46**, 192–203 (2016).

35. E. Smith, M. A. Stark, A. Zarbock, T. L. Burcin, A. C. Bruce, D. Vaswani, P. Foley, K. Ley, IL-17A inhibits the expansion of IL-17A-producing T cells in mice through "short-loop" inhibition via IL-17 receptor., *J. Immunol.* **181**, 1357–64 (2008).

36. C. E. Jones, K. Chan, Interleukin-17 stimulates the expression of interleukin-8, growth-

related oncogene-alpha, and granulocyte-colony-stimulating factor by human airway epithelial cells., *Am. J. Respir. Cell Mol. Biol.* **26**, 748–53 (2002).

37. P. Schwarzenberger, W. Huang, P. Ye, P. Oliver, M. Manuel, Z. Zhang, G. Bagby, S. Nelson, J. K. Kolls, Requirement of endogenous stem cell factor and granulocyte-colony-stimulating factor for IL-17-mediated granulopoiesis., *J. Immunol.* **164**, 4783–9 (2000).

38. J. Mei, Y. Liu, N. Dai, C. Hoffmann, K. M. Hudock, P. Zhang, S. H. Guttentag, J. K. Kolls, P. M. Oliver, F. D. Bushman, G. S. Worthen, Cxcr2 and Cxcl5 regulate the IL-17/G-CSF axis and neutrophil homeostasis in mice., *J. Clin. Invest.* **122**, 974–86 (2012).

39. M. A. Stark, Y. Huo, T. L. Burcin, M. A. Morris, T. S. Olson, K. Ley, Phagocytosis of Apoptotic Neutrophils Regulates Granulopoiesis via IL-23 and IL-17, *Immunity* **22**, 285–294 (2005).

40. M. L. Robinette, A. Fuchs, V. S. Cortez, J. S. Lee, Y. Wang, S. K. Durum, S. Gilfillan, M. Colonna, Immunological Genome Consortium, Transcriptional programs define molecular characteristics of innate lymphoid cell classes and subsets., *Nat. Immunol.* **16**, 306–17 (2015).

41. A. Wallrapp, S. J. Riesenfeld, P. R. Burkett, R.-E. E. Abdulnour, J. Nyman, D. Dionne, M. Hofree, M. S. Cuoco, C. Rodman, D. Farouq, B. J. Haas, T. L. Tickle, J. J. Trombetta, P. Baral, C. S. N. Klose, T. Mahlakõiv, D. Artis, O. Rozenblatt-Rosen, I. M. Chiu, B. D. Levy, M. S. Kowalczyk, A. Regev, V. K. Kuchroo, The neuropeptide NMU amplifies ILC2-driven allergic lung inflammation., *Nature* **549**, 351–356 (2017).

42. T. Y. F. Halim, Y. Y. Hwang, S. T. Scanlon, H. Zaghouani, N. Garbi, P. G. Fallon, A. N. J. McKenzie, Group 2 innate lymphoid cells license dendritic cells to potentiate memory TH2 cell responses., *Nat. Immunol.* **17**, 57–64 (2016).

43. C. J. Oliphant, Y. Y. Hwang, J. A. Walker, M. Salimi, S. H. Wong, J. M. Brewer, A. Englezakis, J. L. Barlow, E. Hams, S. T. Scanlon, G. S. Ogg, P. G. Fallon, A. N. J. McKenzie, MHCII-Mediated Dialog between Group 2 Innate Lymphoid Cells and CD4+ T Cells Potentiates Type 2 Immunity and Promotes Parasitic Helminth Expulsion, *Immunity* **41**, 283–295 (2014).

44. L. Y. Drake, H. Kita, Group 2 innate lymphoid cells in the lung., *Adv. Immunol.* **124**, 1–16 (2014).

45. C. M. Lloyd, R. J. Snelgrove, Type 2 immunity: Expanding our view., *Sci. Immunol.* **3**, eaat1604 (2018).

46. S. Bugl, S. Wirths, M. P. Radsak, H. Schild, P. Stein, M. C. André, M. R. Müller, E. Malenke, T. Wiesner, M. Märklin, J.-S. Frick, R. Handgretinger, H.-G. Rammensee, L. Kanz, H.-G. Kopp, Steady-state neutrophil homeostasis is dependent on TLR4/TRIF signaling., *Blood* **121**, 723–33 (2013).

47. A. Yáñez, S. G. Coetzee, A. Olsson, D. E. Muench, B. P. Berman, D. J. Hazelett, N. Salomonis, H. L. Grimes, H. S. Goodridge, Granulocyte-Monocyte Progenitors and Monocyte-Dendritic Cell Progenitors Independently Produce Functionally Distinct Monocytes, *Immunity* **47**, 890-902.e4 (2017).

48. H. M. Mehta, M. Malandra, S. J. Corey, G-CSF and GM-CSF in Neutropenia., *J. Immunol.* **195**, 1341–9 (2015).

49. K. E. Lawlor, I. K. Campbell, D. Metcalf, K. O'Donnell, A. van Nieuwenhuijze, A. W. Roberts, I. P. Wicks, Critical role for granulocyte colony-stimulating factor in inflammatory arthritis, *Proc. Natl. Acad. Sci.* **101**, 11398–11403 (2004).

50. A. Fattorossi, A. Battaglia, L. Pierelli, P. Malinconico, L. Andreocci, A. Perillo, G. Ferrandina, O. Martelli, A. Rughetti, M. Nuti, E. Cortesi, G. Scambia, Effects of granulocyte-colony-stimulating factor and granulocyte/macrophage-colony-stimulating factor administration on T cell proliferation and phagocyte cell-surface molecules during hematopoietic reconstitution after autologous peripheral blood progenitor cell transplantation., *Cancer Immunol. Immunother.* **49**, 641–8 (2001).

51. K. Hosoki, S. Ying, C. Corrigan, H. Qi, A. Kurosky, K. Jennings, Q. Sun, I. Boldogh, S. Sur, Analysis of a Panel of 48 Cytokines in BAL Fluids Specifically Identifies IL-8 Levels as the Only Cytokine that Distinguishes Controlled Asthma from Uncontrolled Asthma, and Correlates Inversely with FEV1., *PLoS One* **10**, e0126035 (2015).

52. M. Kato, Y. Yamada, K. Maruyama, Y. Hayashi, Serum eosinophil cationic protein and 27 cytokines/chemokines in acute exacerbation of childhood asthma., *Int. Arch. Allergy Immunol.* **152 Suppl**, 62–6 (2010).

53. M. Arpinati, C. L. Green, S. Heimfeld, J. E. Heuser, C. Anasetti, Granulocyte-colony stimulating factor mobilizes T helper 2-inducing dendritic cells., *Blood* **95**, 2484–90 (2000).

54. N. Nowroozilarki, H. H. Öz, C. Schroth, A. Hector, B. Nürnberg, D. Hartl, S. Kolahian, Anti-inflammatory role of CD11b+Ly6G+ neutrophilic cells in allergic airway inflammation in mice., *Immunol. Lett.* **204**, 67–74 (2018).

55. A. N. Salazar Cabrera, R. Berrón Pérez, J. A. Ortega Martell, E. Onuma Takane, Asthma and cyclic neutropenia., *Allergol. Immunopathol. (Madr).* **24**, 25–8 (1996).

56. B. Navabi, J. E. M. Upton, Primary immunodeficiencies associated with eosinophilia., *Allergy Asthma. Clin. Immunol.* **12**, 27 (2016).

57. S. Jurcevic, C. Humfrey, M. Uddin, S. Warrington, B. Larsson, C. Keen, The effect of a selective CXCR2 antagonist (AZD5069) on human blood neutrophil count and innate immune functions., *Br. J. Clin. Pharmacol.* **80**, 1324–36 (2015).

58. H. Watz, M. Uddin, F. Pedersen, A. Kirsten, T. Goldmann, F. Stellmacher, E. Groth, B. Larsson, G. Böttcher, A. Malmgren, M. Kraan, K. F. Rabe, Effects of the CXCR2 antagonist AZD5069 on lung neutrophil recruitment in asthma., *Pulm. Pharmacol. Ther.* **45**, 121–123 (2017).

59. S. Fox, A. E. Leitch, R. Duffin, C. Haslett, A. G. Rossi, Neutrophil apoptosis: relevance to the innate immune response and inflammatory disease., *J. Innate Immun.* **2**, 216–27 (2010).

60. L. J. Hoodless, C. D. Lucas, R. Duffin, M. A. Denvir, C. Haslett, C. S. Tucker, A. G. Rossi, Genetic and pharmacological inhibition of CDK9 drives neutrophil apoptosis to resolve inflammation in zebrafish in vivo., *Sci. Rep.* **5**, 36980 (2016).

61. C. D. Lucas, K. C. Allen, D. A. Dorward, L. J. Hoodless, L. A. Melrose, J. A. Marwick, C. S. Tucker, C. Haslett, R. Duffin, A. G. Rossi, Flavones induce neutrophil apoptosis by down-regulation of Mcl-1 via a proteasomal-dependent pathway., *FASEB J.* **27**, 1084–94 (2013).

62. L. J. Hoodless, C. D. Lucas, R. Duffin, M. A. Denvir, C. Haslett, C. S. Tucker, A. G. Rossi, Genetic and pharmacological inhibition of CDK9 drives neutrophil apoptosis to resolve inflammation in zebrafish in vivo, *Sci. Rep.* **6**, 36980 (2016).

63. D. F. Patel, T. Peiró, A. Shoemark, S. Akthar, S. A. Walker, A. M. Grabiec, P. L. Jackson, T. Hussell, A. Gaggar, X. Xu, J. L. Trevor, J. Li, C. Steele, G. Tavernier, J. E. Blalock, R. M. Niven, L. G. Gregory, A. Simpson, C. M. Lloyd, R. J. Snelgrove, An extracellular matrix fragment drives epithelial remodeling and airway hyperresponsiveness., *Sci. Transl. Med.* **10** (2018), doi:10.1126/scitranslmed.aaq0693.

64. S. Löser, L. G. Gregory, Y. Zhang, K. Schaefer, S. A. Walker, J. Buckley, L. Denney, C. H. Dean, W. O. C. Cookson, M. F. Moffatt, C. M. Lloyd, Pulmonary ORMDL3 is critical for induction of Alternaria-induced allergic airways disease., *J. Allergy Clin. Immunol.* **139**, 1496-1507.e3 (2017).

65. A. Singanayagam, N. Glanville, J. L. Girkin, Y. M. Ching, A. Marcellini, J. D. Porter, M. Toussaint, R. P. Walton, L. J. Finney, J. Aniscenko, J. Zhu, M.-B. Trujillo-Torralbo, M. A. Calderazzo, C. Grainge, S.-L. Loo, P. C. Veerati, P. S. Pathinayake, K. S. Nichol, A. T. Reid, P. L. James, R. Solari, P. A. B. Wark, D. A. Knight, M. F. Moffatt, W. O. Cookson, M. R. Edwards, P. Mallia, N. W. Bartlett, S. L. Johnston, Corticosteroid suppression of antiviral immunity increases bacterial loads and mucus production in COPD exacerbations., *Nat. Commun.* **9**, 2229 (2018).

Acknowledgements: We thank Lorraine Lawrence for histological sectioning and staining.

Funding: RJS is a Wellcome Trust Senior Research Fellow in Basic Biomedical Sciences (209458/Z/17/Z). CML is a Wellcome Trust Senior Fellow in Basic Biomedical Sciences (107059/Z/15/Z). TP is supported by a Marie Curie Intra European Fellowship within the 7th European Community Framework Programme (FP7-PEOPLE-2013-IEF Nº627374). AS is supported by a pump priming grant from the British Lung Foundation (PPRG15-9) and a research grant from the British Medical Association (HC Roscoe 2015 grant). Aspects of the work were funded by an award from the Rosetrees Trust (M612) to RJS, LG and CML. LMC. is funded by core support from Cancer Research UK (A23983 and A17196), the MRC (MR/M01245X/1), and the National Heart & Lung Institute Foundation.

Author Contributions: DFP and RJS designed and interpreted the experiments, performed statistical analysis and prepared the manuscript. DFP, with the assistance of TP, NB, JV, SA, FP, CJP, KS, AS, SAW, LGG and RJS performed the majority of the experiments. LMC and CML provided key reagents and contributed discussions throughout the work.

Declaration of interests: The authors declare that they have no competing interests.

Figure Legends:

Figure 1: Neutrophil depleted mice display augmented type 2 inflammation after 3 weeks of HDM exposure.

(**A**) Balb/c mice were administered HDM or PBS intranasally (i.n.) 3 times per week for up to 3 weeks, and at 24 hours prior to each HDM/PBS administration mice were dosed with either 100 μg of neutrophil depleting antibody, 1A8, or isotype control antibody, 2A3 intraperitoneally (i.p.). At 24 hours, 1 week and 3 week time points (in each instance 24 hours post final HDM/PBS exposure), lung tissue and BALF was collected (Ŧ). Total numbers of neutrophils in the lungs (**B**) and airways (**C**) were determined by flow cytometry. (**D**) Total cell numbers in the lung were assessed after 3 weeks of HDM exposure by trypan blue exclusion. (**E**) Representative H&E stained lung sections from mice exposed to PBS or HDM for 3 weeks and treated with 2A3 or 1A8. (**F**) The number of eosinophils in the lung were quantified by flow cytometry at 3 weeks. The number of $CD4^+$ T cells expressing T1ST2 (**G**) or IL-13 (**H**) in the lung were assessed by flow cytometry after 3 weeks of PBS/HDM exposure. (**I**) After 3 weeks of HDM/PBS exposure, concentrations of HDM-specific IgE and IgG1 in the serum were determined by ELISA. Figures present combined data from 2 independent experiments with 4-6 mice per group in each experiment. Results depicted as mean ± SEM. **P*<0.05, ***P*<0.01, ****P*<0.001, *****P*<0.0001 using Mann–Whitney statistical test.

Figure 2: Augmented T_H2 cytokine production by ILC2s in neutrophil depleted mice administered HDM for 1 week.

(**A**) Balb/c mice were administered HDM or PBS intranasally (i.n.) 3 times per week for 1 week and at 24 hours prior to each HDM treatment, mice were dosed with either 100 μg of neutrophil depleting antibody, 1A8, or isotype control antibody, 2A3 intraperitoneally (i.p.). At 24 hours post the final HDM administration BALF was collected (Ŧ). (**B**) Concentrations

of IL-4, IL-5 and IL-13 protein were assessed in and BALF by ELISA. In some experiments, $CD4^+$ T cells and ILC2s (pooled from 3 mice per data point) were isolated from the airways by FACS, at 24 hours post final HDM exposure, for subsequent mRNA gene expression analysis. (**C**) Relative expression of *Il-4*, *Il-5*, *Il-13* and *Gata-3* in T cells and ILC2s derived from BAL of HDM treated mice, as determined by qPCR. At the same time point, the number of IL-13^+ ILC2s and IL-5^+ ILC2s (**D**) and geometric expression of IL-13 and IL-5 in ILC2s (**E**) in the BAL was assessed by flow cytometry. Figures present combined data from 2 independent experiments with 4-6 mice per group in each experiment (**B, D** and **E**), or from one experiment whereby each data point represents cells pooled from 3 independent mice (**C**). Results depicted as mean ± SEM. *P<0.05, **P<0.01, ***P<0.001, ****P<0.0001 using Mann–Whitney statistical test.

Figure 3: HDM exposed, neutrophil depleted mice exhibit augmented monocytosis, dendritic cell numbers and antigen presentation.

Balb/c mice were administered HDM or PBS intranasally (i.n.) 3 times per week for 1 week. At 24 hours prior to each HDM/PBS administration, mice were treated with either 100 µg of neutrophil depleting antibody, 1A8, or isotype control antibody, 2A3 intraperitoneally (i.p). At 24 hours post final HDM/PBS exposure, lung tissue was collected. (**A**) Lung monocyte subsets identified as $Ly6C^{low}$ and $Ly6C^{high}$ were enumerated by flow cytometry. (**B**) Numbers of lung monocyte-derived dendritic cells (moDCs) were also determined by flow cytometry. The number of moDCs (**C**) and $CD86^+$ moDCs (**D**) in the mediastinal lymph nodes (MLN) were enumerated by flow cytometry. In some experiments, the final dose of HDM was admixed with 100 µg Alexa Fluor 488 labelled OVA (**E**) and mediastinal lymph nodes collected (Ŧ) at 24 hrs post the final HDM/PBS exposure. (**F**) The number of OVA^+ moDCs within the mediastinal lymph nodes were enumerated by flow cytometry. Figures present data combined from 2

independent experiments with 4-6 mice per group for each experiment (**A**-**D**) or from 1 experiment with 5 mice per group (**F**). Results depicted as mean ± SEM. **P*<0.05, ***P*<0.01, ****P*<0.001, *****P*<0.0001 using Mann–Whitney statistical test.

Figure 4: Neutrophil depleted mice display increased numbers of monocyte and dendritic cell progenitors within their bone marrow owing to a dysregulated IL-23 – IL-17 – G-CSF axis.

Balb/c mice were administered HDM or PBS intranasally (i.n.) 3 times per week for 1 week. At 24 hours prior to each HDM/PBS administration, mice were treated with either 100 μg of neutrophil depleting antibody, 1A8, or isotype control antibody, 2A3 intraperitoneally (i.p). At 24 hours post final HDM/PBS exposure, BALF, lung tissue, blood and bone marrow were collected. (**A**) The number of $Ly6C^{low}$ and $Ly6C^{high}$ monocytes in the blood were quantified by flow cytometry. (**B**) The percentage of monocyte dendritic cell progenitors (MDPs) and common dendritic cell progenitors (CDPs) within the bone marrow were assessed by flow cytometry. (**C**) The concentration of G-CSF in the serum, lung homogenate and BALF was determined by ELISA. Expression of *Csf3* (G-CSF gene; **D**), *Il17* (**E**) and *Il23* (**F**) was assessed in whole lung by qPCR. (**G**) Schematic depicting the negative feedback pathway by which tissue neutrophils limit granulopoiesis by modulation of the IL-23 – IL-17 – G-CSF axis. Figures present data from 2 independent experiment with 4-6 mice per group in each experiment. Results depicted as mean ± SEM. *P<0.05, **P<0.01, ***P<0.001, *****P*<0.0001 using Mann–Whitney statistical test.

Figure 5: Neutralization of G-CSF abrogates the augmented monocytes, bone marrow progenitors and T_H2 cytokines observed in neutrophil depleted HDM exposed mice.

(**A**) Balb/c mice were administered HDM intranasally (i.n.) 3 times per week for 1 week. At 24 hours prior to each HDM administration, mice were treated with either 100 μg of neutrophil

depleting antibody, 1A8, or isotype control antibody, 2A3. To neutralize G-CSF, mice were also administered 100 μg anti-G-CSF or isotype control, 2A3, i.p. at 24 hours prior to each HDM dose. At 24 hours post final HDM administration, BAL, lung tissue and bone marrow were collected (Ŧ). The number of lung and airway neutrophils (**B**) and lung $Ly6C^{low}$ and $Ly6C^{high}$ monocytes (**C**) were determined by flow cytometry. (**D**) The percentage of MDPs and CDPs within the bone marrow were assessed by flow cytometry. (**E**) The concentrations of BALF IL-4, IL-5 and IL-13 were assessed by ELISA. (**F**) Geometric mean of IL-13 by lung ILC2s was assessed by flow cytometry. Figures present data combined from 2 independent experiments with 4-6 mice per group in each experiment. Results depicted as mean ± SEM. **P*<0.05, ***P*<0.01, ****P*<0.001 using Mann–Whitney statistical test.

Figure 6: Co-administration of recombinant G-CSF augments numbers of HDM-induced neutrophils, monocytes and bone marrow progenitors and ILC2 cytokine responses.

(**A**) Balb/c mice were administered PBS or HDM intranasally (i.n.) 3 times per week for 1 week. Mice were also administered 100 ng recombinant G-CSF i.n. (in 50 μl PBS) and 2 μg recombinant G-CSF i.p. (in 2000 μl PBS), or respective PBS controls, daily throughout the study. At 24 hours post final HDM administration, BAL, lung tissue and bone marrow were collected (Ŧ). The number of lung and airway neutrophils (**B**) and lung $Ly6C^{low}$ and $Ly6C^{high}$ monocytes (**C**) were determined by flow cytometry. (**D**) The percentage of MDPs and CDPs within the bone marrow were assessed by flow cytometry. (**E**) The concentrations of BALF IL-4, IL-5 and IL-13 were assessed by ELISA. (**F**) Geometric mean of IL-13 by BAL ILC2s was assessed by flow cytometry. Figures present data from 1 experiment with 4-6 mice per group in each experiment. Results depicted as mean ± SEM. **P*<0.05, ***P*<0.01 using Mann–Whitney statistical test.

Figure 7: G-CSF augments T_H2 cytokine production from IL-33 expanded airway Csf3r-expressing ILC2s.

Balb/c mice were administered HDM intranasally (i.n.) 3 times per week for 1 week. At 24 hours post final HDM administration, BAL was collected. (**A**) Relative expression of mRNA *Csf3r* in T cells and ILC2s isolated by FACS from the BAL of HDM exposed mice, as determined by qPCR. (**B**) Balb/c mice were administered 1 μg recombinant IL-33 i.n. 3 times per week for 1 week. At 24 hours post final IL-33 administration, BAL was collected. (**C**) Relative expression of mRNA *Csf3r* in T cells and ILC2s isolated by FACS from the BAL of IL-33 exposed mice, as determined by qPCR. In some experiments, 100 ng recombinant G-CSF was co-administered with IL-33 (**B**), and $CD4^+$ T cells and ILC2s were isolated from the airways by FACS, at 24 hours post final IL-33 administration, for subsequent mRNA gene expression analysis. (**D**) Relative expression of IL-4, and IL-13 in T cells and ILC2s derived from BAL, as determined by qPCR. (**E**) From the same experiments, BALF concentrations of IL-5 and IL-13 were determined by ELISA. Figures present data from 1 experiment with 4-6 mice per group in each experiment. Results depicted as mean ± SEM. **P*<0.05, ***P*<0.01 using Mann–Whitney statistical test.

Figure 8: G-CSF directly augments T_H2 cytokine production from human ILC2s.

(**A**) Human ILC2s were isolated from peripheral blood and expanded in bulk culture with IL-7 (5 ng/ml) and IL-33 (15 ng/ml), before the addition of media or media containing 100 ng/ml recombinant G-CSF for 72 hours. (**B**) Relative expression of *CSF3R* was assessed by qPCR after 72 hours. (**C**) The levels of IL-5 and IL-13 in the ILC2 supernatant were assessed by a multiplex cytokine assay and expressed as a donor specific fold change after G-CSF treatment. (**D**) Expression of *IL5*, *IL13*, and *GATA3* was assessed by qPCR after 72 hours, and presented

as a donor specific fold change after G-CSF treatment. Results depicted as mean ± SEM. *P<0.05, **P<0.01, ***P<0.001 using a paired t-test.

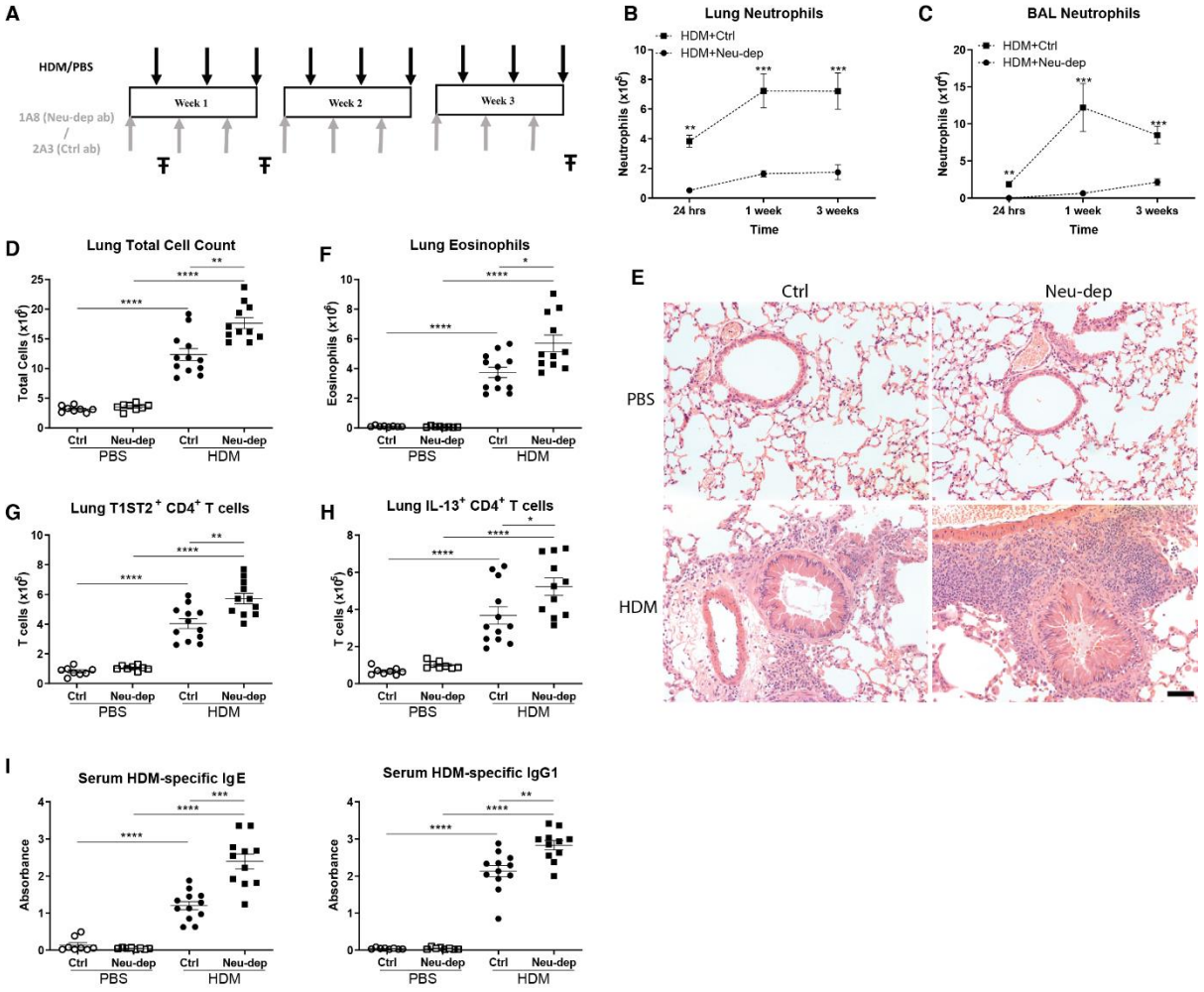
A
HDM/PBS
Week 1
Week 2
Week 3
1A8 (Neu-dep ab)
/
2A3 (Ctrl ab)
B
Lung Neutrophils
HDM+Ctrl
HDM+Neu-dep
Neutrophils (x10⁶)
24 hrs
1 week
3 weeks
Time
C
BAL Neutrophils
HDM+Ctrl
HDM+Neu-dep
Neutrophils (x10⁶)
24 hrs
1 week
3 weeks
Time
D
Lung Total Cell Count
Total Cells (x10⁶)
Ctrl
Neu-dep
Ctrl
Neu-dep
PBS
HDM
E
Ctrl
Neu-dep
PBS
HDM
F
Lung Eosinophils
Eosinophils (x10⁶)
Ctrl
Neu-dep
Ctrl
Neu-dep
PBS
HDM
G
Lung T1ST2+ CD4+ T cells
T cells (x10⁶)
Ctrl
Neu-dep
Ctrl
Neu-dep
PBS
HDM
H
Lung IL-13+ CD4+ T cells
T cells (x10⁶)
Ctrl
Neu-dep
Ctrl
Neu-dep
PBS
HDM
I
Serum HDM-specific IgE
Absorbance
Ctrl
Neu-dep
Ctrl
Neu-dep
PBS
HDM
Serum HDM-specific IgG1
Absorbance
Ctrl
Neu-dep
Ctrl
Neu-dep
PBS
HDM

Figure 1

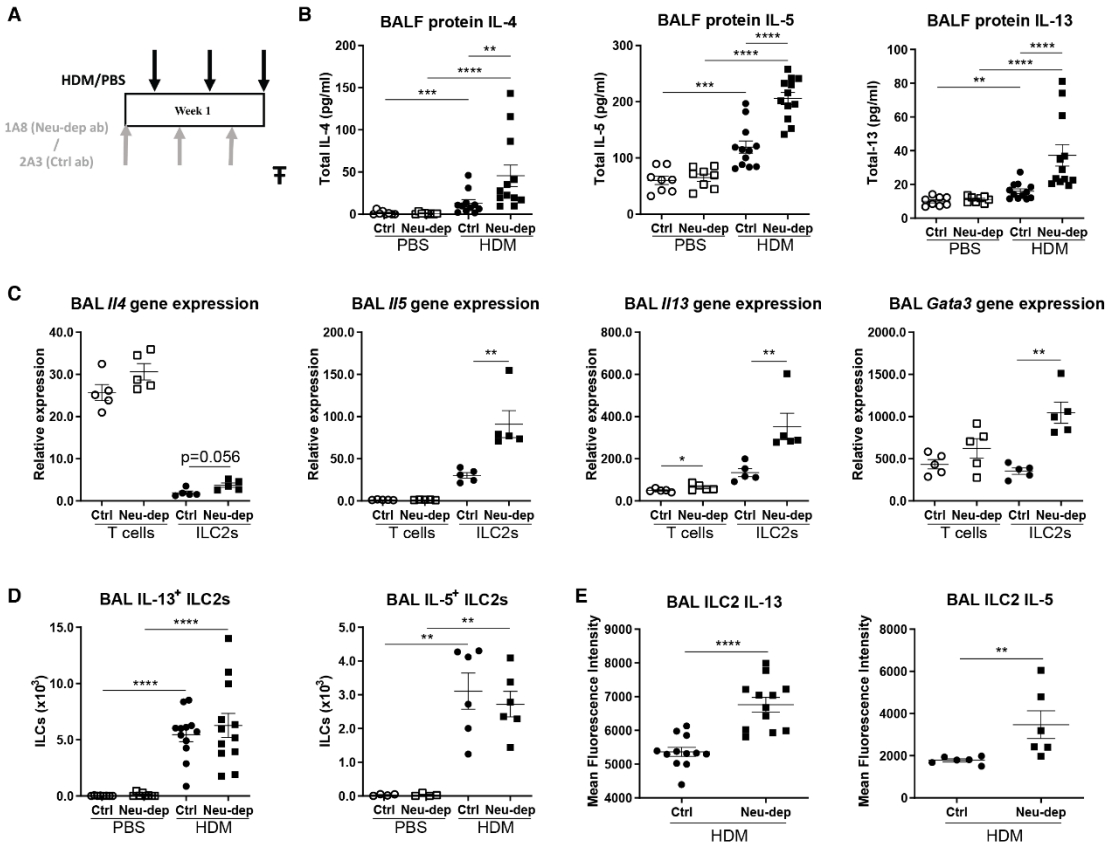
A
HDM/PBS
Week 1
1A8 (Neu-dep ab)
/
2A3 (Ctrl ab)
B
BALF protein IL-4
Total IL-4 (pg/ml)
BALF protein IL-5
Total IL-5 (pg/ml)
BALF protein IL-13
Total-13 (pg/ml)
Ctrl Neu-dep Ctrl Neu-dep
PBS HDM
C
BAL Il4 gene expression
BAL Il5 gene expression
BAL Il13 gene expression
BAL Gata3 gene expression
Relative expression
p=0.056
Ctrl Neu-dep Ctrl Neu-dep
T cells ILC2s
D
BAL IL-13+ ILC2s
BAL IL-5+ ILC2s
ILCs (x10³)
E
BAL ILC2 IL-13
BAL ILC2 IL-5
Mean Fluorescence Intensity
Ctrl Neu-dep
HDM

Figure 2

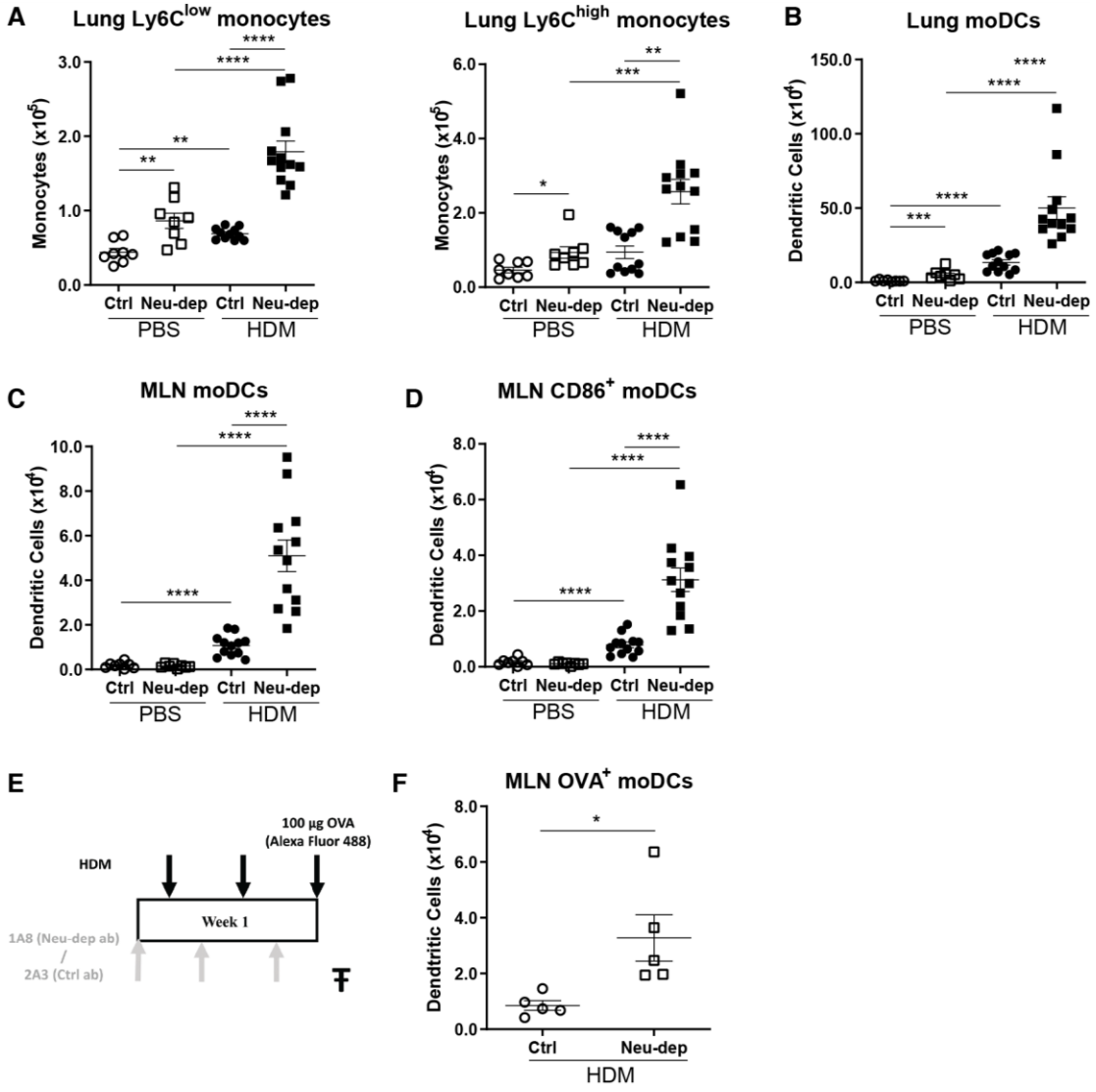
A
Lung Ly6C^low monocytes
Monocytes (x10^5)
Ctrl Neu-dep Ctrl Neu-dep
PBS HDM
Lung Ly6C^high monocytes
Monocytes (x10^5)
B
Lung moDCs
Dendritic Cells (x10^4)
C
MLN moDCs
Dendritic Cells (x10^4)
D
MLN CD86+ moDCs
Dendritic Cells (x10^4)
E
100 µg OVA
(Alexa Fluor 488)
HDM
Week 1
1A8 (Neu-dep ab)
/
2A3 (Ctrl ab)
F
MLN OVA+ moDCs
Dendtritic Cells (x10^4)
Ctrl Neu-dep
HDM

Figure 3

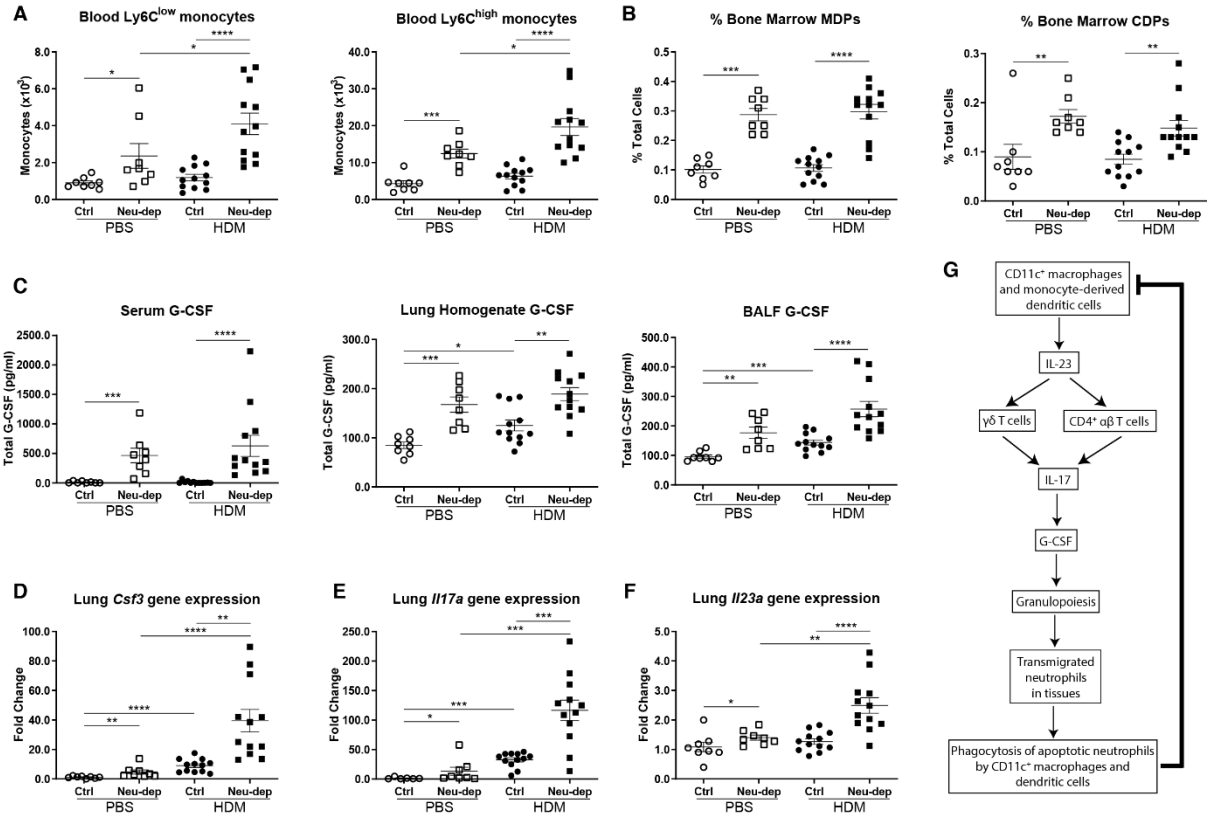
A
Blood Ly6C^low monocytes
Monocytes (x10^3)
Blood Ly6C^high monocytes
Monocytes (x10^3)
B
% Bone Marrow MDPs
% Total Cells
% Bone Marrow CDPs
% Total Cells
C
Serum G-CSF
Total G-CSF (pg/ml)
Lung Homogenate G-CSF
Total G-CSF (pg/ml)
BALF G-CSF
Total G-CSF (pg/ml)
D
Lung Csf3 gene expression
Fold Change
E
Lung Il17a gene expression
Fold Change
F
Lung Il23a gene expression
Fold Change
Ctrl
Neu-dep
PBS
HDM
G
CD11c+ macrophages and monocyte-derived dendritic cells
IL-23
γδ T cells
CD4+ αβ T cells
IL-17
G-CSF
Granulopoiesis
Transmigrated neutrophils in tissues
Phagocytosis of apoptotic neutrophils by CD11c+ macrophages and dendritic cells

Figure 4

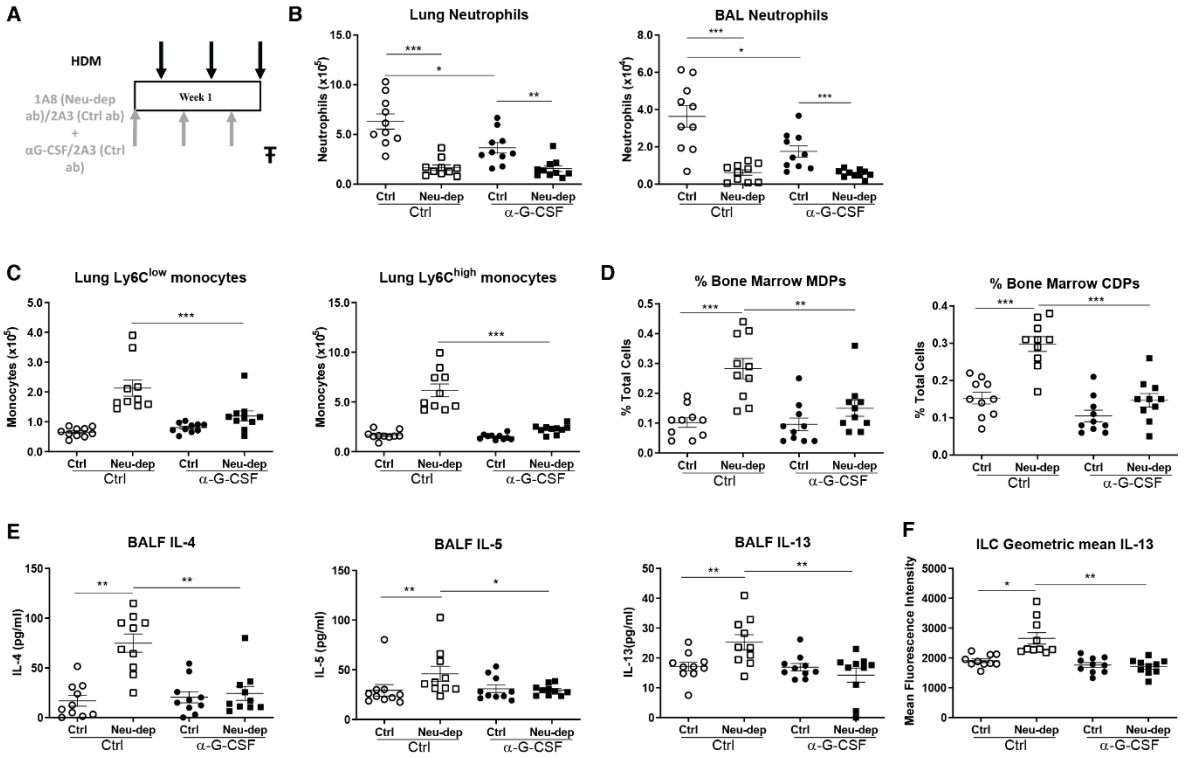
A
HDM
Week 1
1A8 (Neu-dep ab)/2A3 (Ctrl ab)
+
αG-CSF/2A3 (Ctrl ab)
B
Lung Neutrophils
Neutrophils (x10^6)
BAL Neutrophils
Neutrophils (x10^4)
Ctrl
Neu-dep
α-G-CSF
C
Lung Ly6C^low monocytes
Lung Ly6C^high monocytes
Monocytes (x10^6)
D
% Bone Marrow MDPs
% Bone Marrow CDPs
% Total Cells
E
BALF IL-4
BALF IL-5
BALF IL-13
IL-4 (pg/ml)
IL-5 (pg/ml)
IL-13(pg/ml)
F
ILC Geometric mean IL-13
Mean Fluorescence Intensity

Figure 5

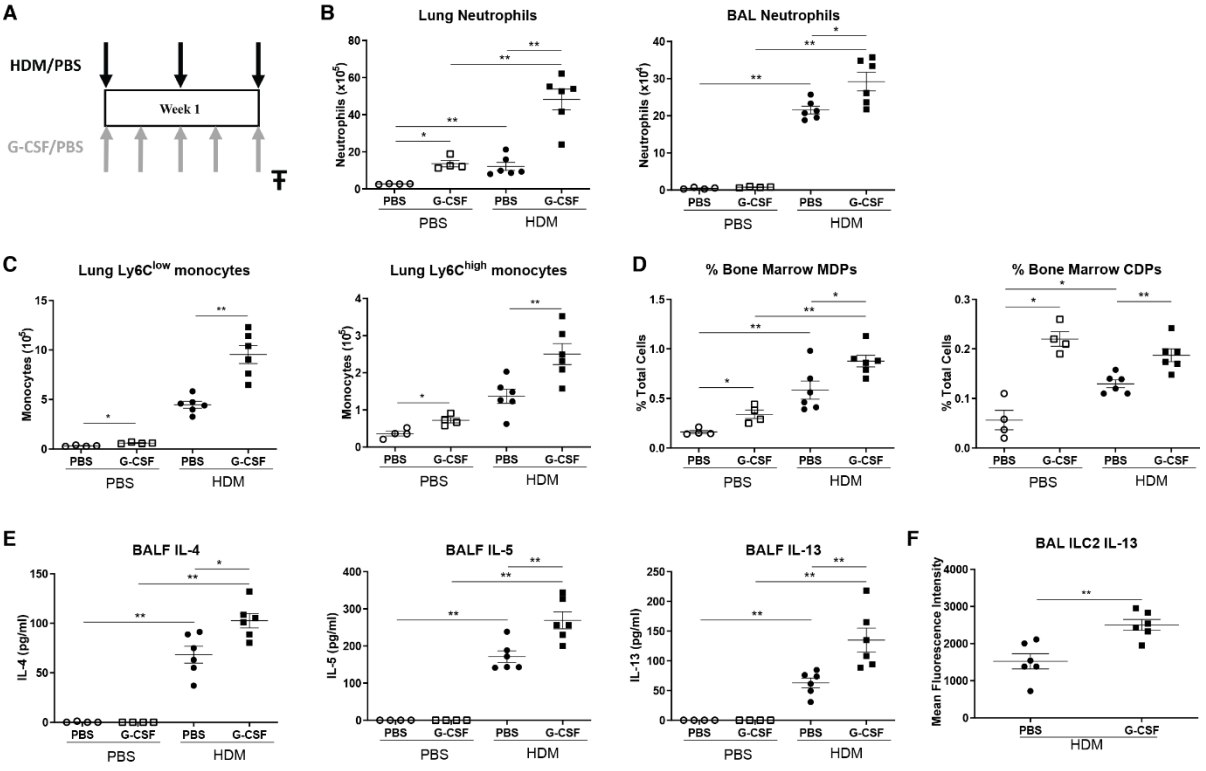
A
HDM/PBS
Week 1
G-CSF/PBS
B
Lung Neutrophils
Neutrophils (x10^6)
BAL Neutrophils
Neutrophils (x10^6)
PBS
G-CSF
HDM
C
Lung Ly6C^low monocytes
Monocytes (10^6)
Lung Ly6C^high monocytes
Monocytes (10^6)
D
% Bone Marrow MDPs
% Total Cells
% Bone Marrow CDPs
% Total Cells
E
BALF IL-4
IL-4 (pg/ml)
BALF IL-5
IL-5 (pg/ml)
BALF IL-13
IL-13 (pg/ml)
F
BAL ILC2 IL-13
Mean Fluorescence Intensity

Figure 6

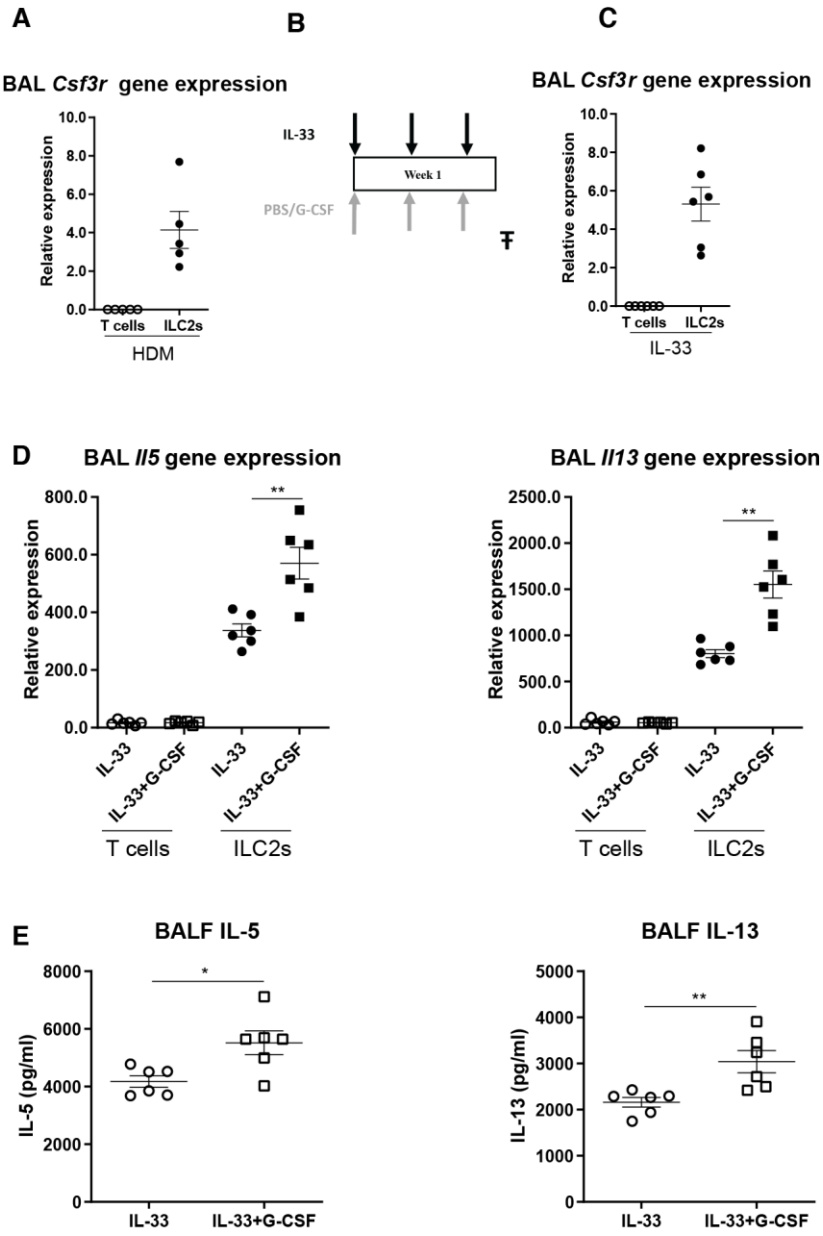
A
B
C
BAL Csf3r gene expression
Relative expression
10.0
8.0
6.0
4.0
2.0
0.0
T cells
ILC2s
HDM
IL-33
Week 1
PBS/G-CSF
BAL Csf3r gene expression
Relative expression
T cells
ILC2s
IL-33
D
BAL Il5 gene expression
Relative expression
800.0
600.0
400.0
200.0
0.0
**
IL-33
IL-33+G-CSF
IL-33
IL-33+G-CSF
T cells
ILC2s
BAL Il13 gene expression
Relative expression
2500.0
2000.0
1500.0
1000.0
500.0
0.0
**
IL-33
IL-33+G-CSF
IL-33
IL-33+G-CSF
T cells
ILC2s
E
BALF IL-5
IL-5 (pg/ml)
8000
6000
4000
2000
0
*
IL-33
IL-33+G-CSF
BALF IL-13
IL-13 (pg/ml)
5000
4000
3000
2000
1000
0
**
IL-33
IL-33+G-CSF

Figure 7

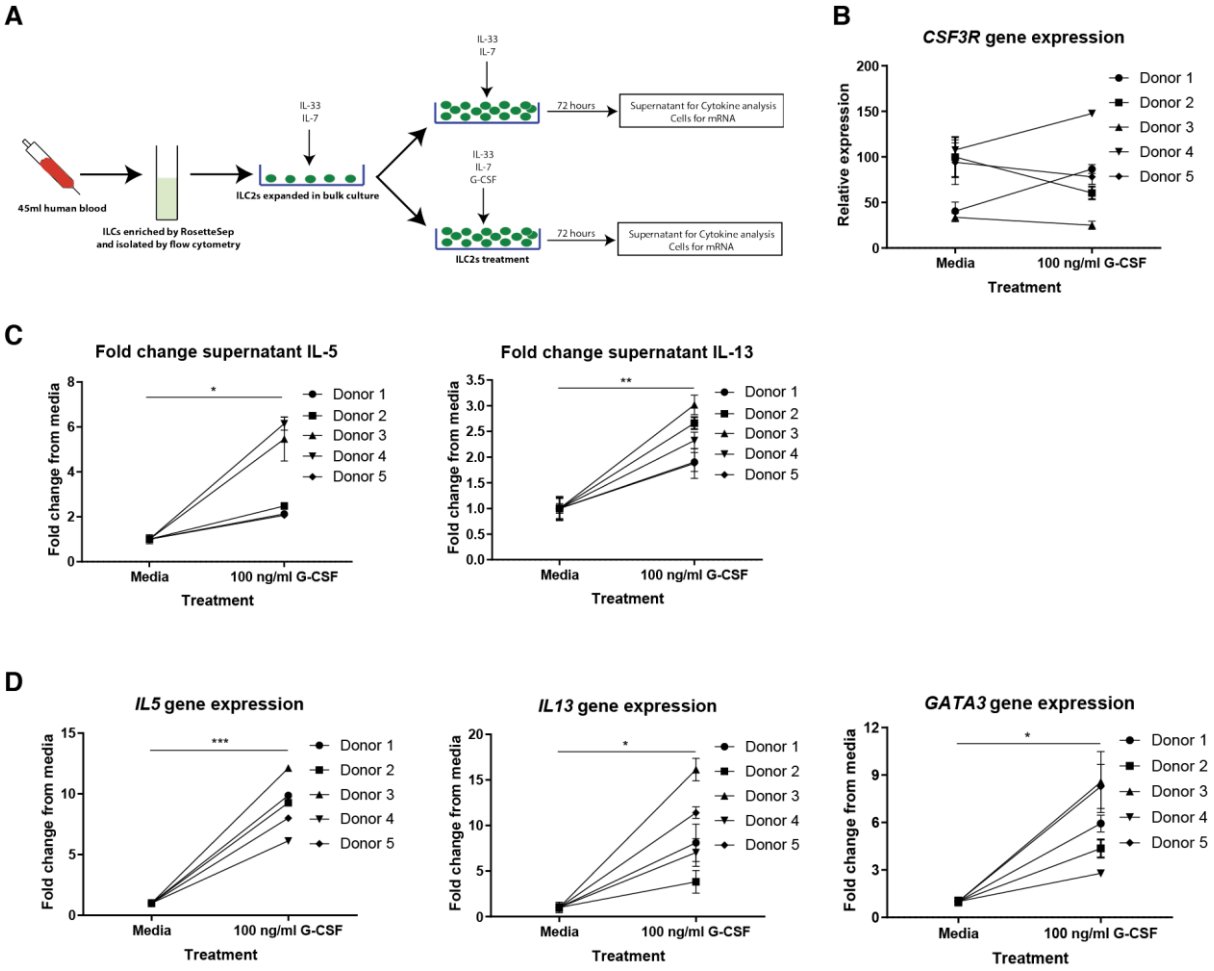
A
45ml human blood
ILCs enriched by RosetteSep
and isolated by flow cytometry
IL-33
IL-7
ILC2s expanded in bulk culture
IL-33
IL-7
72 hours
Supernatant for Cytokine analysis
Cells for mRNA
IL-33
IL-7
G-CSF
ILC2s treatment
72 hours
Supernatant for Cytokine analysis
Cells for mRNA
B
CSF3R gene expression
Relative expression
Donor 1
Donor 2
Donor 3
Donor 4
Donor 5
Media
100 ng/ml G-CSF
Treatment
C
Fold change supernatant IL-5
Fold change from media
Treatment
Fold change supernatant IL-13
Fold change from media
Treatment
D
IL5 gene expression
IL13 gene expression
GATA3 gene expression
Fold change from media
Media
100 ng/ml G-CSF
Treatment

Figure 8

Title: Neutrophils restrain allergic airway inflammation by limiting ILC2 function and monocyte-dendritic cell antigen presentation.

Authors:

Dhiren F. Patel, Teresa Peiró, Nicoletta Bruno, Juho Vuononvirta, Samia Akthar, Franz Puttur, Chloe J. Pyle, Kornelija Suveizdytė, Simone A. Walker, Leo M. Carlin, Lisa G. Gregory, Clare M. Lloyd, Robert J. Snelgrove.

Supplementary Text and Figures

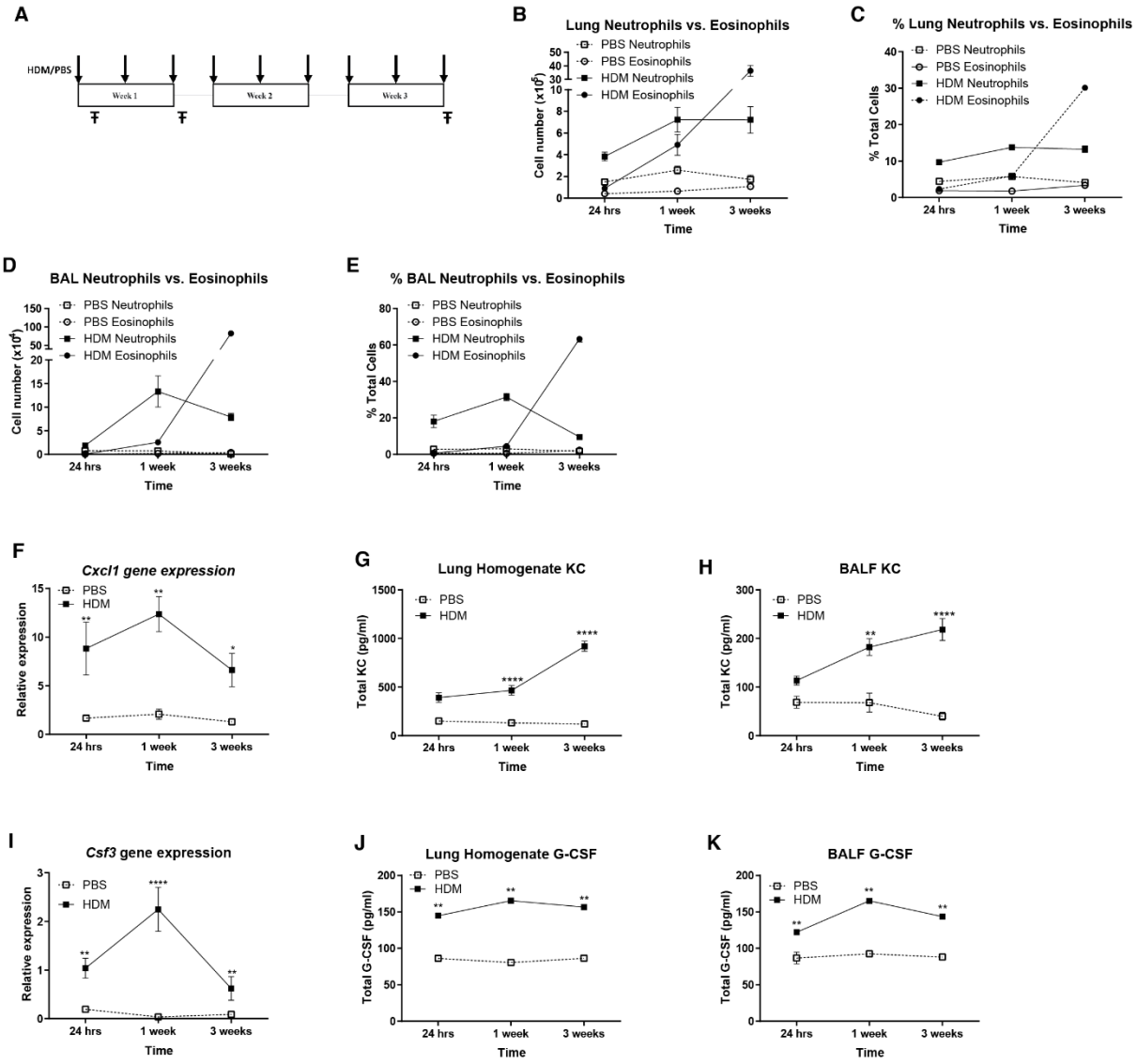

Supplementary Fig. 1: Intranasal administration of HDM induces neutrophilic inflammation in the lungs and airways of mice.

(**A**) Balb/c mice were administered HDM or PBS intranasally (i.n.) 3 times a week for up to 3 weeks, and broncho-alveolar lavage fluid (BALF) and lung tissue collected (Ŧ) at 24 hrs, 1 week and 3 week time points. The number and percentage of eosinophils and neutrophils in the lung tissue (**B** and **C**, respectively) and BAL (**D** and **E**, respectively) were quantified by flow cytometry. (**F**) *Kc* expression was assessed in lung by qPCR. (**G** and **H**) Levels of KC in lung homogenate and BALF were assessed by ELISA at each time point. (**I**) *Csf3* (G-CSF gene) expression was assessed in lung by qPCR. (**J** and **K**) Levels of G-CSF in lung homogenate and

BALF were assessed by ELISA at each time point. Figures present combined data from 2 independent experiments with 4-6 mice per group in each experiment. Results depicted as mean ± SEM. *P<0.05, **P<0.01, ****P<0.0001 using Mann–Whitney statistical test.

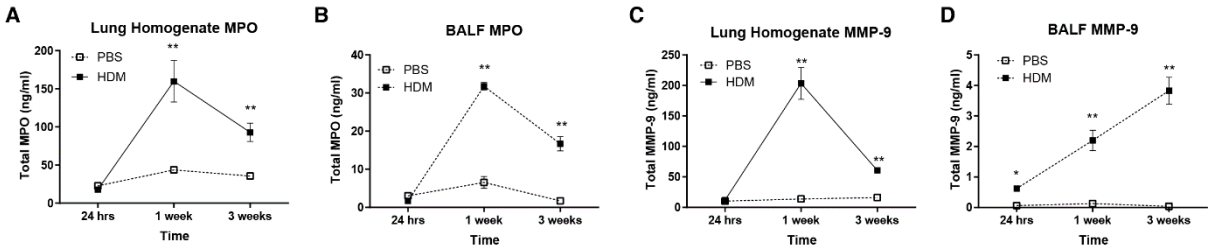

Supplementary Fig. 2: Intranasal administration of HDM induces an increase in neutrophil proteases in the lungs and airways of mice.

Balb/c mice were administered HDM or PBS intranasally (i.n.) 3 times a week for up to 3 weeks, and broncho-alveolar lavage fluid (BALF) and lung tissue collected at 24 hrs, 1 week and 3 week time points. Levels of myeloperoxidase (MPO; **A** and **B**) and matrix metalloproteinase-9 (MMP-9; **C** and **D**) in lung homogenate and BALF were assessed by ELISA at each time point. Figures present combined data from 2 independent experiments with 4-6 mice per group in each experiment. Results depicted as mean ± SEM. *P<0.05, **P<0.01 using Mann–Whitney statistical test.

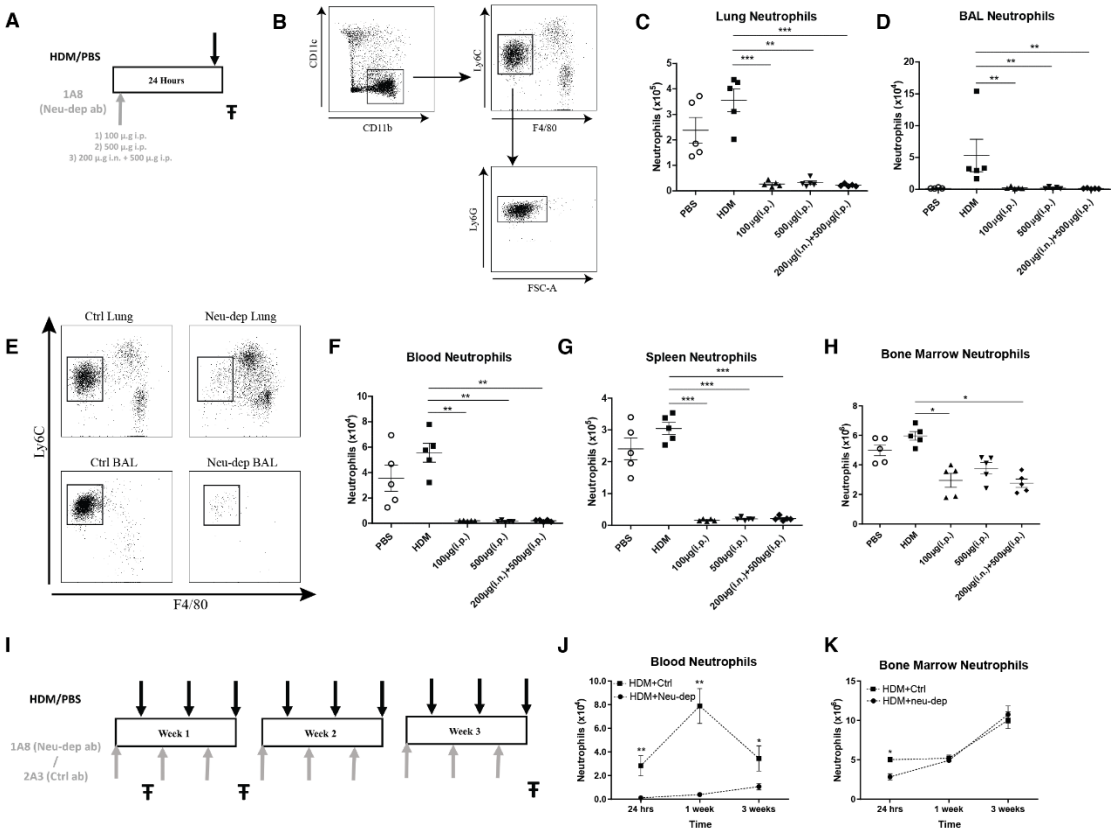

Supplementary Fig. 3: Intraperitoneal administration of anti-Ly6G antibody, 1A8, systemically depletes neutrophils in HDM treated mice.

(**A**) Balb/c mice were administered different doses of anti-Ly6G antibody, 1A8, either intraperitoneally (i.p) or intranasally (i.n.). After 24 hours mice were administered i.n. HDM/PBS, and after a further 24 hours lung tissue, BALF, blood, spleen and bone marrow were collected (Ŧ). (**B**) Flow cytometry gating strategy to identify neutrophils independently of Ly6G expression, whereby neutrophils were defined as $CD11b^{high}CD11c^{low}F480^{low}Ly6C^{intermediate}$ – with validation of population demonstrated in figure by Ly6G expression. The number of neutrophils in the lung (**C**) and BAL (**D**) were determined by flow cytometry. (**E**) Representative flow cytometry plots demonstrating effective neutrophil depletion in lung and airways of mice administered 1A8. The number of neutrophils in the blood (**F**), spleen (**G**) and bone marrow (**H**) were enumerated by flow cytometry. (**I**) Balb/c mice were administered HDM or PBS intranasally (i.n.) 3 times per week

for up to 3 weeks, and at 24 hours prior to each HDM administration, mice were dosed with either 100 μg of neutrophil depleting antibody, 1A8, or isotype control antibody, 2A3, i.p.. At 24 hours, 1 week and 3 week time points (Ŧ), the number of neutrophils were determined in blood (**J**) and bone marrow (**K**) by flow cytometry. Figures represent data 1 experiment with 4-6 mice per group. Results depicted as mean ± SEM. **P*<0.05, ***P*<0.01, ****P*<0.001 using Mann–Whitney statistical test.

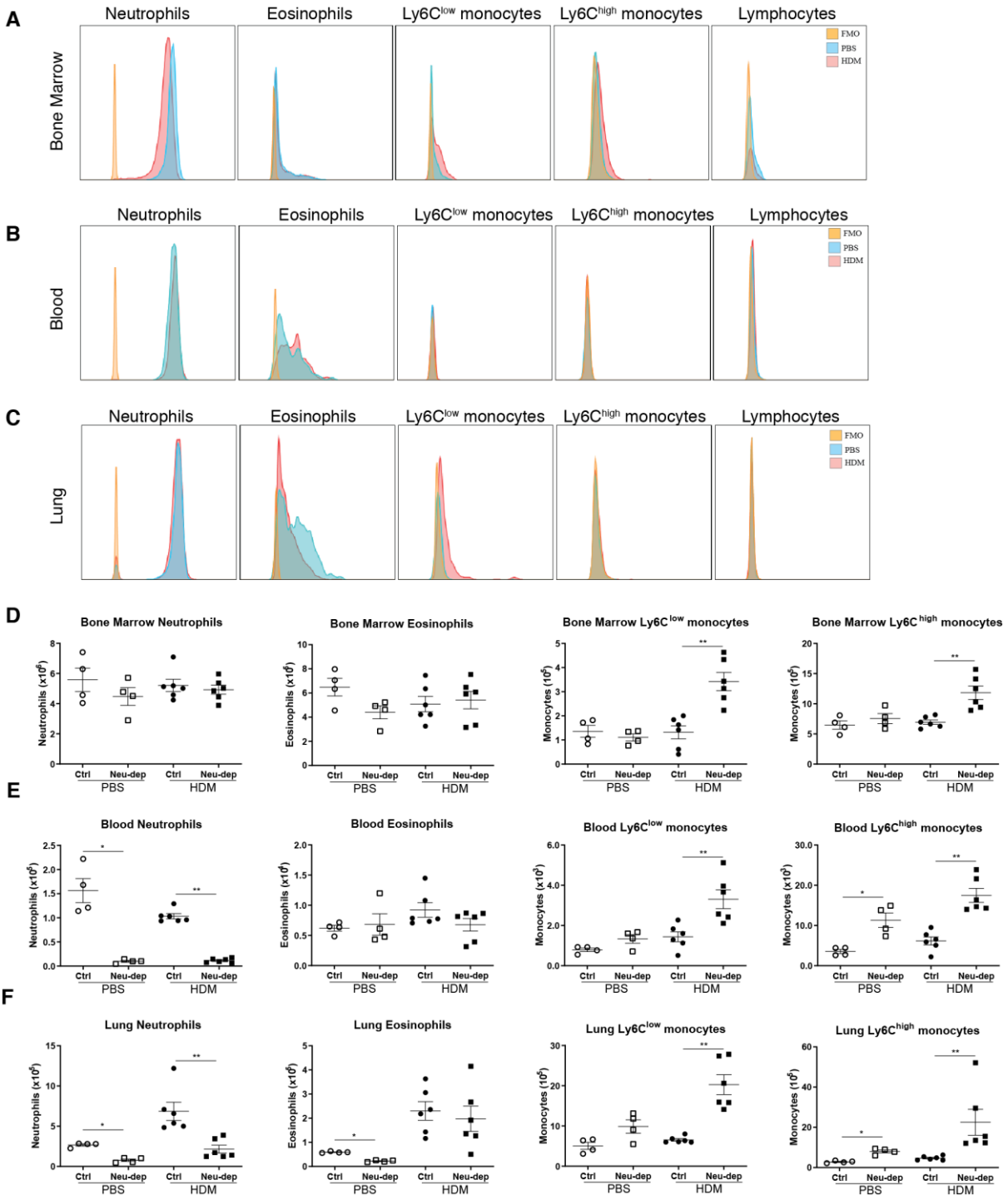
A
Neutrophils
Eosinophils
Ly6C^low monocytes
Ly6C^high monocytes
Lymphocytes
FMO
PBS
HDM
Bone Marrow
B
Blood
C
Lung
D
Bone Marrow Neutrophils
Bone Marrow Eosinophils
Bone Marrow Ly6C^low monocytes
Bone Marrow Ly6C^high monocytes
Neutrophils (x10^6)
Eosinophils (x10^6)
Monocytes (10^6)
Ctrl
Neu-dep
PBS
HDM
E
Blood Neutrophils
Blood Eosinophils
Blood Ly6C^low monocytes
Blood Ly6C^high monocytes
Neutrophils (x10^6)
Eosinophils (x10^6)
Monocytes (x10^3)
F
Lung Neutrophils
Lung Eosinophils
Lung Ly6C^low monocytes
Lung Ly6C^high monocytes
Neutrophils (x10^6)
Eosinophils (x10^6)
Monocytes (10^6)

Supplementary Fig. 4: Intraperitoneal administration of anti-Ly6G antibody, 1A8, specifically depletes neutrophils.

Balb/c mice were administered HDM or PBS intranasally (i.n.) 3 times per week for 1 week, and at 24 hours prior to each HDM/PBS administration mice were dosed with either 100 μg of neutrophil depleting antibody, 1A8, or isotype control antibody, 2A3 intraperitoneally (i.p.). At 24 hours post final HDM/PBS exposure, bone marrow, blood and lung tissue was collected. Representative histogram overlays are presented depicting Ly6G expression on neutrophils, eosinophils, $Ly6C^{low}$ monocytes, $Ly6C^{high}$ monocytes and lymphocytes in bone marrow (**A**), blood (**B**) and lung tissue (**C**) of PBS and HDM treated mice. Orange = FMO; Blue = PBS; Red = HDM. Total numbers of neutrophils, eosinophils, $Ly6C^{low}$ monocytes and $Ly6C^{high}$ monocytes in bone marrow (**D**), blood (**E**) and lung tissue (**F**) of PBS and HDM treated mice after 2A3 / 1A8 treatment. Figures represent data 1 experiment with 4-6 mice per group. Results depicted as mean ± SEM. $*P<0.05$, $**P<0.01$ using Mann–Whitney statistical test.

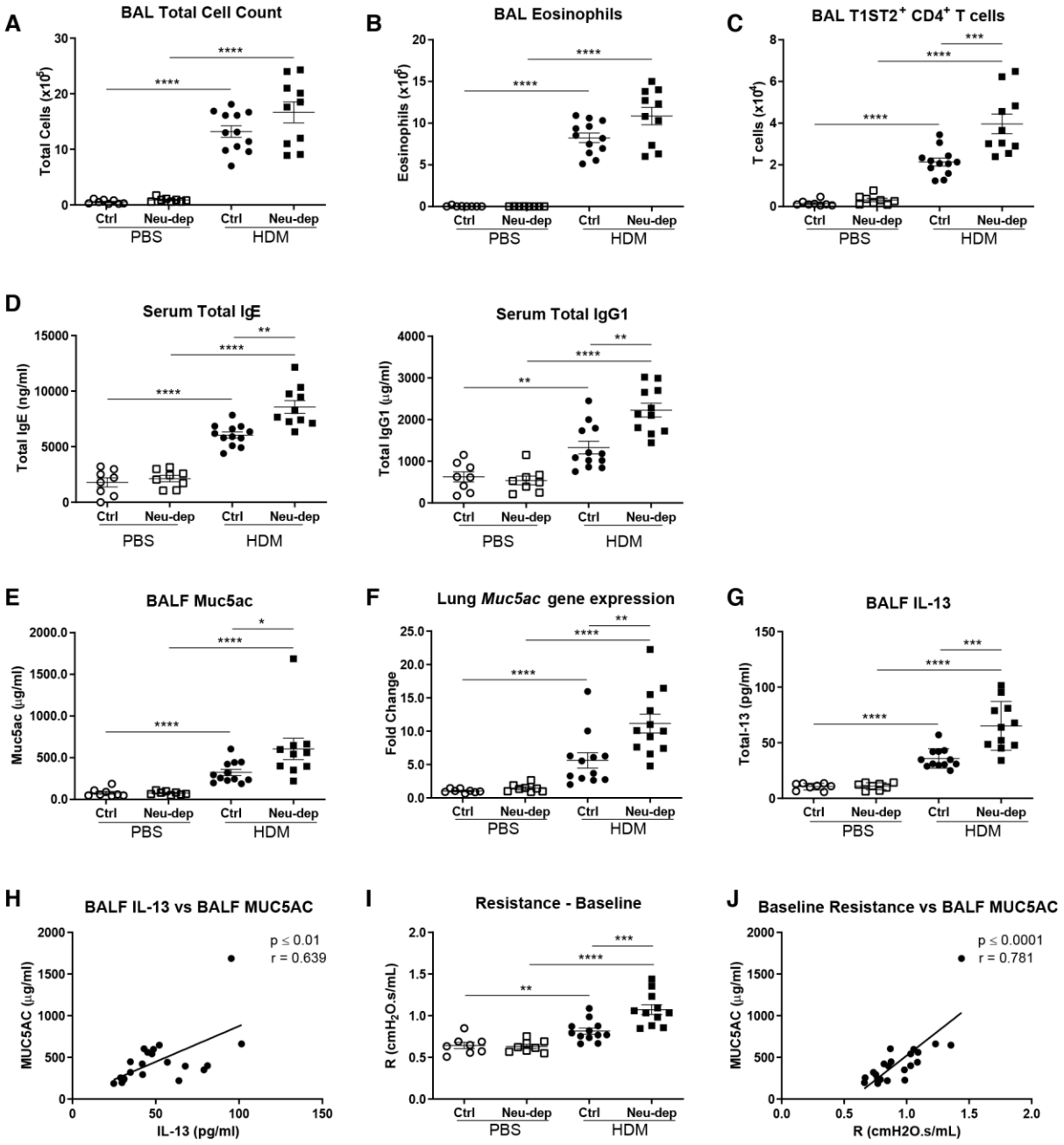

Supplementary Fig. 5: Neutrophil depleted mice display augmented type 2 inflammation, epithelial remodelling and airway resistance after 3 weeks of HDM exposure.

Balb/c mice were administered HDM or PBS intranasally (i.n.) 3 times per week for 3 weeks, and at 24 hours prior to each HDM/PBS administration mice were dosed with either 100 µg of neutrophil depleting antibody, 1A8, or isotype control antibody, 2A3 intraperitoneally (i.p.). At 24 hours post final HDM/PBS exposure blood, lung tissue and BALF was collected. (**A**) Total cell numbers in the airways were assessed by trypan blue exclusion. (**B**) The number of

eosinophils in the airways were quantified by flow cytometry. (**C**) The number of $CD4^+$ T cells expressing T1ST2 in the airways were assessed by flow cytometry. (**D**) Concentrations of total IgE and IgG1 in the serum were determined by ELISA. (**E**) Expression of *Muc5ac* was determined in lung tissue of mice by qPCR. Concentrations of MUC5AC (**F**) and IL-13 (**G**) protein were assessed in and BALF by ELISA. (**H**) Correlation between BALF IL-13 and MUC5AC concentration for all HDM groups. Airway resistance (R) at baseline was assessed by Flexivent (**I**) and correlated with BALF MUC5AC concentration for all HDM groups (**J**). Figures present combined data from 2 independent experiments with 4-6 mice per group in each experiment. Results depicted as mean ± SEM. **P*<0.05, ***P*<0.01, ****P*<0.001, *****P*<0.0001 using Mann–Whitney statistical test. Correlation analysis was performed using Spearman rank test.

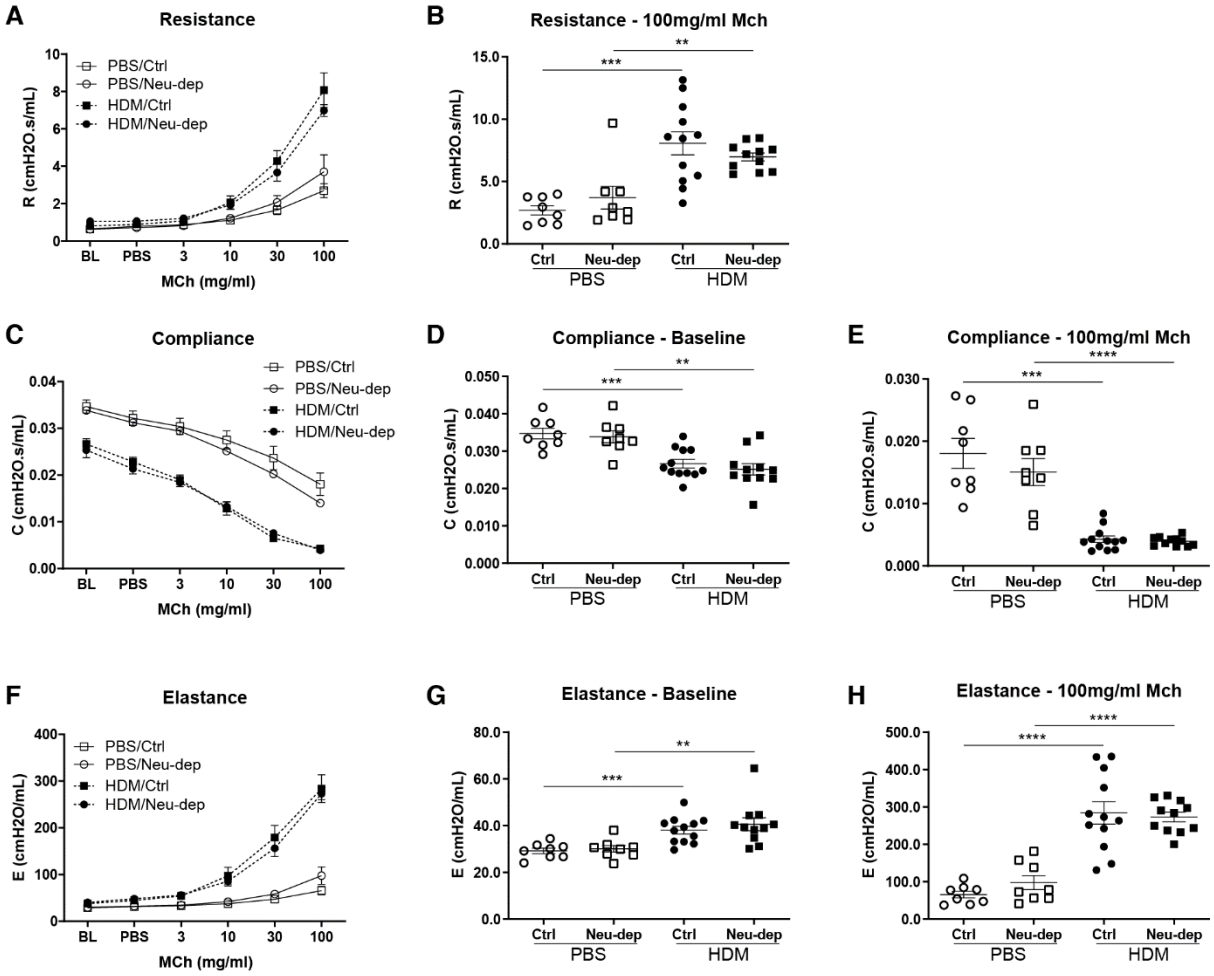

Supplementary Fig. 6: Neutrophil depleted mice display comparable airway hyperresponsiveness after 3 weeks of HDM exposure.

Balb/c mice were administered HDM or PBS intranasally (i.n.) 3 times per week for 3 weeks, and at 24 hours prior to each HDM/PBS administration mice were dosed with either 100 µg of neutrophil depleting antibody, 1A8, or isotype control antibody, 2A3 intraperitoneally (i.p.). (**A**) Airway Resistance (R) to increasing doses of methacholine (Mch) was measured 24 hrs post the final HDM/PBS exposure. (**B**) Airway resistance at 100 mg/ml Mch. (**C**) Lung compliance (C) to increasing doses of Mch was measured 24 hrs post the final HDM/PBS exposure. Lung compliance at baseline (**D**) and 100 mg/ml Mch (**E**). (**F**) Tissue elastance (E) to increasing doses of Mch was measured 24 hrs post the final HDM/PBS exposure. Tissue elastance at baseline (**G**) and 100 mg/ml Mch (**H**). Figures present combined data from 2

independent experiments with 4-6 mice per group in each experiment. Results depicted as mean ± SEM. $^{**}P<0.01$, $^{***}P<0.001$, $^{****}P<0.0001$ using Mann–Whitney statistical test.

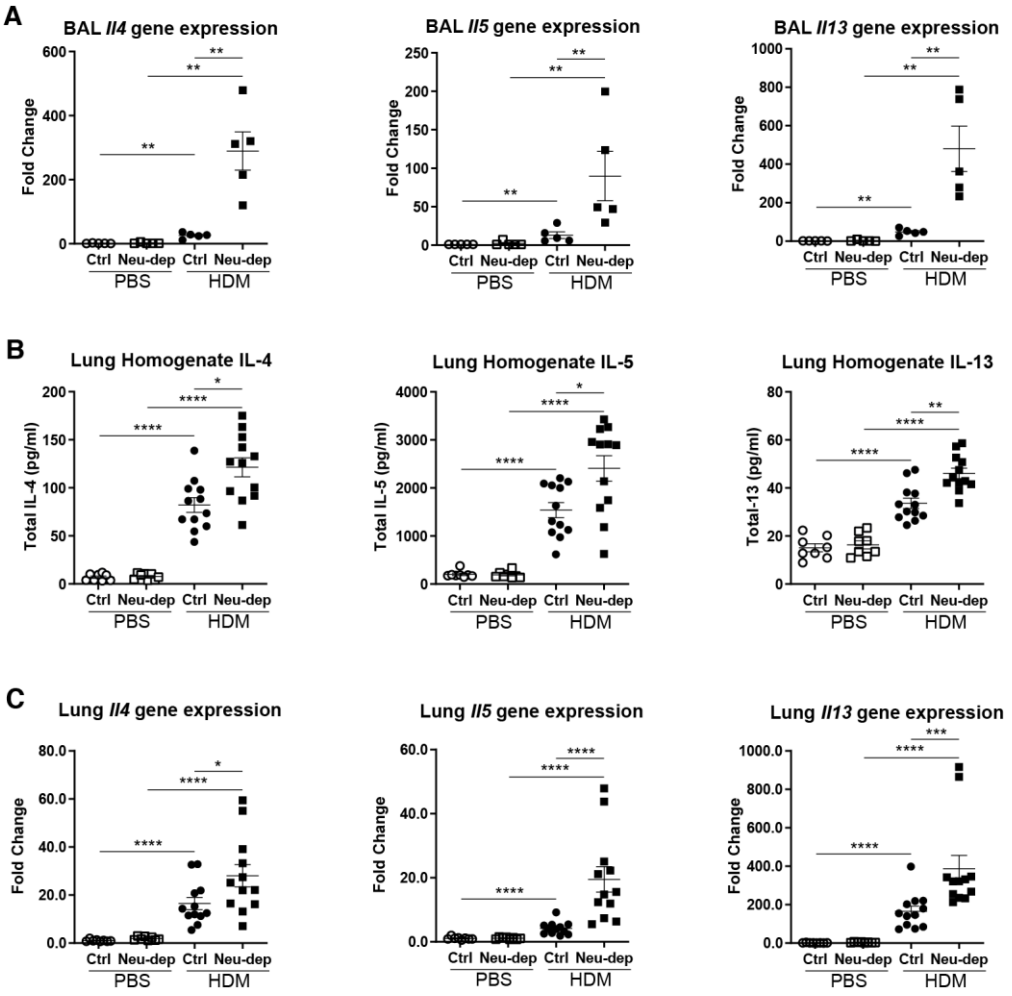

Supplementary Fig. 7: Augmented T_H2 cytokine levels in neutrophil depleted mice administered HDM for 1 week.

Balb/c mice were administered HDM or PBS intranasally (i.n.) 3 times per week for 1 week and at 24 hours prior to each HDM treatment, mice were dosed with either 100 μg of neutrophil depleting antibody, 1A8, or isotype control antibody, 2A3 intraperitoneally (i.p.). At 24 hours post the final HDM administration BAL cells and lung tissue were collected. (**A**) Expression of *Il4*, *Il5* and *Il13* were determined in BAL-derived cells by qPCR. (**B**) Concentrations of IL-4, IL-5 and IL-13 protein were assessed in lung homogenate by ELISA. (**C**) Expression of *Il4*, *Il5* and *Il13* were determined in whole lung by qPCR. Figures present combined data from 1 experiment with 4-6 mice per group (**A**) or from 2 independent experiments with 4-6 mice per

group in each experiment (**B** and **C**). Results depicted as mean ± SEM. *P<0.05, **P<0.01, ***P<0.001, ****P<0.0001 using Mann–Whitney statistical test.

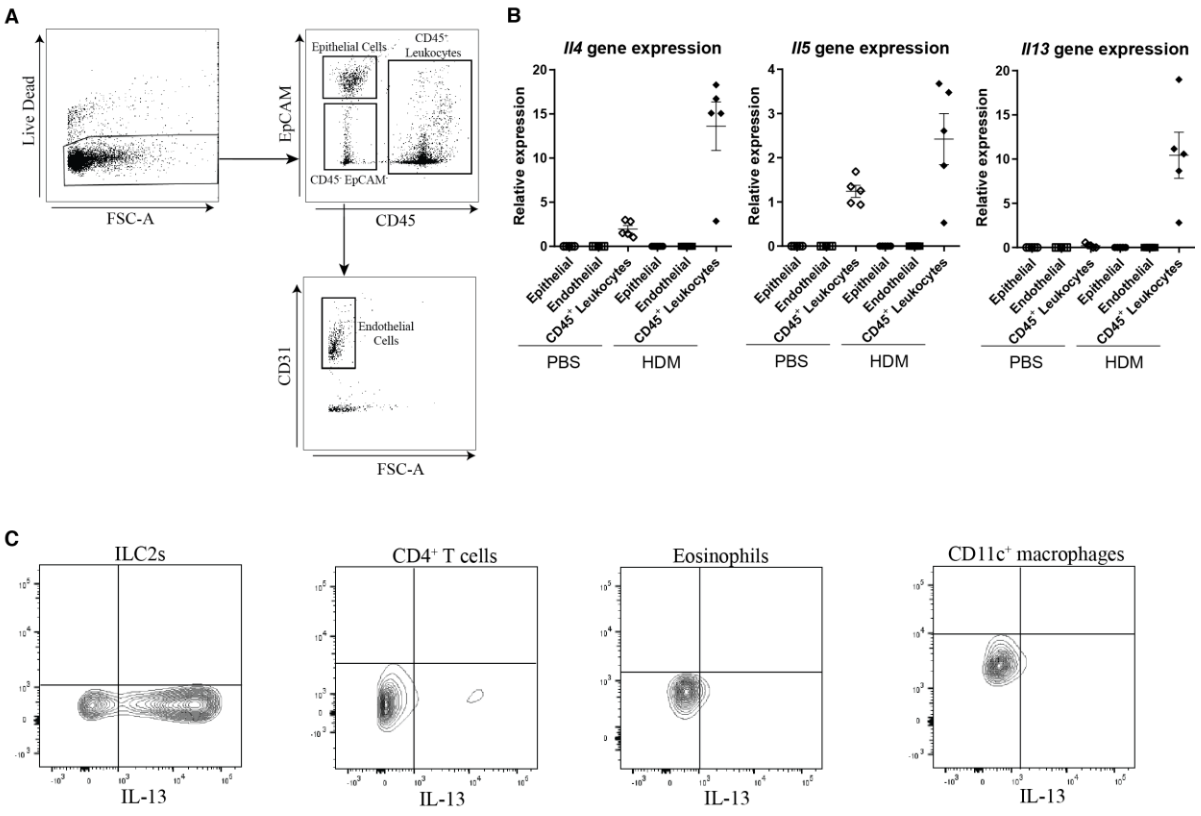

Supplementary Fig. 8: ILC2s are the predominant source of IL-13 after 1 week of HDM administration.

Balb/c mice were administered HDM or PBS intranasally (i.n.) 3 times per week for 1 week. (**A**) Gating strategy utilized in some experiments to isolate lung $CD45^+$ leukocytes, $CD45^-EpCAM^+$ epithelial cells and $CD45^-EpCAM^-CD31^+$ endothelial cells by fluorescence-activated cell sorting (FACS) at 24 hours post the final PBS / HDM administration. (**B**) Relative expression of *Il4*, *Il5* and *Il13* was determined in isolated populations by qPCR. Female IL-13 *gfp*-reporter mice were administered HDM intranasally (i.n.) 3 times per week for 1 week. At 24 hours post final HDM exposure, BALF was collected to identify $IL\text{-}13^+$ cell populations by flow cytometry. (**C**) Representative contour plots depicting IL-13 expression by airway ILCs, $CD4^+$ T cells, eosinophils and $CD11c^+$ macrophages. Figures present data from 1 experiment with 4-6 mice per group. Results depicted as mean ± SEM.

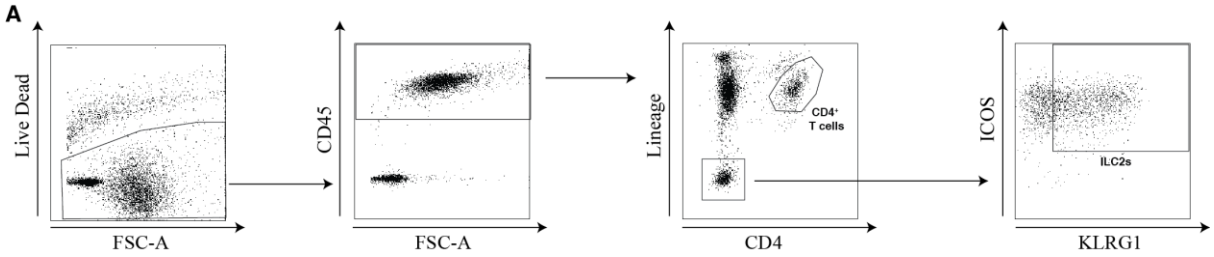

Supplementary Fig. 9: Gating strategy for isolation of ILC2s and $CD4^+$ T cells by fluorescence activated cell sorting.

A gating strategy was deployed to sort ILC2s and $CD4^+$ T cells independent of intracellular cytokine staining. Total live cells were assessed for CD45 to isolate live leukocytes. Leukocytes were subsequently interrogated for the expression of common lineage markers in a self-made lineage cocktail (TCRβ, CD5, CD19, TCRγδ, CD11b, CD11c, FCεR1, GR-1, F4/80, TER-119 and NKp46) with $CD4^+$ T cells being identified as Lin^+ $CD4^+$. Lineage negative cells were interrogated for the expression of ICOS and ILC2-defining maker, KLRG1, with ILC2s being identified as $ICOS^+$ $KLRG1^+$.

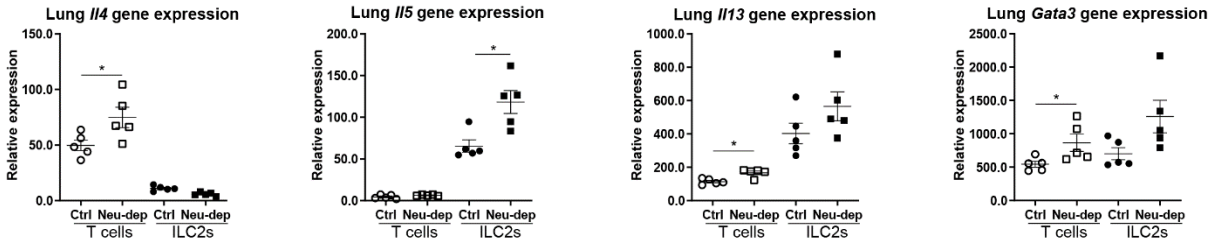

Supplementary Fig. 10: Augmented IL-5 and IL-13 levels in lungs of neutrophil depleted mice administered HDM for 1 week are primarily derived from ILC2s.

Balb/c mice were administered HDM intranasally (i.n.) 3 times per week for 1 week and at 24 hours prior to each HDM treatment, mice were dosed with either 100 µg of neutrophil depleting antibody, 1A8, or isotype control antibody, 2A3 intraperitoneally (i.p.). At 24 hours post the final HDM exposure, $CD4^+$ T cells and ILC2s were isolated from lung tissue by fluorescence activated cell sorting (FACS) for subsequent mRNA gene expression analysis. Relative expression of IL-4, IL-5, IL-13 and GATA-3 in T cells and ILC2s derived from lung tissue, as determined by qPCR. Figures present data from 1 experiment with 5 mice per group. Results depicted as mean ± SEM. *$P<0.05$ using Mann–Whitney statistical test.

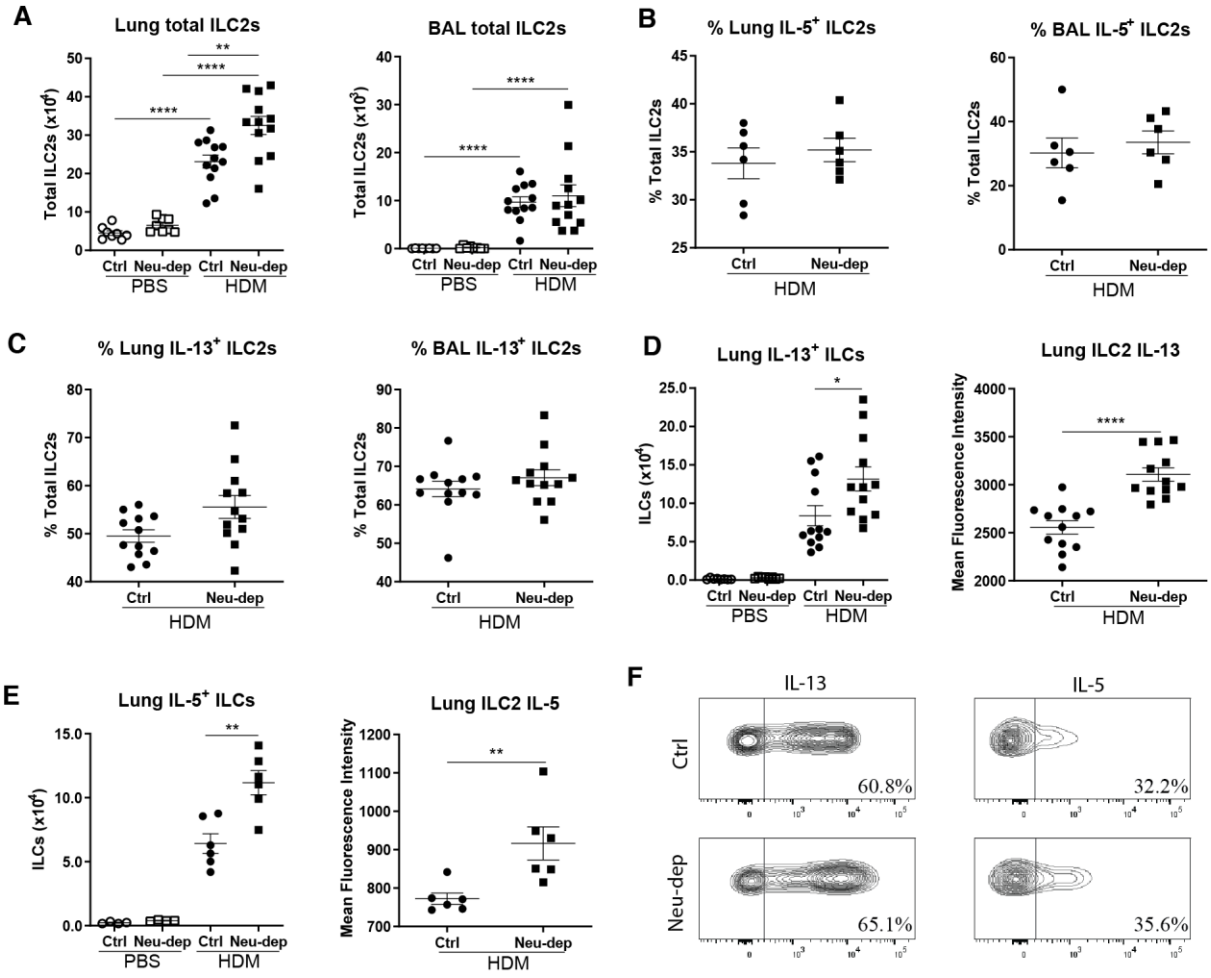

Supplementary Fig. 11: ILC2s from neutrophil depleted mice administered HDM for 1 week produce more IL-5 and IL-13 on a per cell basis.

Balb/c mice were administered HDM or PBS intranasally (i.n.) 3 times per week for 1 week and at 24 hours prior to each HDM treatment, mice were dosed with either 100 μg of neutrophil depleting antibody, 1A8, or isotype control antibody, 2A3 intraperitoneally (i.p.). (**A**) At 24 hours post final PBS/HDM administration, the total number of ILC2s in lung tissue and BAL was determined by flow cytometry. The percentage of lung and BAL ILC2s producing IL-5 (**B**) and IL-13 (**C**) were determined by flow cytometry. (**D**) The number of IL-13$^+$ ILC2s and geometric expression of IL-13 on ILC2s in the lung was assessed by flow cytometry. (**E**) Similarly, the number of IL-5$^+$ ILC2s and geometric mean of IL-5 on ILC2s in the lung was assessed by flow cytometry. (**F**) Representative contour plots depicting IL-13 and IL-5

expression by ILC2s from the lungs of mice administered HDM for 1 week in combination with 2A3 or 1A8. Figures present data from 2 independent experiments with 4-6 mice per group in each experiment (**A**, **C** and **D**) or from 1 experiment with 4-6 mice per group (**B** and **E**). Results depicted as mean ± SEM. *P<0.05, **P<0.01, ****P<0.0001 using Mann–Whitney statistical test.

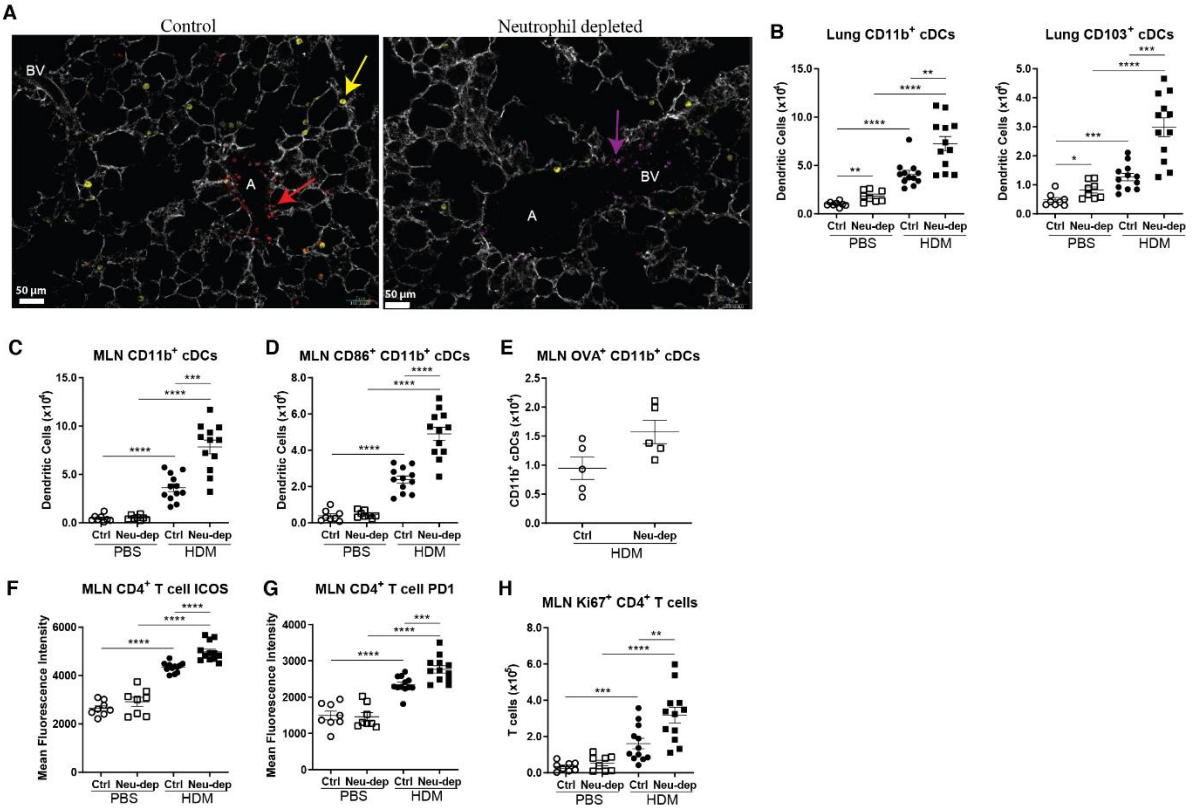

Supplementary Fig. 12: HDM exposed, neutrophil depleted mice exhibit augmented dendritic cell numbers and antigen presentation.

Balb/c mice were administered HDM or PBS intranasally (i.n.) 3 times per week for 1 week. At 24 hours prior to each HDM/PBS administration, mice were treated with either 100 µg of neutrophil depleting antibody, 1A8, or isotype control antibody, 2A3 intraperitoneally (i.p). At 24 hours post final HDM/PBS exposure, lung tissue and mediastinal lymph nodes (MLNs) were collected. (**A**) Representative images of precision cut lung slices from control and neutrophil depleted mice exposed to HDM for 1 week, showing monocytes (CD115; magenta), airway macrophages (CD11c; yellow), neutrophils (Ly6G; red) and endothelial cells (CD31; white). Airways (A) and blood vessels (BV) are annotated. (**B**) Numbers of lung $CD11b^+$ conventional dendritic cells ($CD11b^+$ cDCs) and $CD103^+$ cDCs were determined by flow cytometry. The number of mediastinal lymph node (MLN) $CD11b^+$ cDCs (**C**), $CD86^+$ $CD11b^+$ cDCs (**D**), were enumerated by flow cytometry. In some experiments, the final dose of HDM

was admixed with 100 µg Alexa Fluor 488 labelled OVA and MLNs collected at 24 hrs post the final HDM/PBS exposure. (**E**) The number of OVA^+ $CD11b^+$ cDCs in the MLNs were determined by flow cytometry. MLN $CD4^+$ T cell geometric mean expression of ICOS (**F**) and PD-1 (**G**), and the number of Ki-67^+ $CD4^+$ T cells (**H**) were also enumerated by flow cytometry. Figures present data combined from 2 independent experiments with 4-6 mice per group for each experiment (**B-D** and **F-H**) or from 1 experiment with 5 mice per group (**E**). Results depicted as mean ± SEM. **P*<0.05, ***P*<0.01, ****P*<0.001; *****P*<0.0001 using Mann–Whitney statistical test.

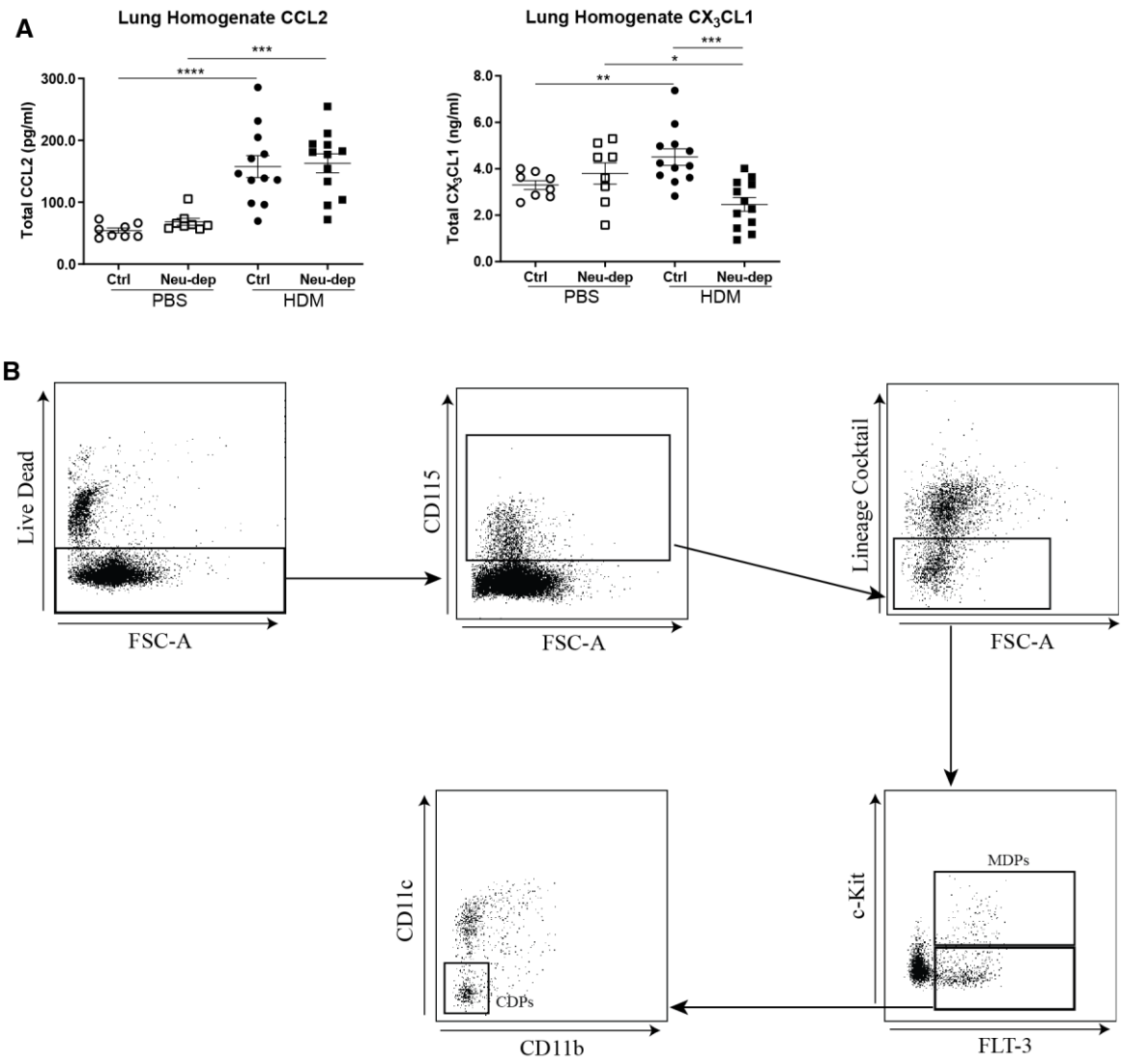

Supplementary Fig. 13: Lung concentrations of classical monocyte chemokines and flow cytometry gating strategy to identify monocyte dendritic cell progenitors (MDPs) and common dendritic cell progenitors (CDPs).

(**A**) Balb/c mice were administered HDM or PBS intranasally (i.n.) 3 times per week for 1 week. At 24 hours prior to each HDM/PBS administration, mice were treated with either 100 µg of neutrophil depleting antibody, 1A8, or isotype control antibody, 2A3 intraperitoneally (i.p). At 24 hours post final HDM/PBS exposure, lung tissue was collected. The concentration of CCL2 and CX3CL1 in lung homogenate was assessed by ELISA. Figures present data combined from 2 independent experiments with 4-6 mice per group for each experiment.

Results depicted as mean ± SEM. $^{**}P<0.01$, $^{***}P<0.001$; $^{****}P<0.0001$ using Mann–Whitney statistical test. (**B**) A gating strategy was deployed to enumerate MDPs and CDPs in bone marrow by flow cytometry. Total live cells were assessed for CD115 expression, with $CD115^+$ cells subsequently further interrogated for expression of common leukocyte markers in a lineage cocktail (CD3, CD19, SiglecF, Ly6G, NKp46 and CD90.2). $CD115^+Lin^-$ cells were then interrogated for relative expression of c-Kit and FLT3, with $c\text{-}Kit^+FLT3^+$ defined as MDPs. Cells that were $c\text{-}Kit^-FLT3^+$ were further analysed for expression of CD11c and CD11b, with $CDllc^-CD11b^-$ cells identified as CDPs.

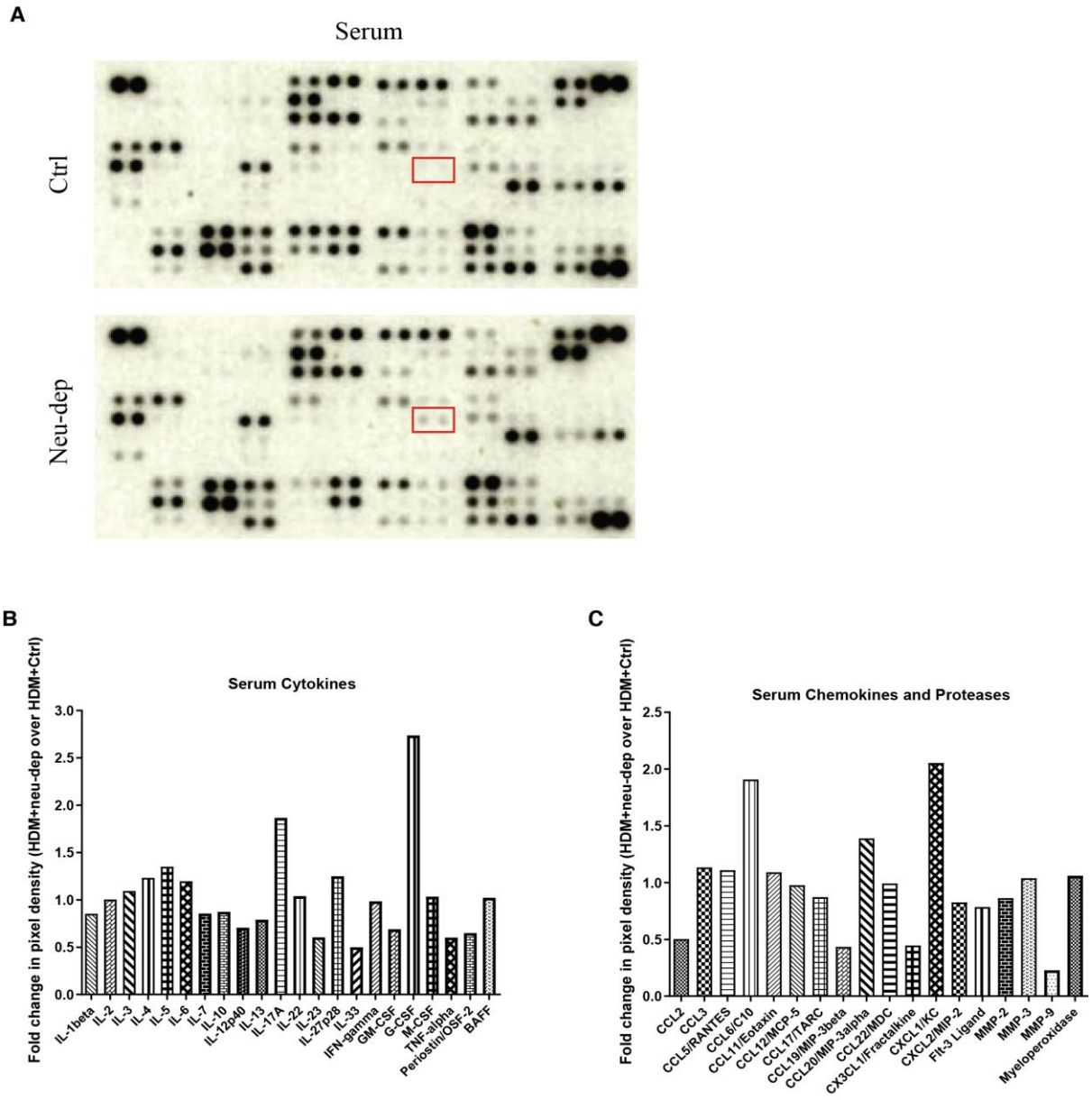

Supplementary Fig. 14: G-CSF is elevated in the serum of neutrophil depleted mice administered HDM.

Balb/c mice were administered HDM intranasally (i.n.) 3 times per week for 1 week. At 24 hours prior to each HDM administration, mice were treated with either 100 µg of neutrophil depleting antibody, 1A8, or isotype control antibody, 2A3, intraperitoneally (i.p). At 24 hours post final HDM exposure, serum was collected for proteome profiler analysis. (**A**) Images of the proteome profiler blots from control and neutrophil depleted mice administered HDM for 1 week. Red boxes denote the position of G-CSF on respective blots. (**B**) Fold change in serum

cytokine pixel density in HDM-exposed neutrophil depleted mice over respective control mice. (**C**) Fold change in serum chemokine and protease pixel density in HDM-exposed neutrophil depleted mice over respective control mice.

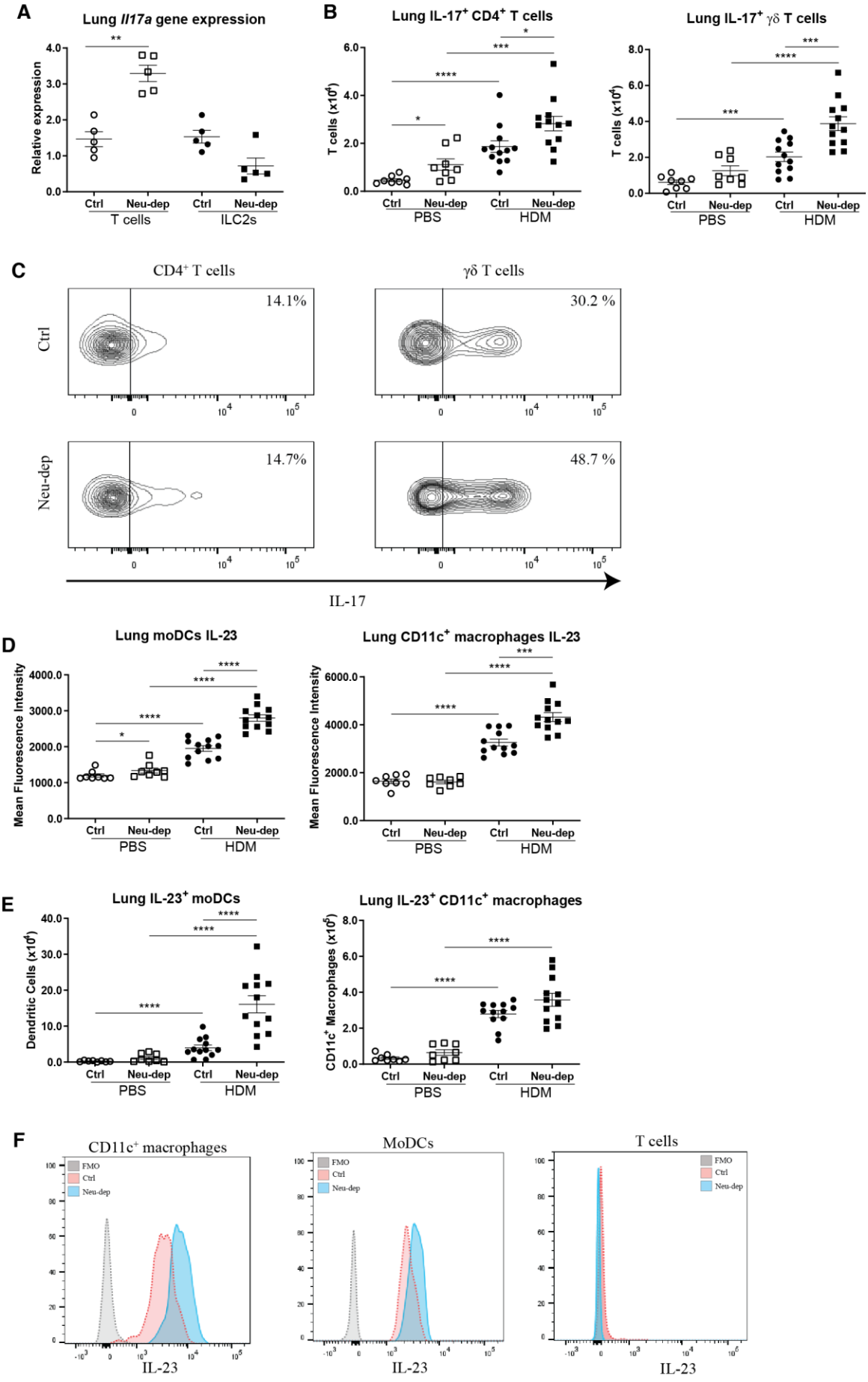
A
Lung Il17a gene expression
Relative expression
Ctrl
Neu-dep
T cells
ILC2s
B
Lung IL-17+ CD4+ T cells
Lung IL-17+ γδ T cells
T cells (x10⁶)
PBS
HDM
C
CD4+ T cells
γδ T cells
14.1%
30.2 %
14.7%
48.7 %
Ctrl
Neu-dep
IL-17
D
Lung moDCs IL-23
Lung CD11c+ macrophages IL-23
Mean Fluorescence Intensity
E
Lung IL-23+ moDCs
Lung IL-23+ CD11c+ macrophages
Dendritic Cells (x10⁶)
CD11c+ Macrophages (x10⁵)
F
CD11c+ macrophages
MoDCs
T cells
FMO
Ctrl
Neu-dep
IL-23

Supplementary Fig. 15: Neutrophil depleted mice administered HDM produce elevated levels of IL-17 and IL-23.

Balb/c mice were administered HDM or PBS intranasally (i.n.) 3 times per week for 1 week. At 24 hours prior to each HDM/PBS administration, mice were treated with either 100 μg of neutrophil depleting antibody, 1A8, or isotype control antibody, 2A3 intraperitoneally (i.p). At 24 hours post final HDM/PBS exposure, lung tissue was collected. (**A**) *Il17* expression was determined in isolated lung populations of $CD4^+$ T cell and ILC2s by qPCR. (**B**) The number of lung IL-17^+ $CD4^+$ T cells and IL-17^+ γδ T cells were determined by flow cytometry. (**C**) Representative contour plots depicting IL-17 expression by $CD4^+$ T cells and IL-17^+ γδ T cells from 2A3 and 1A8 treated mice after 1 week of HDM administration. (**D**) The number of lung IL-23^+ $CD11c^+$ macrophages and IL-23^+ moDCs were determined by flow cytometry. (**E**) Geometric mean of IL-23 expression by $CD11c^+$ macrophages and moDCs as adjudged by flow cytometry. (**F**) Representative histogram overlays of IL-23 expression by $CD11c^+$ macrophages and moDCs. Histogram overlay for IL-23 expression by T cells is also presented to demonstrate specificity of binding of the anti-IL-23 antibody. Grey = FMO; Red = HDM/2A3; Blue = HDM/1A8. Figures present data from 1 experiment with 5 mice per group (**A**) or from 2 independent experiment with 4-6 mice per group in each experiment (**B**, **D** and **E**). Results depicted as mean ± SEM. *P<0.05, **P<0.01, ***P<0.001, ****P<0.0001 using Mann–Whitney statistical test.

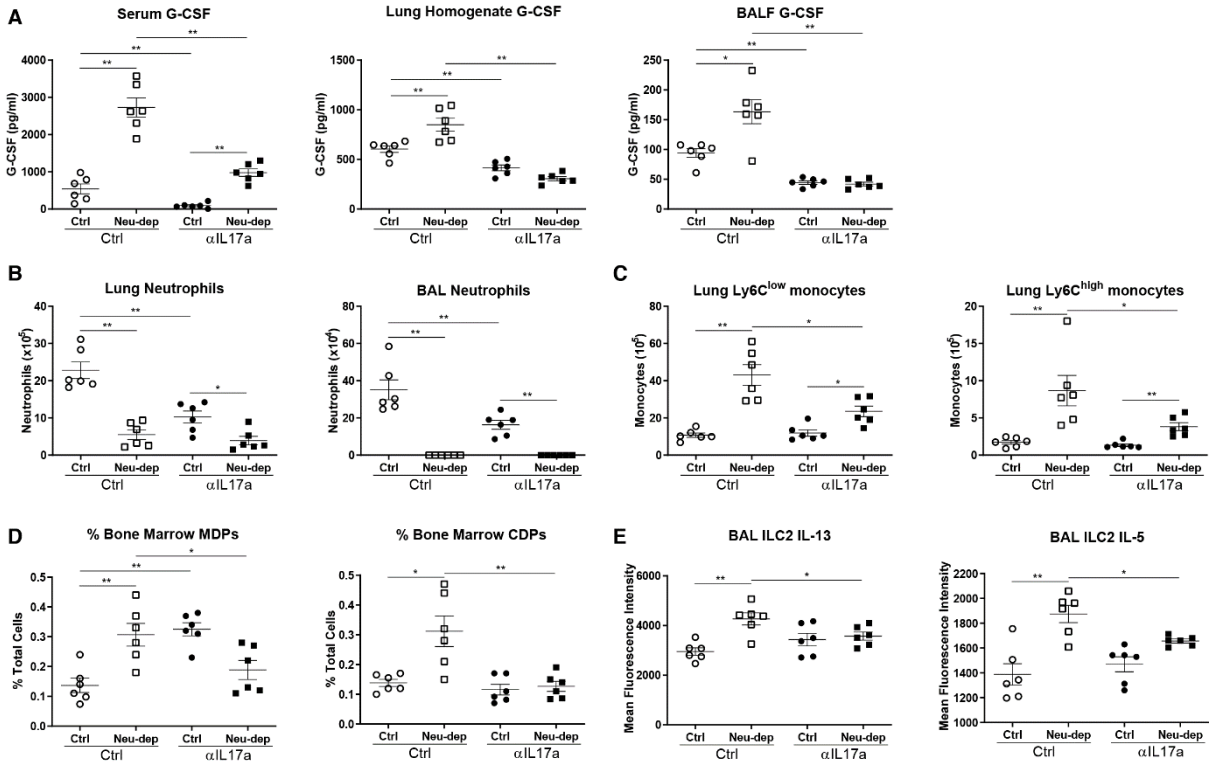

Supplementary Fig. 16: Neutralization of IL-17 reverts the effects of neutrophil depletion in HDM administered mice.

Balb/c mice were administered HDM intranasally (i.n.) 3 times per week for 1 week. At 24 hours prior to each HDM administration, mice were treated with either 100 µg of neutrophil depleting antibody, 1A8, or isotype control antibody, 2A3. To neutralize IL-17, mice were also administered 20 µg anti-IL-17 or isotype control, 2A3, i.p. at 24 hours prior to each HDM dose. At 24 hours post final HDM administration, serum, lung tissue, BAL and bone marrow were collected. (**A**) The concentrations of G-CSF in serum, lung homogenate and BALF were assessed by ELISA. (**B**) The number of neutrophils in the lung and BAL were determined by flow cytometry. (**C**) The number of lung Ly6C^{low} and Ly6C^{high} monocytes were determined by flow cytometry. (**D**) The percentage of monocyte dendritic cell progenitors (MDPs) and common dendritic cell progenitors (CDPs) within the bone marrow were assessed by flow cytometry. (**E**) Geometric mean of IL-13 and IL-5 expression by airway ILCs was assessed by

flow cytometry. Figures present data from 1 experiment with 4-6 mice per group Results depicted as mean ± SEM. *P<0.05, **P<0.01using Mann–Whitney statistical test.

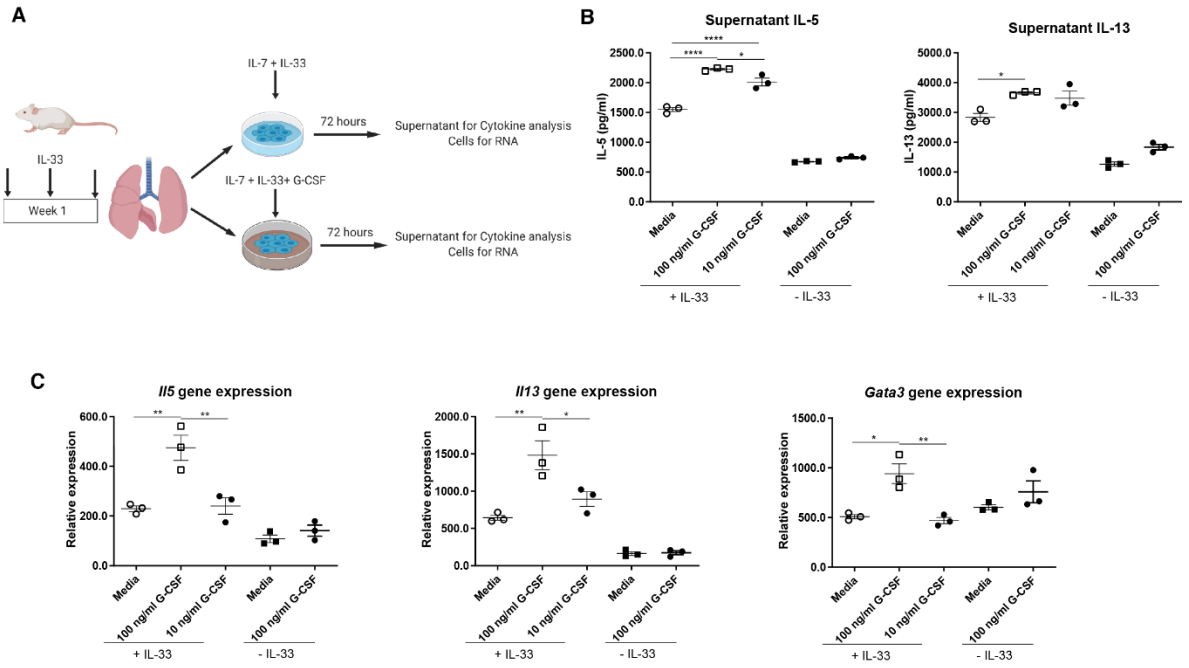

Supplementary Fig. 17: G-CSF directly augments T_H2 cytokine production from mouse ILC2s.

(**A**) Balb/c mice were administered 1 µg recombinant IL-33 i.n. 3 times per week for 1 week. At 24 hours post final IL-33 administration, lungs were collected and ILC2s isolated by fluorescence activated cell sorting. ILC2s were subsequently cultured with combinations of IL-7 (5ng/ml) / IL-33 (10 ng/ml) and /or recombinant G-CSF (10 or 100 ng/ml), as depicted within the figure, for 72 hours. (**B**) The levels of IL-5 and IL-13 in the ILC2 supernatant were assessed by ELISA. (**C**) Relative expression of *Il5*, *Il13*, and *Gata3* was assessed by qPCR after 72 hours. Results depicted as mean ± SEM. *P<0.05 using an ANOVA test followed by a Bonferonni correction.

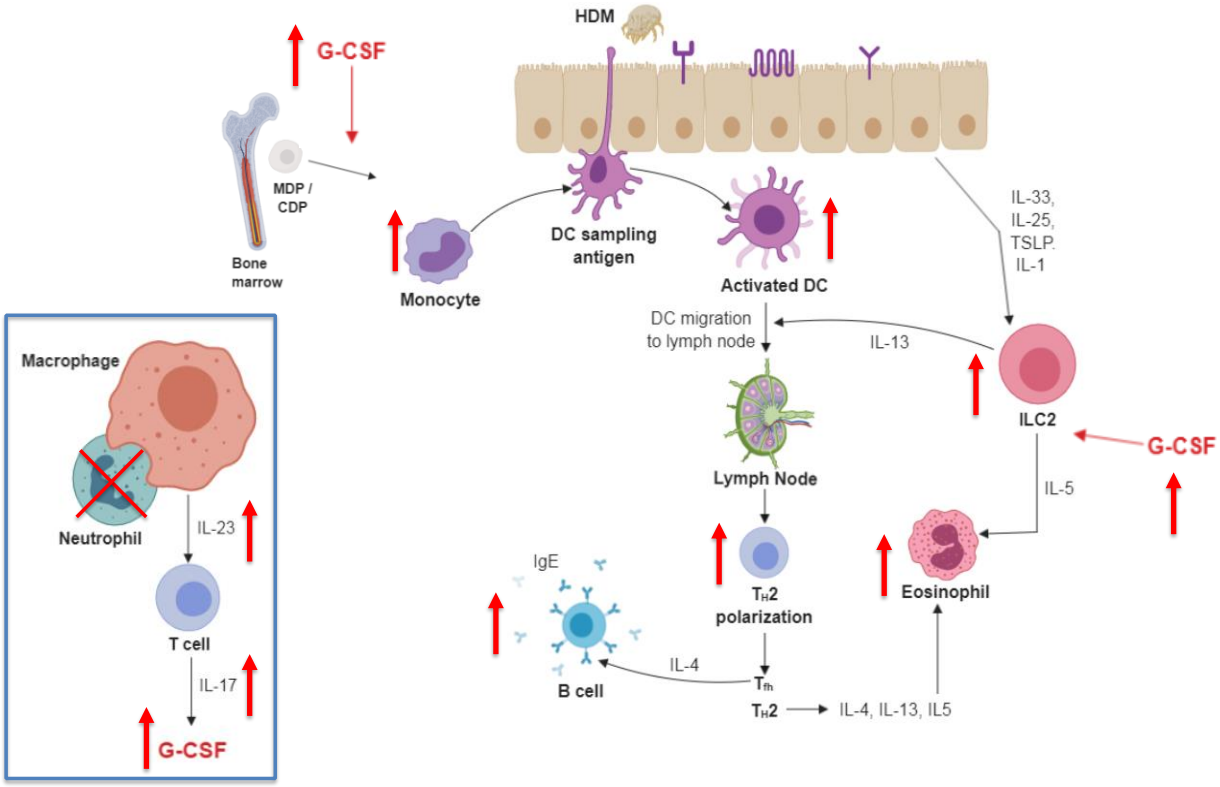

Supplementary Fig. 18: Neutrophil depletion alters the IL-23 – IL-17 – G-CSF regulatory feedback pathway to exacerbate T_H2 cytokine production and allergen sensitisation.

Inset: Lung $CD11c^+$ macrophages produce IL-23, which functions to promote IL-17 production by $CD4^+$ and γδ T cells. IL-17 subsequently induces G-CSF production, which drives neutrophil granulopoiesis and efflux from the bone marrow. Neutrophils transmigrate into an allergen exposed lung, before undergoing apoptosis and being phagocytosed by resident macrophages, whose IL-23 production is subsequently diminished. In the absence of tissue neutrophils, this feedback cycle becomes dysregulated giving rise to increased IL-23, IL-17 and G-CSF. *Main Figure*: In an allergen exposed lung, accumulated G-CSF acts on the expanded ILC2 population to promote their IL-5 and IL-13 production. Concomitantly, G-CSF drives the expansion of bone marrow progenitors, MDPs and CDPs, leading to a monocytosis and increase in lung moDCs. The increased population of moDCs sample allergen, become activated and migrate to the local draining mediastinal lymph node to activate T cells in the

context of the heightened T_H2 cytokine milieu. This ultimately results in augmented T_H2 polarisation and type 2 antibody responses.

Supplementary Table 1: Raw data file. See uploaded document.

Supplementary Table 2: List of antibodies utilised for flow cytometry staining.

Cell type	Surface marker phenotype	Monoclonal antibody conjugate	Dilution
Neutrophils	$CD11b^{high}$	CD11b-PerCP (ThermoFisher Scientific)	1/400
	$CD11c^{-}$	CD11c-APC (BD Biosciences)	1/200
	F480-	F4/80-PE (ThermoFisher Scientific)	1/50
	$Ly6G^{high}$	Ly6G-FITC (BD Biosciences)	1/100
	$Ly6C^{int}$	Ly6C-PE-Cy7 (BD Biosciences)	1/100
Eosinophils	$CD11b^{high}$	CD11b-PerCP (ThermoFisher Scientific)	1/400
	$CD11c^{low}$	CD11c-APC (BD Biosciences)	1/200
	$SiglecF^{high}$	SiglecF-BV421 (Biolegend)	1/200
	$Ly\text{-}6G^{low}$	Ly6G-FITC (BD Biosciences)	1/100
Alveolar macrophages	$CD11b^{-}$	CD11b-PerCP (eBioscience)	1/400
	$CD11c^{+}$	CD11c-APC (BD Biosciences)	1/200
	$F4/80^{high}$	F4/80-PE (eBioscience)	1/50
	$Siglec\text{-}F^{+}$	Siglec-F-BV421 (Biolegend)	1/200
Ly6Chigh monocytes	Myeloid Lin^{-}	CD3-PE, CD19-PE, CD90.2-PE, Nkp46-PE, Ly6G-PE, Siglec-F-PE (ThermoFisher Scientific)	1/100
	$CD11b^{+}$	CD11b-PerCP (ThermoFisher Scientific)	1/400
	$CD11c^{-}$	CD11c-FITC (BD Biosciences)	1/100
	$F4/80^{high}$	F4/80-PE-DAZZLE (Biolegend)	1/50
	$Ly6C^{high}$	Ly6C-Alexa Fluor 700 (Biolegend)	1/200
	Further confirmed via FSC vs. SSC plot		
Ly6Clow monocytes	Myeloid Lin^{-}	CD3-PE, CD19-PE, CD90.2-PE, Nkp46-PE, Ly6G-PE, Siglec-F-PE (ThermoFisher Scientific)	1/100
	$CD11b^{+}$	CD11b-PerCP (ThermoFisher Scientific)	1/400
	$CD11c^{-}$	CD11c-FITC (BD Biosciences)	1/100
	$F4/80^{high}$	F4/80-PE-DAZZLE (Biolegend)	1/50
	$Ly6C^{low}$	Ly6C-Alexa Fluor 700 (Biolegend)	1/200
	Further confirmed via FSC vs. SSC plot		
Monocyte-Derived DCs	Myeloid Lin^{-}	CD3-PE, CD19-PE, CD90.2-PE, Nkp46-PE, Ly6G-PE, Siglec-F-PE (ThermoFisher Scientific)	1/100
	$CD11c^{+}$	CD11c-FITC (BD Biosciences)	1/100

	$CD11b^{high}$	CD11b-PerCP (ThermoFisher Scientific)	1/400
	$CD103^{-}$	CD103-APC (Biolegend)	1/100
	$MHCII^{high}$	I-A/I-E-BV421 (Biolegend)	1/200
	$CD64^{+}$	CD64-PE-Cy7	1/50
CD11b+ cDCs	Myeloid Lin^{-}	CD3-PE, CD19-PE, CD90.2-PE, Nkp46-PE, Ly6G-PE, Siglec-F-PE (ThermoFisher Scientific)	1/100
	$CD11c^{+}$	CD11c-FITC (BD Biosciences)	1/100
	$CD11b^{high}$	CD11b-PerCP (ThermoFisher Scientific)	1/400
	$CD103^{-}$	CD103-APC (Biolegend)	1/100
	$MHCII^{high}$	I-A/I-E-BV421 (Biolegend)	1/200
	$CD64^{-}$	CD64-PE-Cy7	1/50
CD103+ cDCs	Myeloid Lin^{-}	CD3-PE, CD19-PE, CD90.2-PE, Nkp46-PE, Ly6G-PE, Siglec-F-PE (ThermoFisher Scientific)	1/100
	$CD11c^{+}$	CD11c-FITC (BD Biosciences)	1/100
	$CD11b^{-}$	CD11b-PerCP (ThermoFisher Scientific)	1/400
	$CD103^{+}$	CD103-APC (Biolegend)	1/100
	$MHCII^{high}$	I-A/I-E-BV421 (Biolegend)	1/200
	$CD64^{-}$	CD64-PE-Cy7	1/50
MDPs	Myeloid Lin^{-}	CD3-PE, CD19-PE, CD90.2-PE, Nkp46-PE, Ly6G-PE, Siglec-F-PE (ThermoFisher Scientific)	1/100
	$CD11c^{-}$	CD11c-FITC (BD Biosciences)	1/100
	$CD115^{+}$	CD115-APC (Biolegend)	1/50
	ckit/$CD117^{+}$	CD117-Pe-CY7 (ThermoFisher Scientific)	1/50
	Flt-3^{+}	CD135-PE-DAZZLE (Biolegend)	1/50
	$MHCII^{low}$	I-A/I-E-BV421 (Biolegend)	1/200
MDPs	Myeloid Lin^{-}	CD3-PE, CD19-PE, CD90.2-PE, Nkp46-PE, Ly6G-PE, Siglec-F-PE (ThermoFisher Scientific)	1/100
	$CD11c^{-}$	CD11c-FITC (BD Biosciences)	1/100
	$CD115^{+}$	CD115-APC (Biolegend)	1/50
	ckit/$CD117^{-}$	CD117-Pe-CY7 (ThermoFisher Scientific)	1/50
	Flt-3^{+}	CD135-PE-DAZZLE (Biolegend)	1/50
	$MHCII^{low}$	I-A/I-E-BV421 (Biolegend)	1/200
ILCs	ILC Lin^{-}	TCRβ-APC, CD5-APC, CD19-APC, TCRγδ-APC, CD11b-APC, CD11c-APC, FCεR1-APC, GR-1-APC, F4/80-APC, TER-119-APC, CD3-APC, Nkp46-APC (Biolegend)	1/100
	$ICOS^{+}$	CD278/ICOS-PE-Cy7 (Biolegend)	1/100
	$KLRG1^{+}$	KLRG1-PerCP (Biolegend)	1/50
	$CD45^{+}$	CD45-BV711 (Biolegend)	1/100
CD4 T-cells	$CD3^{+}$	CD3-PE-Cy7 (eBioscience)	1/200

	$CD4^+$	CD4-PerCP (BD Biosciences)	1/200
	$CD8^-$	CD8-APC (BD Biosciences)	1/200
CD8 T-cells	$CD3^+$	CD3-PE-Cy7 (eBioscience)	1/200
	$CD4^-$	CD4-PerCP (BD Biosciences)	1/200
	$CD8^+$	CD8-APC (BD Biosciences)	1/200
MLN Monocyte-Derived DCs	Myeloid Lin^-	CD3-PE, CD19-PE, CD90.2-PE, Nkp46-PE, Ly6G-PE, Siglec-F-PE (ThermoFisher Scientific)	1/100
	$CD11c^+$	CD11c-FITC (BD Biosciences)	1/100
	$CD11b^{high}$	CD11b-PerCP (ThermoFisher Scientific)	1/400
	$CD103^-$	CD103-APC (Biolegend)	1/100
	$MHCII^{high}$	I-A/I-E-BV421 (Biolegend)	1/200
	$CD64^+$	CD64-PE-Cy7 (Biolegend)	1/50
	CD86 (to assess expression)	CD86-Alexa Fluor 700 (Biolegend)	1/100
MLN CD11b+ cDCs	Myeloid Lin^-	CD3-PE, CD19-PE, CD90.2-PE, Nkp46-PE, Ly6G-PE, Siglec-F-PE (ThermoFisher Scientific)	1/100
	$CD11c^+$	CD11c-FITC (BD Biosciences)	1/100
	$CD11b^{high}$	CD11b-PerCP (ThermoFisher Scientific)	1/400
	$CD103^-$	CD103-APC (Biolegend)	1/100
	$MHCII^{high}$	I-A/I-E-BV421 (Biolegend)	1/200
	$CD64^-$	CD64-PE-Cy7	1/50
	CD86 (to assess expression)	CD86-Alexa Fluor 700 (Biolegend)	1/100
MLN CD4 T-cells	$CD3^+$	CD3-PE-Cy7 (ThermoFisher Scientific)	1/200
	$CD4^+$	CD4-PerCP (BD Biosciences)	1/200
	$CD8^-$	CD8-APC (BD Biosciences)	1/200
	ICOS (to assess expression)	CD278/ICOS-PE-Cy7 (Biolegend)	1/100
	PD1 (to assess expression)	CD297-PEDAZZLE (Biolegend)	1/100
Epithelial Cells	$EpCAM^+$	EpCAM-PE (ThermoFisher Scientific)	1/100
	$CD45^-$	CD45-PerCP (ThermoFisher Scientific)	1/100
	$CD31^-$	CD31-APC (Biolegend)	1/100
Endothelial Cells	$EpCAM^-$	EpCAM-PE (ThermoFisher Scientific)	1/100
	$CD45^-$	CD45-PerCP (ThermoFisher Scientific)	1/100
	$CD31^+$	CD31-APC (Biolegend)	1/100
Human ILC enrichment	Lin^-	Lin-FITC (ThermoFisher Scientific)	1/30
	$CD45^+$	CD45-PerCP (ThermoFisher Scientific)	1/100
	$CRTH2^+$	CRTH2-BV421 (Biolegend)	1/100